

AFWL-TR-77-234

# LEVEL II

② JDC  
na AFWL-TR  
77-234  
ADE 200/67

DDC FILE COPY AD A059811



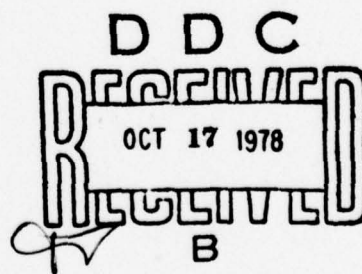
## ADVANCED LASER CONCEPTS

TRW Space Systems Group  
One Space Park  
Redondo Beach, CA 90278

May 1978

Final Report

Approved for public release; distribution unlimited.



AIR FORCE WEAPONS LABORATORY  
Air Force Systems Command  
Kirtland Air Force Base, NM 87117

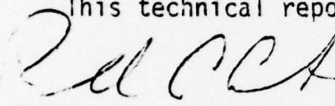
78 09 05 129

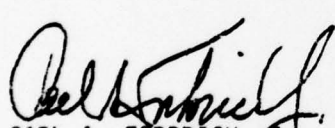
This final report was prepared by TRW, Space Systems Group, Redondo Beach, California, under Contract F29601-76-C-0065, Job Order 12560309 with the Air Force Weapons Laboratory, Kirtland Air Force Base, New Mexico. Capt S. Davis and Capt R. Armstrong were the Project Officers-in-Charge.

When US Government drawings, specifications, or other data are used for any purpose other than a definitely related Government procurement operation, the Government thereby incurs no responsibility nor any obligation whatsoever, and the fact that the Government may have formulated, furnished, or in any way supplied the said drawings, specifications, or other data is not to be regarded by implication or otherwise as in any manner licensing the holder or any other person or corporation or conveying any rights or permission to manufacture, use, or sell any patented invention that may in any way be related thereto.

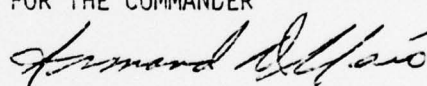
This report has been reviewed by the Office of Information (OI) and is releasable to the National Technical Information Service (NTIS). At NTIS it will be available to the general public, including foreign nations.

This technical report has been reviewed and is approved for publication.

  
RUSSELL A. ARMSTRONG  
Capt, USAF  
Project Officer

  
CARL A. FORBRICH, Jr.  
Lt Col, USAF  
Chief, Chemical Laser Branch

FOR THE COMMANDER

  
ARMAND D. MAIO  
Lt Col, USAF  
Chief, Advanced Laser Technology Division



UNCLASSIFIED

(18) AFWL, SBIE

SECURITY CLASSIFICATION OF THIS PAGE (When Data Entered)

(19) REPORT DOCUMENTATION PAGE		READ INSTRUCTIONS BEFORE COMPLETING FORM	
REPORT NUMBER AFWL TR-77-234 AD-E200267		3. RECIPIENT'S CATALOG NUMBER	
4. TITLE (and Subtitle) (6) <u>ADVANCED LASER CONCEPTS</u>		5. TYPE OF REPORT & PERIOD COVERED (9) Final Report	
7. AUTHOR(s)		8. CONTRACT OR GRANT NUMBER(s) (15) F29601-76-C-0065	
9. PERFORMING ORGANIZATION NAME AND ADDRESS TRW Space Systems Group One Space Park Redondo Beach, CA 90278		10. PROGRAM ELEMENT, PROJECT, TASK AREA & WORK UNIT NUMBERS (16) 62301F (17) 12560309 (17) 03	
11. CONTROLLING OFFICE NAME AND ADDRESS Air Force Weapons Laboratory (ALC) Kirtland Air Force Base, NM 87117		12. REPORT DATE (11) May 1978	
14. MONITORING AGENCY NAME & ADDRESS (if different from Controlling Office)		13. NUMBER OF PAGES 112	
		15. SECURITY CLASS. (of this report) UNCLASSIFIED	
		15a. DECLASSIFICATION/DOWNGRADING SCHEDULE	
16. DISTRIBUTION STATEMENT (of this Report)  Approved for public release; distribution unlimited. (12) 447P			
17. DISTRIBUTION STATEMENT (of the abstract entered in Block 20, if different from Report)			
18. SUPPLEMENTARY NOTES A doublet pi (X doublet sigma)			
19. KEY WORDS (Continue on reverse side if necessary and identify by block number)			
Chemical Laser Spectroscopy CN NF	F <sub>2</sub> /H <sub>2</sub> /CN C1 Flames F <sub>2</sub> /H <sub>2</sub> /N F <sub>4</sub> Flames Chemiluminescence Kinetics	Emission/absorption Population Distribution	
20. ABSTRACT (Continue on reverse side if necessary and identify by block number) (UNCLASSIFIED) Studies directed toward the development of a chemically pumped electronic transition laser are described. A small-scale HF/DF laser device was used to study excited state production in hydrogen-fluorine reactive flows. The number densities of the A <sup>2</sup> Π and X <sup>2</sup> Σ states of CN in hydrogen-fluorine cyanogen compound flames were measured. It was concluded that a population inversion between these two states was not achieved even though extremely high densities of the A <sup>2</sup> Π state of CN were formed. The pure chemical production of the b <sup>1</sup> Σ <sup>+</sup> and a <sup>1</sup> Δ			

DD FORM 1 JAN 73 1473

EDITION OF 1 NOV 65 IS OBSOLETE

UNCLASSIFIED

SECURITY CLASSIFICATION OF THIS PAGE (When Data Entered)

78 09 05 129  
409 637

a singlet delta

A doublet pi

A singlet sigma plus

alt

UNCLASSIFIED

SECURITY CLASSIFICATION OF THIS PAGE (When Data Entered)

states of NF was also demonstrated. For these studies, fluorine atoms formed in the precombustor of the laser were mixed with hydrogen to produce hydrogen atoms. These hydrogen atoms then reacted with  $\text{NF}_2$  radicals produced by the heating of  $\text{N}_2\text{F}_4$  to produce the NF excited states. The densities measured were too low for laser production. However, the system may be scalable to laser proportions.

ACCESSION for	
NTIS	White Section <input checked="" type="checkbox"/>
DDC	Buff Section <input type="checkbox"/>
UNANNOUNCED	<input type="checkbox"/>
JUSTIFICATION	
BY	
DISTRIBUTION/AVAILABILITY CODES	
Dist. avail. and/or SPECIAL	
A	

UNCLASSIFIED

SECURITY CLASSIFICATION OF THIS PAGE (When Data Entered)

## TABLE OF CONTENTS

	<u>Page</u>
1.0 INTRODUCTION . . . . .	1
2.0 STUDY OF CN PRODUCTION IN HYDROGEN-FLUORINE FLAMES . . . . .	3
2.1 BACKGROUND AND INTRODUCTION . . . . .	3
2.2 EXPERIMENTAL . . . . .	7
2.2.1 Experimental Apparatus . . . . .	7
2.2.2 Diagnostic Equipment . . . . .	7
2.2.3 Choice of CN-Lines Used for Emission/Absorption Experiments . . . . .	16
2.2.4 Choice of System Components for Study . . . . .	17
2.3 RESULTS . . . . .	22
2.3.1 Experiments to Optimize Emission Intensities . . . . .	22
2.3.2 Results of Emission/Absorption Experiments for F <sub>2</sub> /H <sub>2</sub> /CNC1 and F <sub>2</sub> /D <sub>2</sub> /CNC1 Flames . . . . .	26
2.3.3 Results of Temperature Measurements. . . . .	26
2.3.4 Spatial Intensity Distributions in F <sub>2</sub> /D <sub>2</sub> / CNC1 Flames . . . . .	37
2.3.5 Effects of Total Pressure . . . . .	47
2.3.6 Visible Spectroscopy . . . . .	51
2.3.7 Data Reduction . . . . .	53
2.3.8 CN-Donors Other Than CNC1 . . . . .	57
2.4 DISCUSSION. . . . .	61
3.0 CHEMICAL PRODUCTION OF NF EXCITED STATES . . . . .	64
3.1 EXPERIMENTAL . . . . .	65
3.1.1 Experimental Apparatus . . . . .	65
3.1.2 Diagnostics. . . . .	66
3.1.3 Gas Handling . . . . .	72

## TABLE OF CONTENTS (Continued)

	<u>Page</u>
3.2 RESULTS . . . . .	72
3.2.1 Preliminary Experiments . . . . .	73
3.2.2 Experiments with the 13:1 Area Expansion Ratio Nozzle . . . . .	78
3.2.3 Experiments with the 4:1 Area Expansion Ratio Nozzle . . . . .	85
3.2.4 Experiments with the 8:1 Area Expansion Ratio Nozzle . . . . .	91
3.2.5 Experiments with the 15 cm Device . . . . .	95
3.3 DISCUSSION . . . . .	103



## 1.0 INTRODUCTION

TRW, along with other government contractors, universities and government and national laboratories, has been engaged in research programs over the past several years with the principal objective of development of an electronic transition chemical laser. These studies were motivated by a need of the Advanced Research Projects Agency and the Air Force for the development of a high energy chemically pumped laser in the wavelength region between 300 nanometers and 2000 nanometers with the potential for high average power for minimum system weight. To date, there have been no demonstrations of a pure chemical electronic transition laser. Also, much of the research has been hampered by the sparsity of data available on most molecules.

The major effort of the present contract was concentrated on studies of ways of pumping the  $A^2\Pi$  state of the CN molecule. The second part of the contract concentrated on studies of the chemical pumping of the  $b^1\Sigma^+$  and  $a^1\Delta$  states of NF. These studies continued an effort begun under Contract F29601-73-A-0036-001 which was funded by ARPA and monitored by the Air Force Weapons Laboratory.

The objective of the program was to determine whether the chemical energy released in hydrogen-fluorine reactive flows could be used to populate the upper level of a candidate laser molecule. Primary emphasis was on CN and NF as candidate laser and energy transfer species because of the data available on these systems. In the case of CN, the spectroscopy and potential energy curves are known and critical radiative lifetimes have been measured. CN has also lased on the  $A^2\Pi - X^2\Sigma$  transition in pulsed flash photolysis

and discharge experiments. In the case of NF, the spectroscopy for the pertinent states has been studied and recent studies at Aerospace Corporation have established pertinent lifetime and kinetic data which makes the system appear interesting. Thus, the candidate species are well characterized.

The report is divided into two sections. The first section concentrates on studies of the CN system. Detailed studies of production of CN in a combustion system are reported with measurements of upper and lower state concentrations. The second section reports on studies of the production of NF excited states by strictly chemical means. Both studies were conducted using TRW's small scale chemical laser facility which will be described in detail.

## 2.0 STUDY OF CN PRODUCTION IN HYDROGEN-FLUORINE FLAMES

### 2.1 BACKGROUND AND INTRODUCTION

Towards the end of the technical effort on Contract F29601-A-73-0036-001, extremely intense emission from the  $A^2\Pi$  state of the CN molecule was observed in hydrogen-fluorine-cyanogen flames. This observation was very encouraging because of the identification of properties of this state of CN which indicate that it could be a good candidate for chemical laser production. The desirable properties of the CN molecule are:

- A 7 microsecond lifetime (1) which is long enough to make a mixing laser possible and also to allow achievement of high power in a laser system.
- Displacement of the  $A^2\Pi$  and  $X^2\Sigma$  potential energy curves ( $r_e$  for  $X^2\Sigma^+$  is 1.1798;  $r_e$  for  $A^2\Pi$  is 1.2332 (2). A potential energy diagram of CN showing the transitions of interest is presented in figure 1.
- The fact that the  $A^2\Pi - X^2\Sigma$  transition of CN has been lased in both flash photolysis<sup>(3)</sup> and electric discharge systems.<sup>(4)</sup>

Preliminary experiments under the previous contract indicated that the cyanogen-fluorine-hydrogen flame system might be capable of creating a population inversion between the  $A^2\Pi$  state and certain vibrational levels of the  $X^2\Sigma^+$  state of CN. A summary of these experiments is given below.

Red emission was first observed in tests in which  $NF_3$ ,  $F_2$  and  $H_2$  were being burned in the precombustor of a combustion driven laser and cyanogen and deuterium added downstream. Adjustment of flows to optimize emission showed maximum intensities when only fluorine, cyanogen and hydrogen

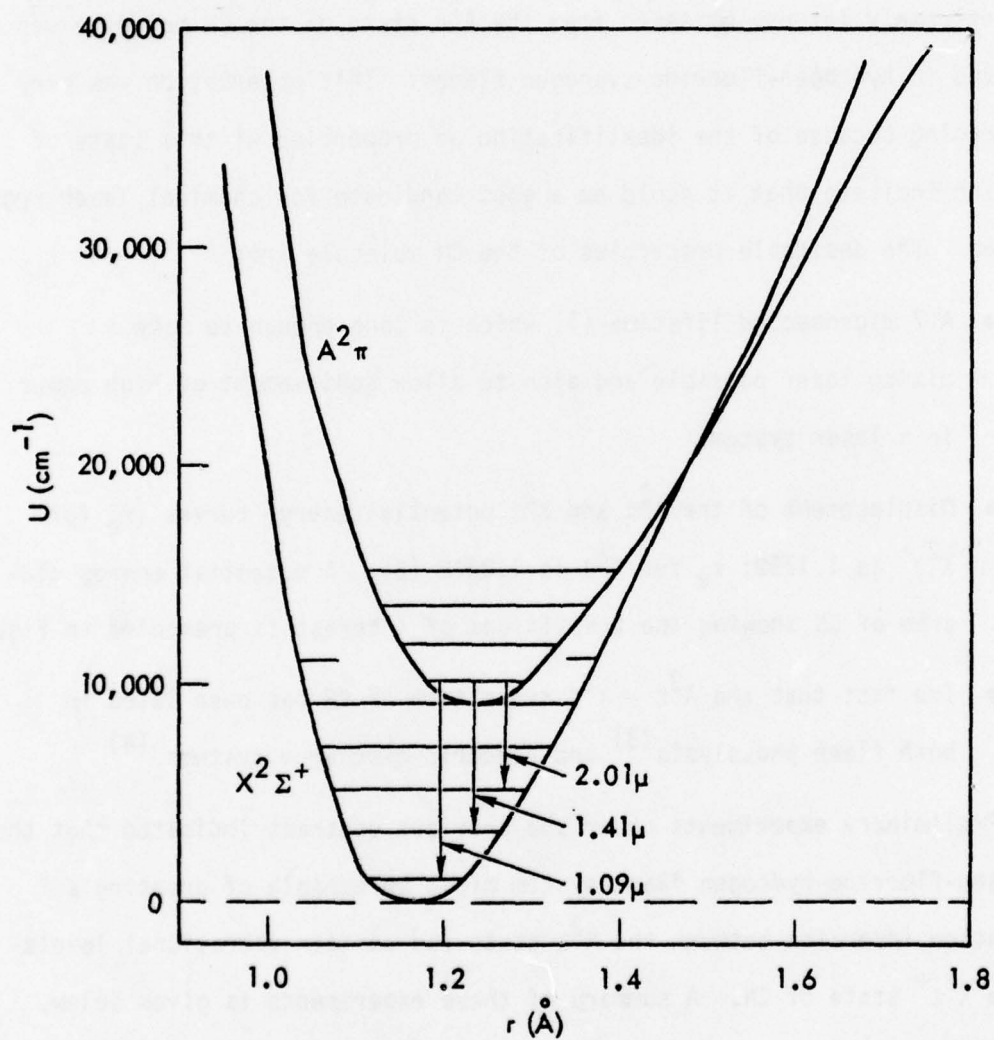


Figure 1. Potential energy curves for CN.



were present. Spectral studies showed that this emission was CN ( $A^2\Pi \rightarrow X^2\Sigma$ ) red band emission. The emission intensity in the 0-0 band of the CN ( $A^2\Pi \rightarrow X^2\Sigma$ ) system at  $1.1\mu$  was optimized by appropriate adjustment of flows and pressure. The number density in this band was determined by scanning the emission with a calibrated spectrometer, integrating the chemiluminescent intensity and using the radiative lifetime of the CN ( $A^2\Pi$ ) state to calculate the number density. Such a determination gave a number density of the order of  $10^{15}$  molecules/cm<sup>3</sup> in the 0-0 band of CN alone. This corresponds to approximately 3% of the number density of the cyanogen present.

The suggestion was made that some of the CN  $A^2\Pi$  state is formed by vibrational to electronic energy transfer from HF ( $v \geq 3$ ). To test this thesis, deuterium was substituted for hydrogen in the experiments. With deuterium, the CN ( $A^2\Pi$ ) state could be populated from transfer from DF ( $v \geq 4$ ). It was found that comparable CN ( $A^2\Pi$ ) emission intensities could be obtained with deuterium although somewhat different ratios of  $F_2$ : (CN)<sub>2</sub>: H<sub>2</sub>(D<sub>2</sub>) were required. This result can be explained if transfer rates from HF and DF to CN are equally fast or if some other mechanism pumps the CN.

Cyanogen was next replaced by cyanogen chloride. The logic was that the weaker CN-Cl bond compared with the NC-CN bond should facilitate CN production. Indeed, it was found that CNCl burned with a more stable flame, with less H<sub>2</sub> or D<sub>2</sub> and gave higher number densities of CN excited state at lower cavity pressures than when (CN)<sub>2</sub> was present.

A preliminary attempt was made to determine the CN  $X^2\Sigma$  state population using absorption spectroscopy. A microwave lamp giving CN ( $B^2\Sigma \rightarrow X^2\Sigma$ ) emission was used as the source. A spectrometer with an EMI6256

photomultiplier was used to monitor the source emission. Source intensity with and without the CN-R/F<sub>2</sub>/D<sub>2</sub> flame was monitored and corrections made for the CN (B<sup>2</sup><sub>Σ</sub> → X<sup>2</sup><sub>Σ</sub>) emission from the flame. With the (CN)<sub>2</sub> flame, approximately 95% of the emission was absorbed in a 15 cm path. This is in the nonlinear absorption region making it difficult to set an upper bound on CN ground state population. However, in the CNCl flame only 5% of the source intensity was absorbed indicating that the ground state population is less than ~10<sup>13</sup> molecules/cm<sup>3</sup>. Unfortunately, emission and absorption experiments were not performed under identical flow conditions so these tests were very preliminary.

Some lasing tests were conducted using two mirror configurations. First tests were tried with gold coated mirrors with a hole outcoupler mounted external to the Brewster angle windows. The next tests were conducted with mirrors dielectrically coated for maximum reflectance at 1.4 μ (the 0-1 CN (A<sup>2</sup><sub>Π</sub> → X<sup>2</sup><sub>Σ</sub>) transition). These mirrors were mounted inside the cavity. No lasing was indicated with the gold-coated mirrors. With the dielectric mirrors a ratio of 20 between tuned and spoiled cavities could be achieved. However, a spectral scan with very poor resolution indicated no line narrowing.

The tests described above were conducted only for a very limited range of experimental conditions and were inconclusive for determination of whether the flame system could be made to lase. Thus, the current program was initiated to evaluate the potential of fluorine-hydrogen flames as a means of exciting the A<sup>2</sup><sub>Π</sub> state of CN.

The object of the research conducted under this program was to conduct

very detailed studies of the cyanogen flame system to evaluate its lasing potential. This section reports on the results of these detailed studies.

## 2.2 EXPERIMENTAL

### 2.2.1 Experimental Apparatus

The hardware used for these experiments was a 15 cm gain length laser nominally used for HF/DF laser studies. A photograph of the device is shown in Figure 2. The device is built in rectangular modules constructed of aluminum. For these studies, only fluorine flowed through the precombustor of the laser. Thus, the precombustor was used as an injection port for fluorine. The fluorine passed from the precombustor through a "side-on" type of injector. This consisted of a rectangular supersonic nozzle, with fuel injected from a series of holes located along the two long edges of the nozzle. The hydrogen and cyanogen compounds were premixed in the line leading to the injector and injected into the fluorine flow through the "side-on" injector holes. The cavity, where mixing occurred, could be reviewed either through Brewster angle windows to allow viewing along the laser axis or through chemiluminescence windows to allow viewing perpendicular to the laser axis.

For absorption experiments, a source of CN ( $A^2\Pi - X^2\Sigma$ ) emission was required. The smallest scale HF laser described in detail in section 3.2 was used as a burner for this purpose.

### 2.2.2 Diagnostic Equipment

The most important diagnostics performed on this system were absorption to measure ground state populations and emission to measure excited state

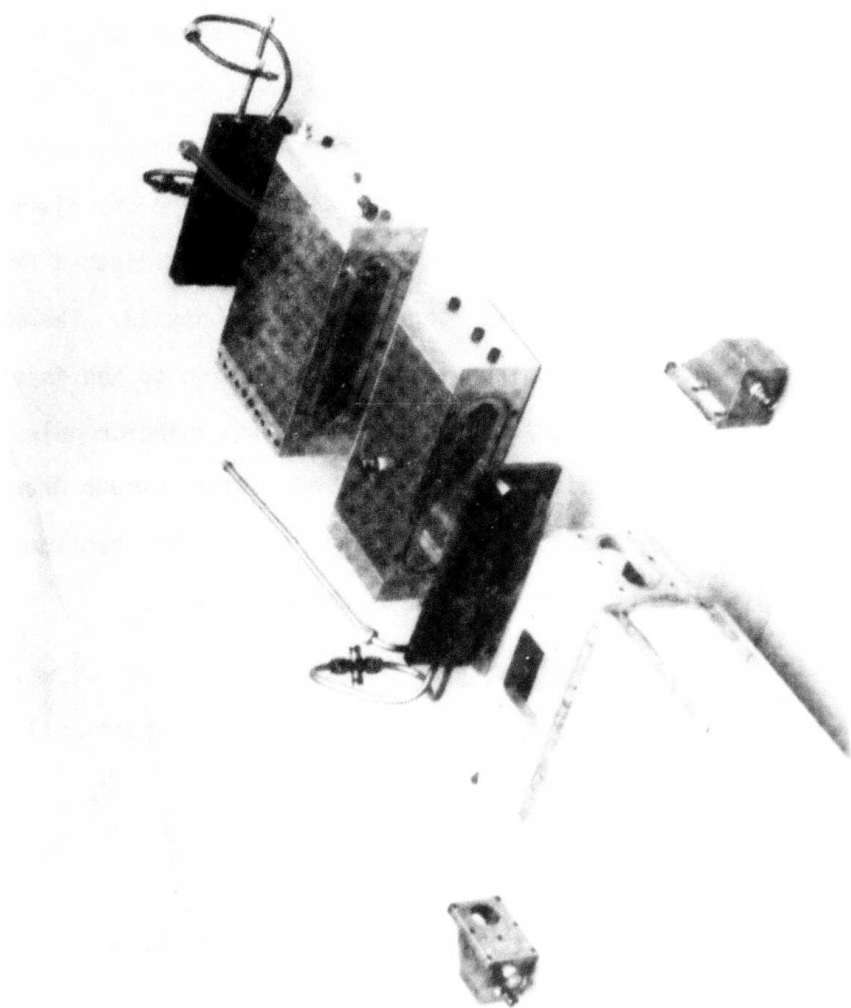


Figure 2. Components of 15 cm gain HF laser device.



population. It was found that absorption of an isolated line of the (0,0) band of the ( $A^2\Pi \rightarrow X^2\Sigma$ ) transition of CN could be used to determine the concentration of the  $X^2\Sigma$  state of CN. As noted above, a small HF laser in which fluorine, hydrogen and cyanogen were burned was used as the source for the emission experiments. Upper state concentrations could be determined by observation in emission of the same line used for the absorption experiments.

A schematic drawing of the experimental configuration used to perform emission/absorption experiments is shown in Figure 3. A photograph of the actual experiment is shown in Figure 4. The arrangement had the two lasers in series. The optical system was designed so that radiation from either the burner or the reaction cell could be monitored. Since the same CN line could be used for both emission and absorption measurements, it was possible to easily accumulate emission and absorption data almost simultaneously using the same spectrometer. This was done using two choppers and two lockin amplifiers. One chopper at 98 hertz was placed at the entrance slit of the spectrometer. This was used to isolate the signal from the burner from that of the reaction cell. The other chopper at 167 hertz was placed between the burner and reaction cell. This was used to record absorption data. A two pen recorder was used to record the data.

The spectrometer used for these experiments was a 0.3 meter McPherson. It was equipped with a 600 line/mm grating blazed at  $1.6\mu$ . A PbS detector cooled to 77°K was used for detection. A 700 nm cuton filter was used to prevent higher order radiation from hitting the grating and entering the detection system.

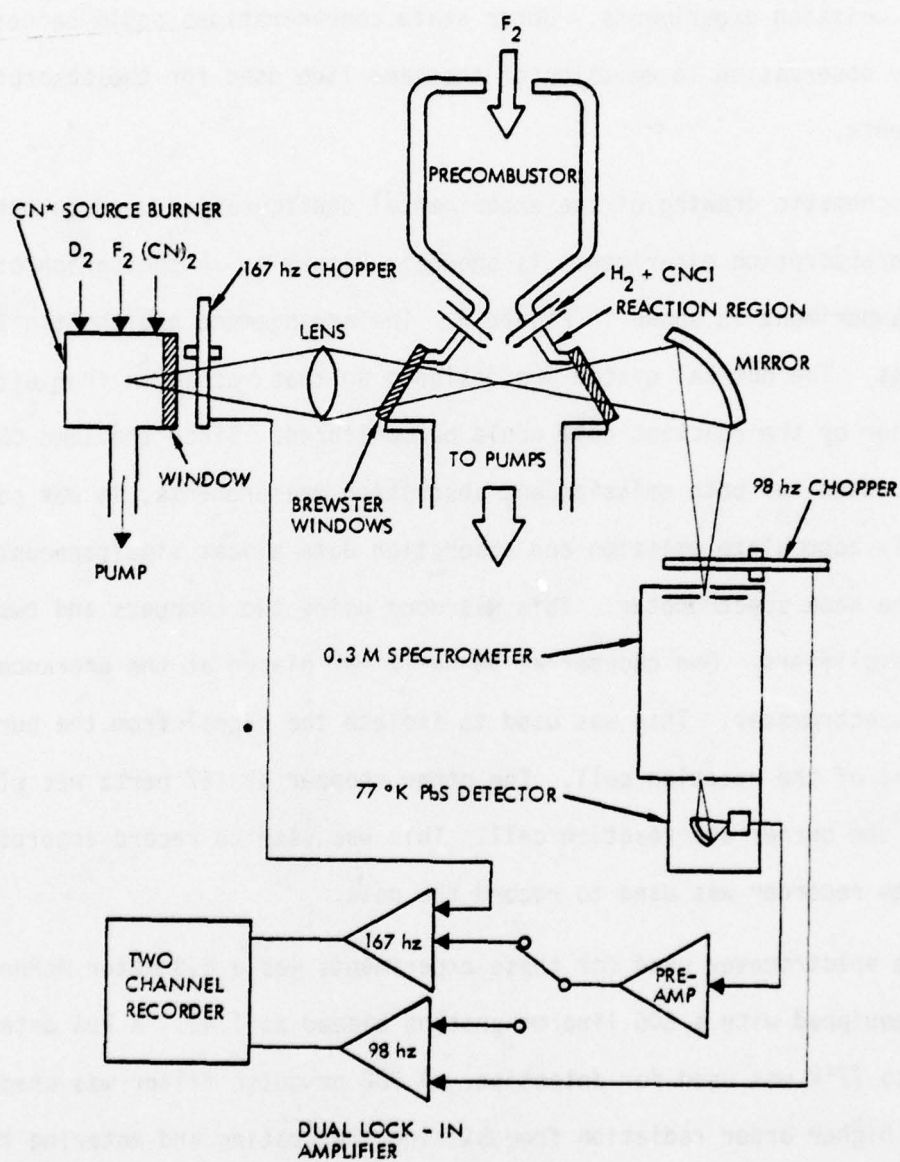


Figure 3. Schematic of experimental configuration for emission/absorption experiments.

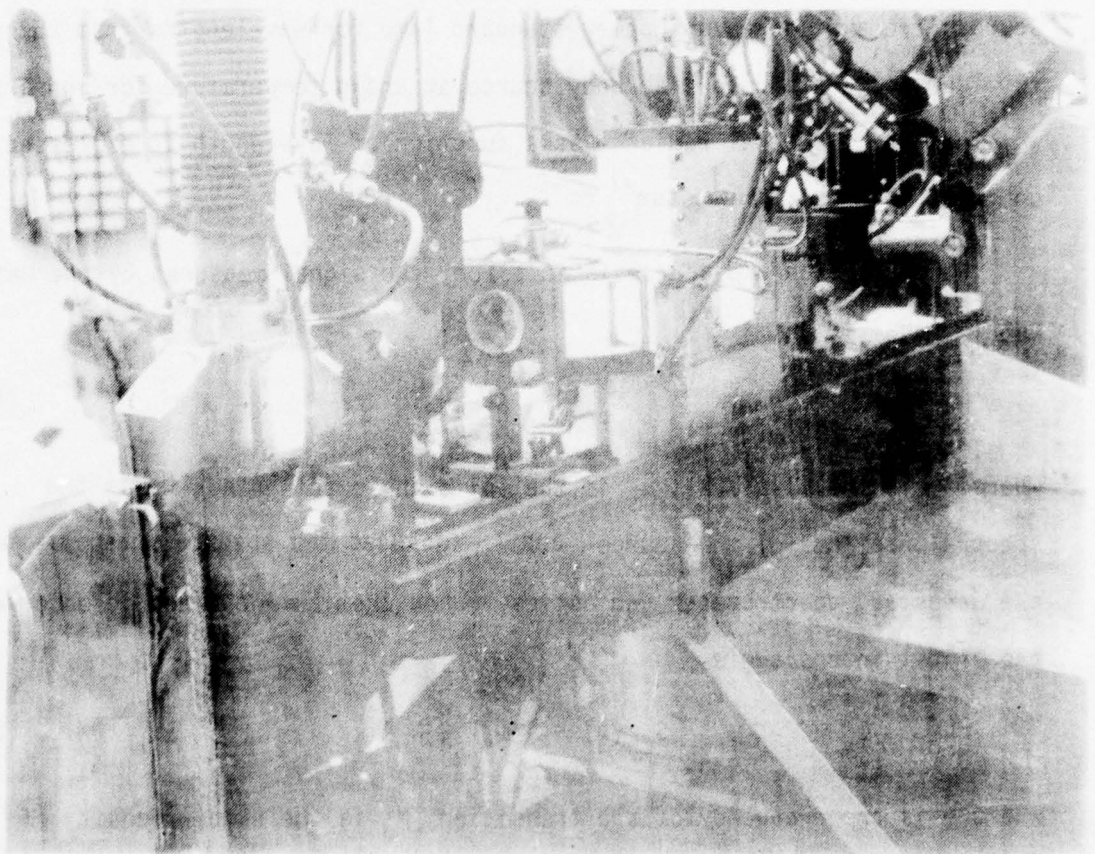


Figure 4. Equipment used for absorption/ emission experiments.

For determination of excited state number densities from emission intensities, the entire spectral detection setup including optics, spectrometer and detector was calibrated. This was done by placing a calibrated light source in the same optical position as the chemiluminescence source. Care was taken in optical design to insure the optics are completely filled and that the slit image is smaller than the standard source. Two standard sources are available, an Eppley standard lamp for wavelengths from 250 nm to 1  $\mu\text{m}$  and a standard blackbody source at known temperature for infrared wavelengths. Spectral radiance as a function of wavelength is expressed in units of watts micron<sup>-1</sup> ster<sup>-1</sup> cm<sup>-2</sup>.

When the standard source is in place, the signal measured by the detector is equal to

$$S_p(\lambda) = A_s \omega_s N_\lambda T_\lambda \quad (1)$$

where  $A_s$  is the slit area,  $\omega_s$  is the solid angle collected,  $N_\lambda$  is the spectral radiance of the source, and  $T_\lambda$  includes the spectral response of the detector, spectrometer and optics. When chemiluminescence is observed, the signal intensity is

$$S_{ch}(\lambda) = A_s \omega_s T_\lambda \frac{h\nu}{4\pi} N_u A_{ul}^2 \quad (2)$$

where  $\nu$  is the frequency of the transition,  $N_u$  is the number density of species in the upper state,  $A_{ul}$  is the Einstein coefficient for the observed transition and  $l$  is the optical path length.

$N_u$  can be obtained by dividing equation (2) by equation (1). It can be expressed as

$$N_u = \frac{N_\lambda}{S_p(\lambda)} S_{ch}(\lambda) \frac{4\pi}{h\nu} \frac{1}{A_{ul}^2} \quad (3)$$



For broad transitions,  $N_u$  is obtained by integration of the entire area under the emission curve. If intensity in only one vibrational band is observed, equation (3) can be divided by the Franck-Condon factor of that transition to give the total upper vibrational state number density. Peak heights were used to determine number densities. These were checked by integration of the area under the emission line to insure that the two techniques were in agreement.

A Polaroid portrature camera was used to photograph the medium to determine homogeneity. This proved to be a very useful diagnostic technique for determining what was happening in the cavity.

Temperatures were determined using emission spectroscopy of either HF, DF or CN. For these tests the spectrometer was fitted with a 600 line/mm grating blazed at  $3\mu$  for HF/DF experiments or a 1200 line/mm grating blazed at 750 nm for CN experiments. For these tests, only relative peak heights were important so the spectrometer needed to be calibrated only relatively, not absolutely.

In order to compute CN ground state densities from absorbances using the formulas in Section 2.3.7, several requirements need to be fulfilled. The first requirement is the accurate measure of the absorbance for an individual spectral line as has been described earlier. A second requirement is that both the source and medium be Doppler-broadened or that the type of broadening present be known.

Considerations of Doppler width and pressure broadening coefficients lead to the conclusion that Doppler half-widths should exceed the collision broadening half-width by about one order of magnitude at  $T = 3000^\circ\text{K}$  and pressures of 10 to 100 torr.

The Doppler width (full width at half-maximum) is given by

$$\frac{\Delta W_D}{W} = \frac{2\sqrt{R \ln 2}}{C} \sqrt{\frac{T}{M}} \approx 7 \cdot 10^{-6} \quad (4)$$

while the collision width is given by the classical Lorentz expression

$$\Delta W_L = \frac{2}{\pi C} \sigma_L^2 N \sqrt{2\pi RT \left( \frac{1}{M_1} + \frac{1}{M_2} \right)} \quad (5)$$

where  $M_1$  and  $M_2$  are molecular weights of CN and its principal collision partner,  $N$  the total number density, and  $\sigma_L^2$  is an "optical" collision cross section which generally is about  $5 \cdot 10 \text{ cm}^2$ . The value of  $\Delta W_L$  is about  $1.7 \times 10^{-3} \text{ cm}^{-1}$  at 10 torr and  $8.5 \times 10^{-3} \text{ cm}^{-1}$  at 50 torr. At  $1.1\mu$  and  $3000^\circ\text{K}$ ,  $\Delta W_D$  is about  $0.07 \text{ cm}^{-1}$ . Therefore, the Doppler width is a factor of 10 larger than the collision width, indicating that the assumption of Doppler broadening is justified under the run conditions of these experiments. However, it was considered desirable to verify this experimentally. Also, a third requirement for computation of CN ground state densities is that the source line is not self-absorbed.

To measure linewidths and to check for self absorption, a scanning Fabray-Perot interferometer was used. Plates with 98.5% reflectivity at  $1.15\mu$  were obtained and the system was adjusted for a free spectral range of 0.026 nm. Optical tables were mounted around the laser to provide a table support for the optics and the system was aligned using  $1.15\mu$  He - Ne laser. Figure 5 shows a scan with the Fabray-Perot interferometer of the alignment laser. The two features in the scan are due to two separate laser lines. The fine structure observed is due to the laser mode structure. When an attempt was made to scan the output from the CN burner, no fringes were observed even though numerous adjustments and a

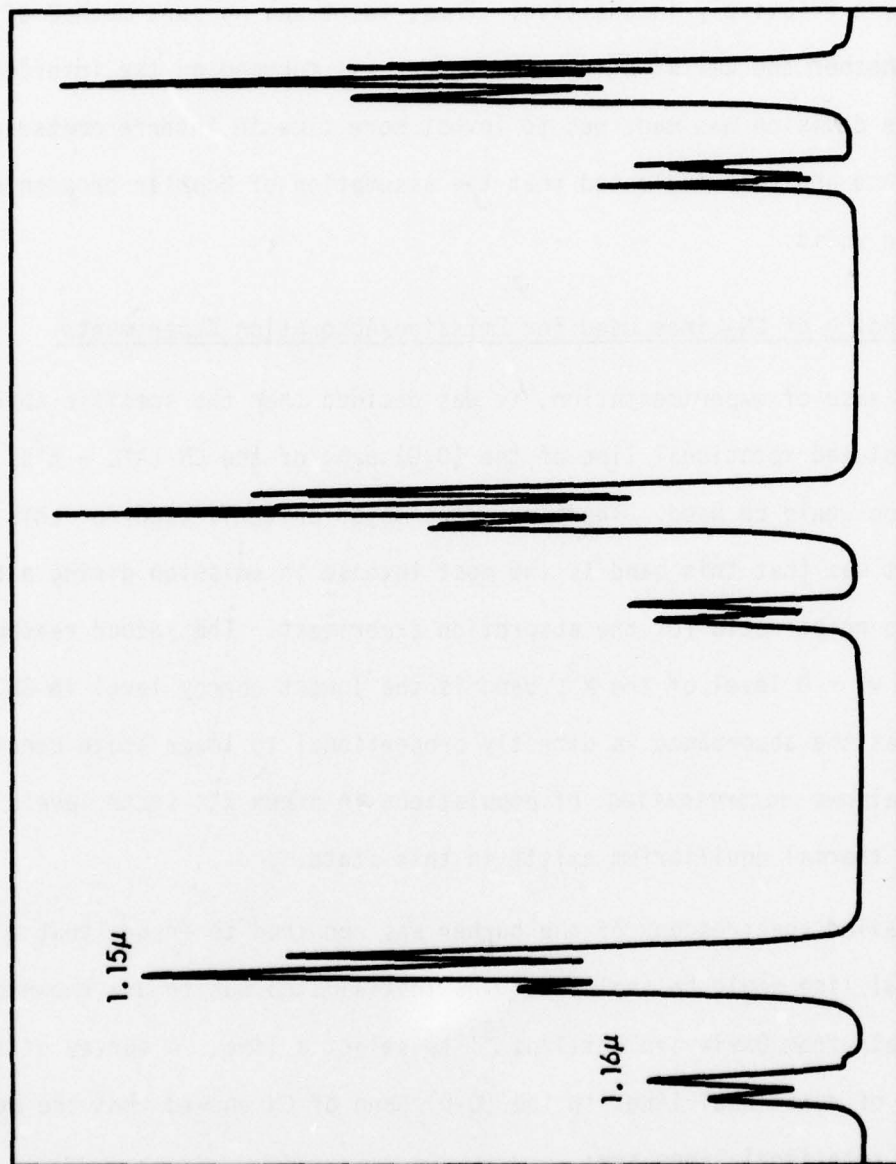


Figure 5. Interferogram of He-Ne Laser at  $1.15\mu$  with a free spectral range of  $0.026\text{ nm}$ . The mode structure of the laser is observed.

large amount of time were devoted to this task. It was felt the difficulty was due to the fact that the experiments were conducted in the infrared spectral range where visual alignment was impossible and where detector systems are relatively insensitive. Thus, there was no sure method of determining whether the emission from the burner was focused on the interferometer. Thus, the decision was made not to invest more time in interferometer measurements since analysis indicated that the assumption of Doppler broadening should be valid.

### 2.2.3 Choice of CN-Lines Used for Emission/Absorption Experiments

For ease of experimentation, it was decided that the specific absorption of an isolated rotational line of the (0,0) band of the CN ( $A^2\Pi \rightarrow X^2\Sigma$ ) transition would be used. There were two major criteria used for this choice. The first was that this band is the most intense in emission giving a better signal to noise ratio for the absorption experiment. The second reason was that the  $v'' = 0$  level of the  $X^2\Sigma$  band is the lowest energy level in CN. This means that the absorbance is directly proportional to lower state density. It also allows determination of populations in other  $X^2\Sigma$  state levels by assuming thermal equilibrium exists in this state.

Detailed spectroscopy of the burner was required to insure that a single rotational line could be isolated. The initial step was to use known spectroscopic data from Davis and Phillips<sup>(5)</sup> to select a line. A survey of the location of rotational lines in the (0-0) band of CN showed that the most isolated rotational lines are:



P <sub>1</sub> (10)	$\lambda = 1105.2114 \text{ nm}$	nearest line 0.32 nm away
P <sub>1</sub> (14)	$\lambda = 1108.7934 \text{ nm}$	nearest line 0.26 nm away
Q <sub>1</sub> (16)	$\lambda = 1104.1444 \text{ nm}$	nearest line 0.24 nm away
Q <sub>1</sub> (20)	$\lambda = 1107.2666 \text{ nm}$	nearest line 0.26 nm away
Q <sub>1</sub> (24)	$\lambda = 1111.1783 \text{ nm}$	nearest line 0.25 nm away
Q <sub>1</sub> (25)	$\lambda = 1112.2790 \text{ nm}$	nearest line 0.22 nm away

High resolution spectra were then run using the McPherson spectrometer to verify that these lines could be isolated with the chosen optical system. It was found that 0.1 nm resolution could be easily achieved with this system. The spectrum of the CN flame was scanned over the six candidate P<sub>1</sub> and Q<sub>1</sub> branch lines. It was found that the Q<sub>1</sub> branch lines were more intense than the P<sub>1</sub> branch lines and hence easier to use for reference. A portion of the high resolution spectrum showing the Q<sub>1</sub>(24) and Q<sub>1</sub>(25) lines is shown in Figure 6. The Q<sub>1</sub>(24) line was somewhat arbitrarily chosen from the list of candidate lines as the reference line for the absorption and emission experiments. Peak heights were monitored rather than attempting to integrate the area of the line for each measurement.

#### 2.2.4 Choice of System Components for Study

The first step in this program was to decide which cyanogen-containing compounds would be most desirable for study. The first criteria for selection of CN-containing compounds were low boiling points and commercial availability.

Table 1 lists the most volatile CN-containing compounds with their respective boiling points, dissociation energies and heats of formation. Using this table as a guide, CNBr, CH<sub>3</sub>CN and CH<sub>3</sub>NC were eliminated from consideration by their relatively high boiling points and

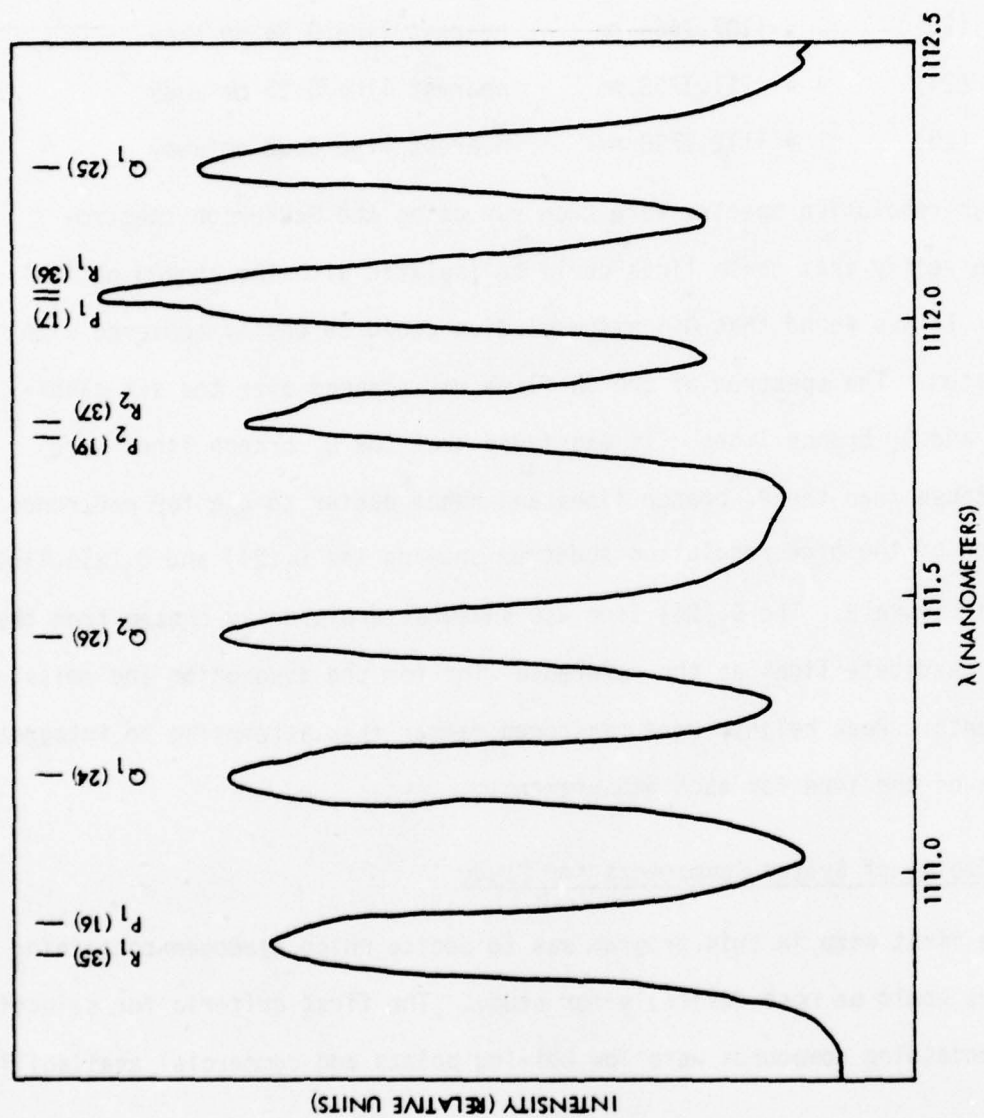


Figure 6. High resolution spectral scan of the CN burner.

low vapor pressures.  $\text{CNF}$  and  $\text{CH}_3\text{NC}$  could be eliminated because they were not commercially available and are difficult to store even when synthesized. This preliminary screening left  $\text{HCN}$ ,  $(\text{CN})_2$ ,  $\text{CNCI}$ ,  $\text{CF}_3\text{CN}$  and  $\text{C}_2\text{F}_5\text{CN}$  as potential CN-donors.

The second criteria for selection was their capability of producing the CN radical in the reaction with either fluorine or hydrogen atoms. Table 2 summarizes the reactions of hydrogen and fluorine atoms with the CN-containing compounds and their corresponding reaction enthalpies. This table indicates that CN radicals can be produced in the reaction of either F or H atoms with any CN-containing compound with the exception of cyanogen. However, none of these reactions produces the 26 kcal/mole required to excite CN to the A state.

With the above considerations added to ease of procurement,  $\text{HCN}$  and  $\text{CICN}$  were established as the primary candidates for study. Backup candidates were  $\text{CF}_3\text{CN}$ ,  $\text{C}_2\text{F}_5\text{CN}$  and  $(\text{CN})_2$ . Flames using both hydrogen and deuterium were studied.

Choice of gases to use in the reference burner were guided by practical considerations. Cyanogen was used as the CN-radical source because of its ready commercial availability. Deuterium was used in place of hydrogen to avoid any interference from the HF 2-0 overtone emission.

Gas flows were monitored by the pressure behind calibrated orifices. All gas flowrates were carefully calibrated using Matheson 8142, 8163 or 8164 mass flow meters with a Matheson 8143 flow indicator.

Conventional gas handling techniques were used for all gases. The only problem encountered was with  $\text{CNCI}$  which appeared to react with the pump oil forming a solid compound which eventually caused the pump to stop running.

Table 1.  
Boiling Points, Dissociation Energies and Heats of  
Formation of Several CN-Containing Compounds

Compound	Boiling Point, °C	D <sup>a</sup> (kcal)	D <sup>b</sup> (kcal)	ΔH <sub>f</sub> <sup>b</sup>	ΔH <sub>f</sub> <sup>c</sup>
*HCN	26	114	120	32.39	32.3
(CN) <sub>2</sub>	-20.7	112	128	73.4	73.87
*CNCI	13.8	-	97	32.8	32.97
CNBr	61.6	-	83	46.1	44.5
CNF <sup>d</sup>	-46.2	-	≤ 111	≥ 7.4	8.6
CH <sub>3</sub> CN	82	103	~ 110		
CH <sub>3</sub> NC	59.6				
*CF <sub>3</sub> CN	-68°C				-118.4
C <sub>2</sub> F <sub>5</sub> CN	-35°C				

\*Most desirable compounds to study.

- a. T. L. Cottrell, The Strengths of Chemical Bonds (Butterworth's, London, 1958).
- b. D. D. Davis and H. Okabe, J. Chem. Phys. 49, 5526 (1969).
- c. D. R. Stull and H. Prophet, Eds., JANAF Thermodynamic Tables. Second Edition, NSRDS-NBS37, June 1971.
- d. Liquid cyanogen fluoride, CNF, is rapidly converted to polymeric materials at room temperature. However, it can be stored in the gas phase at atmospheric pressure. The compound has to be synthesized.



Table 2.  
Reactions of Hydrogen and Fluorine Atoms  
With CN-Containing Compounds

Compounds	Reactions	$\Delta H$ (Kcal)
HCN	$H + HCN \rightarrow H_2 + CN$ $F + HCN \rightarrow HF + CN$ $F + HCN \rightarrow FCN + H$	+16 -14.9 + 9
$(CN)_2$	$H + (CN)_2 \rightarrow HCN + CN$ $F + (CN)_2 \rightarrow FCN + CN$	+ 7.9 +16.6
CNCI	$H + CNCI \rightarrow HCl + CN$ $H + CNCI \rightarrow HCN + Cl$ $F + CNCI \rightarrow FCN + Cl$ $F + CNCI \rightarrow FCl + CN$	- 5.9 -23.7 -14.9 +37
CNBr	$H + CNBr \rightarrow HBr + CN$ $H + CNBr \rightarrow HCN + Br$ $F + CNBr \rightarrow FCN + Br$ $F + CNBr \rightarrow FBr + CN$	- 5.9 -39.1 -30.3 +23
CNF	$H + CNF \rightarrow HF + CN$ $H + CNF \rightarrow HCN + F$ $F + CNF \rightarrow F_2 + CN$	-23.5 - 8.8 +75.3
$CH_3CN$	$H + CH_3CN \rightarrow CH_4 + CN$ $H + CH_3CN \rightarrow HCN + CH_3$ $F + CH_3CN \rightarrow CH_3F + CN$ $F + CH_3CN \rightarrow CH_2CN + HF$	
$CF_3CN$	$H + CF_3CN \rightarrow CF_3H + CN$ $H + CF_3CN \rightarrow HF + CF_2CN$ $H + CH_3CN \rightarrow HCN + CF_3$ $F + CF_3CN \rightarrow CF_4 + CN$ $F + CF_3CN \rightarrow FCN + CF_3$	~ 0 N.A. -14.1 -22

Care had to be taken to change the pump oil often when using this compound and even with this precaution, pump performance degraded with time. The pump eventually had to be returned to the manufacturer to be rebuilt.

## 2.3 RESULTS

### 2.3.1 Experiments to Optimize Emission Intensities

Most experiments on the CN system were performed for a fixed position in the cavity, i.e., both the optics and laser positions were fixed. For these experiments, the observation region was approximately 0.5 cm below the mixing nozzle. Later tests were run at various cavity positions. These results will be discussed in section 2.3.4.

The first tests performed were designed to optimize the emission from the  $A^2\Pi$  state of CN. For these tests, the spectrometer was set to monitor CN emission as a function of flowrate of an individual species. Some representative plots obtained in this optimization procedure are shown in Figures 7 through 9 for the  $F_2/D_2/CNCl$  system. Figure 7 shows a plot of the CN emission intensity versus fluorine flow with  $D_2$ ,  $CNCl$  constant at two separate cavity pressures. Note that the emission intensity is sharply peaked and that the peak is dependent on pressure. Figure 8 shows the dependence of emission intensity on deuterium flow with fluorine and cyanogen chloride flows constant. Again the emission intensity peaks at a certain deuterium flow and the position at which it peaks is dependent on pressure. Figure 9 shows the dependence of CN emission intensity on cyanogen chloride flow for fixed  $F_2$  and  $D_2$  flows. The signal changes very slowly with  $CNCl$  flow once a critical flow is reached.

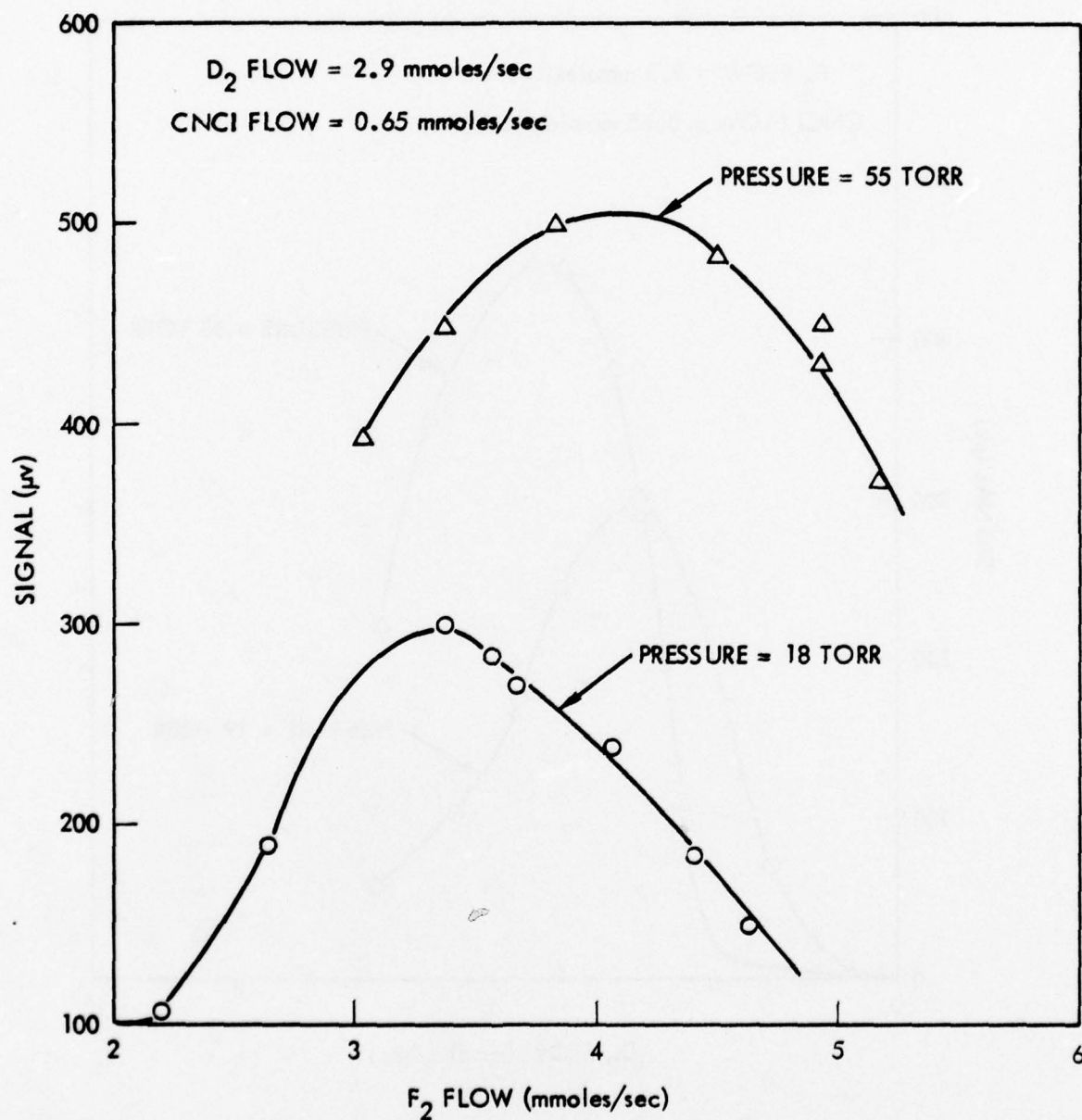


Figure 7. Plot of emission intensity versus fluorine flow with D<sub>2</sub>, CNCI constant.

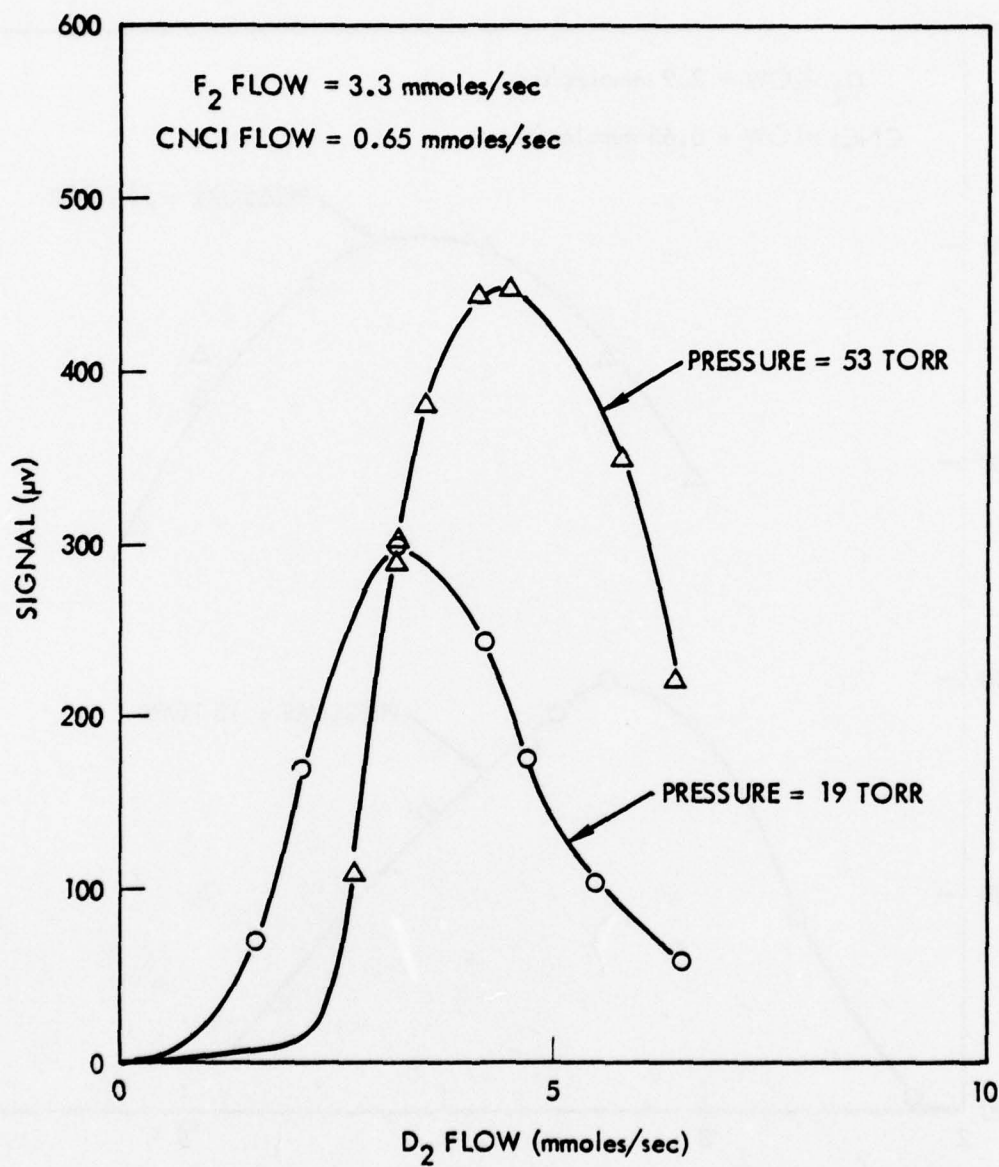


Figure 8. Plot of emission intensity versus deuterium flow with  $\text{F}_2$ ,  $\text{CNCI}$  constant.



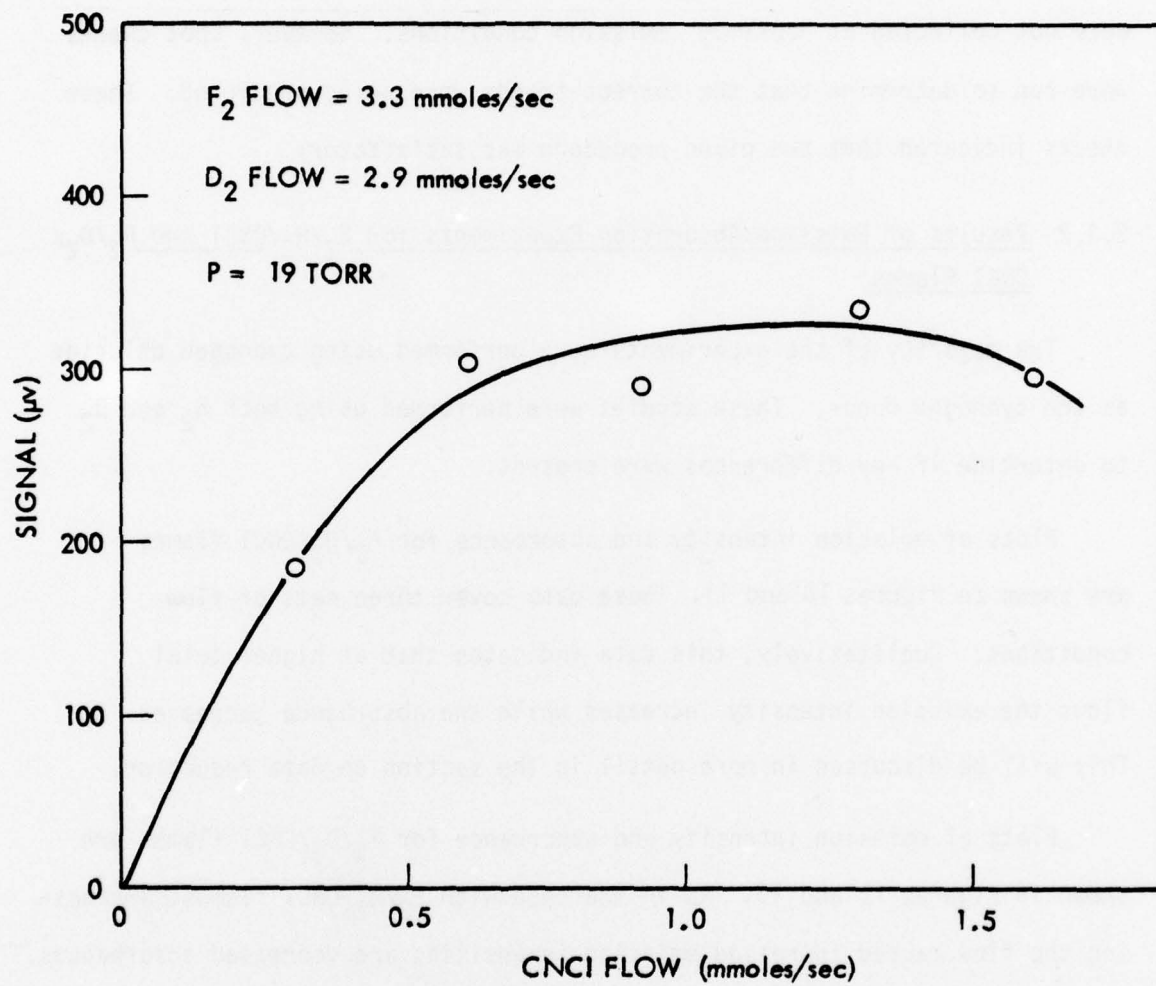


Figure 9. Plot of emission intensity versus CNCI flow with  $\text{F}_2$ ,  $\text{D}_2$  constant.

For many of the experiments performed, the  $F_2$ ,  $D_2$  and  $CNCl$  flows were optimized at a given pressure. Then data was accumulated by keeping flows constant and changing the pressure by throttling the pump. Thus, all data were not collected at "optimum" emission conditions. However, spot checks were run to determine that the correct trends were being predicted. These checks indicated that the given procedure was satisfactory.

### 2.3.2 Results of Emission/Absorption Experiments for $F_2/H_2/CNCl$ and $F_2/D_2/CNCl$ Flames

The majority of the experiments were performed using cyanogen chloride as the cyanogen donor. These studies were performed using both  $H_2$  and  $D_2$  to determine if any differences were present.

Plots of emission intensity and absorbance for  $F_2/H_2/CNCl$  flames are shown in Figures 10 and 11. These data cover three sets of flow conditions. Qualitatively, this data indicates that at higher total flows the emission intensity increases while the absorbance decreases. This will be discussed in more detail in the section on data reduction.

Plots of emission intensity and absorbance for  $F_2/D_2/CNCl$  flames are shown in Figures 12 and 13. As in the case with  $F_2/H_2/CNCl$  flames, increasing the flow caused increased emission intensities and decreased absorbances. Thus, qualitatively, it appeared that increased flows were tending to increase upper state densities while decreasing those of the lower state.

### 2.3.3 Results of Temperature Measurements

Accurate temperature data was required both to reduce the data in Section 2.3.2 to number densities in individual rotational-vibrational levels of the  $A^2\Pi$  and  $X^2\Sigma$  states of  $CN$  and also to extend this data to cover

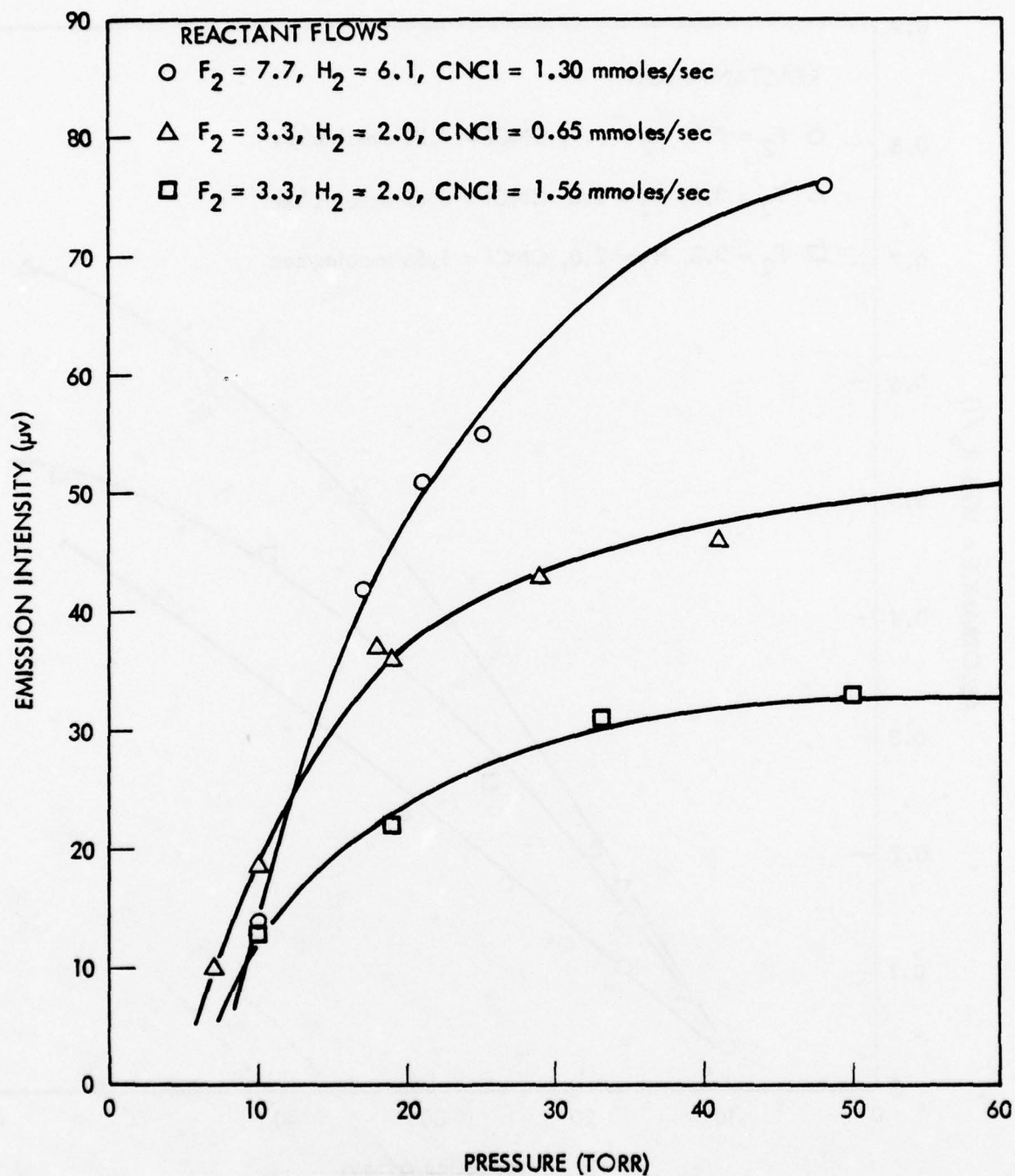


Figure 10. Plot of emission intensity as a function of pressure for several  $H_2$ ,  $F_2$ ,  $CNCl$  flow conditions.

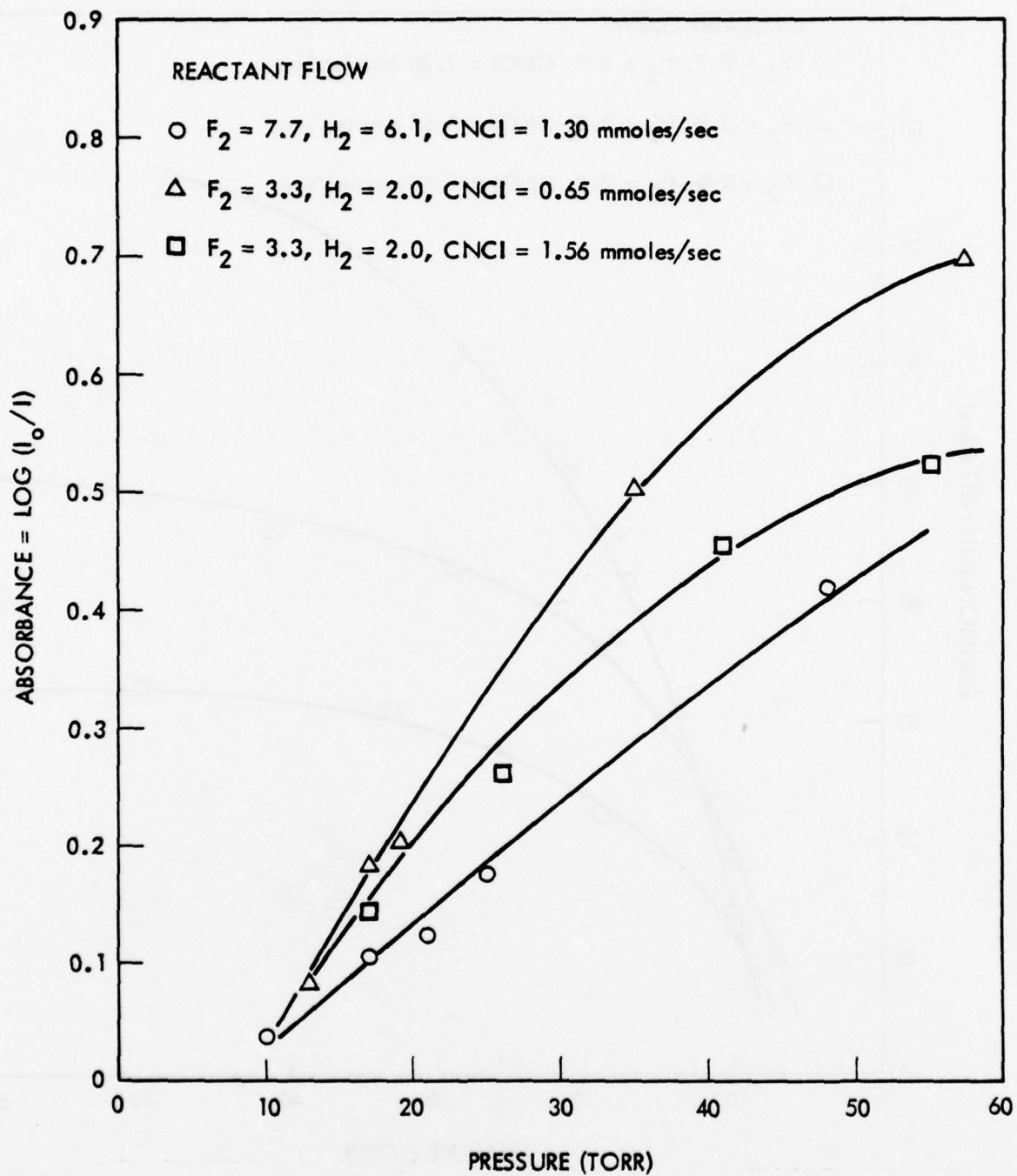


Figure 11. Plot of absorbance as function of pressure for several  $H_2$ ,  $F_2$ ,  $CNCl$  flow conditions.



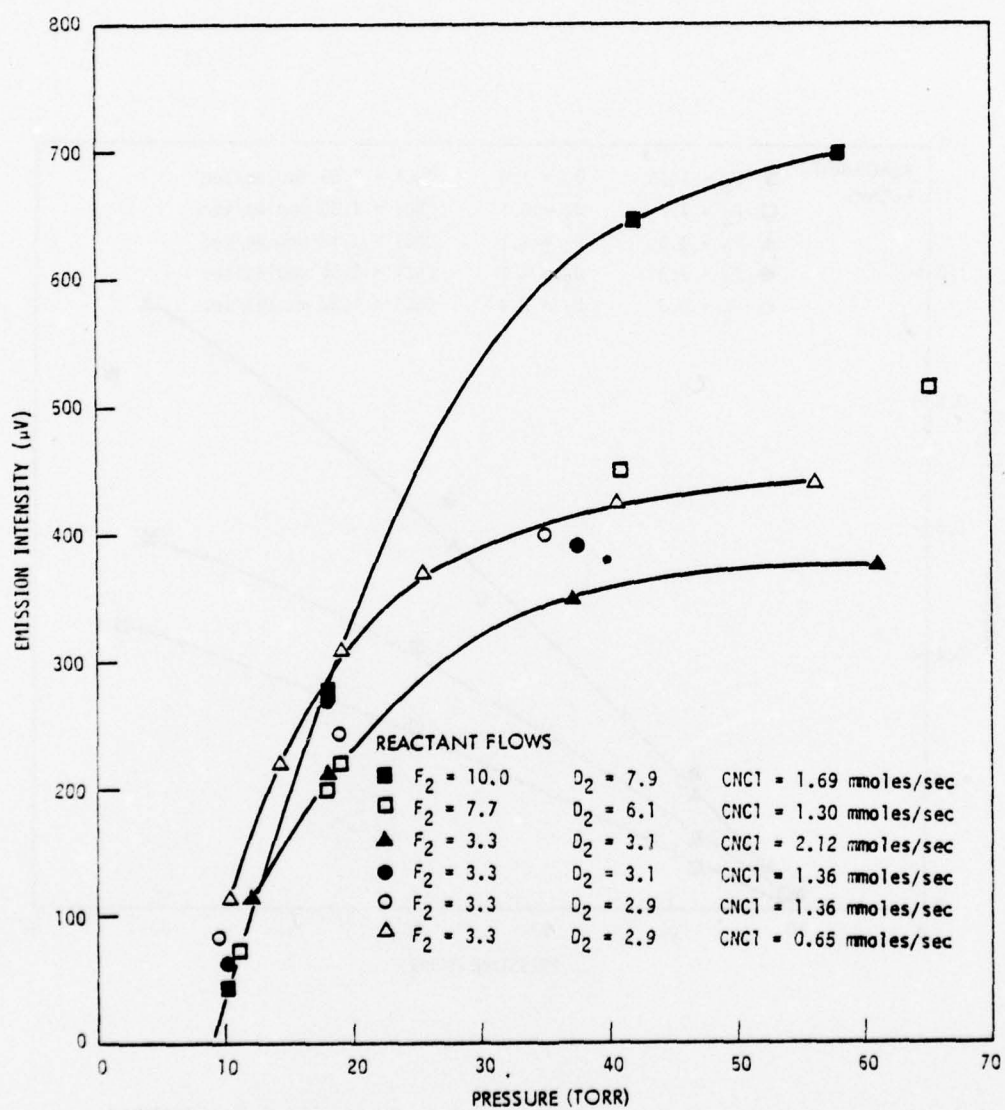


Figure 12. Plot of emission intensity as a function of pressure for several  $F_2$ ,  $D_2$ ,  $\text{CNCI}$  flow conditions.

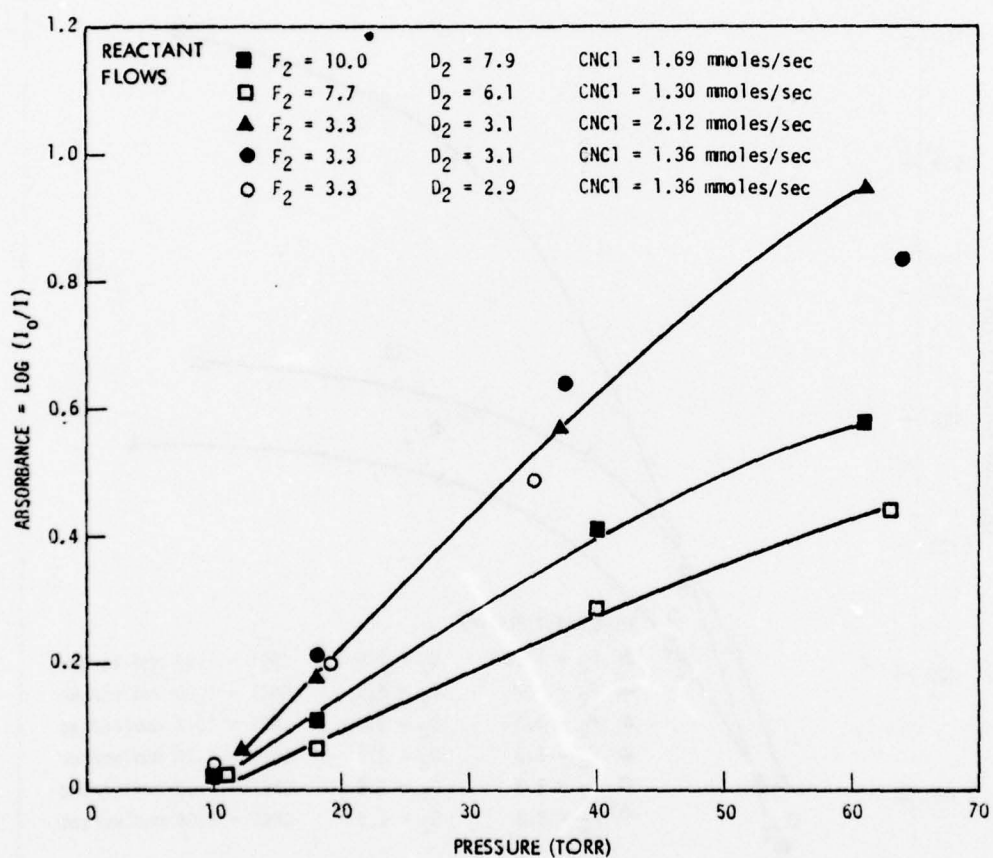


Figure 13. Plot of absorbance versus pressure for several  $F_2$ ,  $D_2$ , CNC1 flow conditions.

populations to other rotational-vibrational levels. Preliminary measurements used chemiluminescence from the R-branch of the 1-0 HF vibrational transition to determine temperature. These data are summarized in Figure 14 where plots of temperature versus pressure are shown. These data indicate that the temperature increases linearly with pressure and decreases with increased CNCl flow. A check of these temperature measurements was made making the assumption that the vibrational levels of the A state of CN were in thermal equilibrium. For this determination the relative number densities in vibronic levels of CN were plotted versus the vibrational quantum number  $v'$ . The slope of this plot was used to determine the temperature. There was a discrepancy of approximately 1000°K in temperatures determined by these two methods. It is most likely that the HF temperatures were incorrect since high concentrations of ground state HF were present in the flame that the 1-0 transition could have shown self absorption. This problem has occurred before<sup>(6)</sup> for determination of high HF temperatures.

Temperature data were next taken using high resolution spectra of DF. Simultaneously, low resolution spectra of CN covering the spectral range from 680 to 780 nm were taken to determine the vibrational temperature of CN for  $\Delta v = 3$  transitions. Typical plots of DF number density in various rotational-vibrational states versus  $J(J + 1)$  where  $J$  is the rotational quantum number are shown in Figure 15. Note that the data from the 1-0 band is very scattered and has a different slope from the data obtained using the 2-1 and 3-2 branches. This can be explained by DF self-absorption of emission from the 1-0 band. This is consistent with problems encountered in determination of temperature from HF data. The temperatures obtained from the slopes of the 3-2 and 2-1 bands were in agreement.

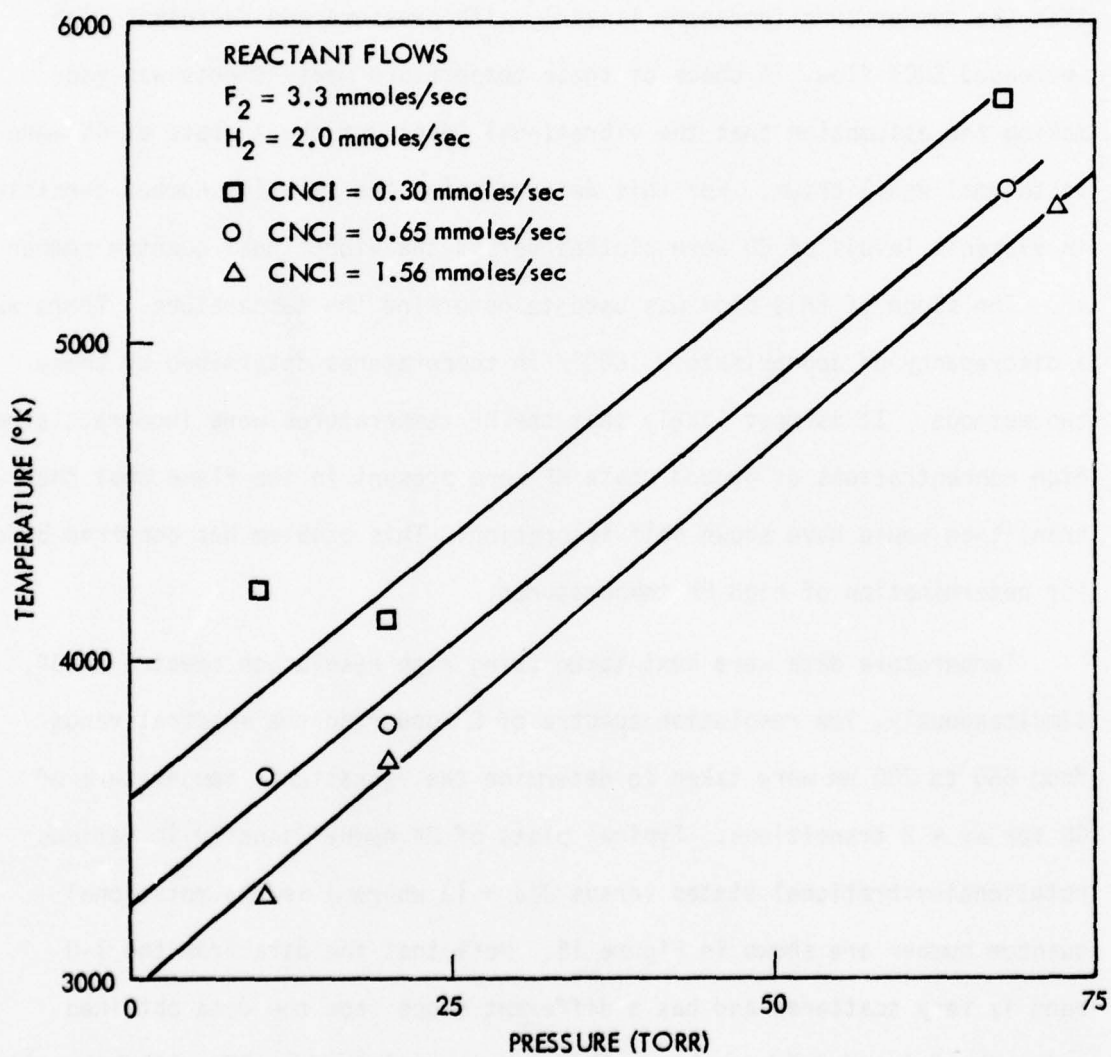


Figure 14. Plot of HF chemiluminescence temperature versus pressure in  $F_2/H_2/CNCl$  flame.



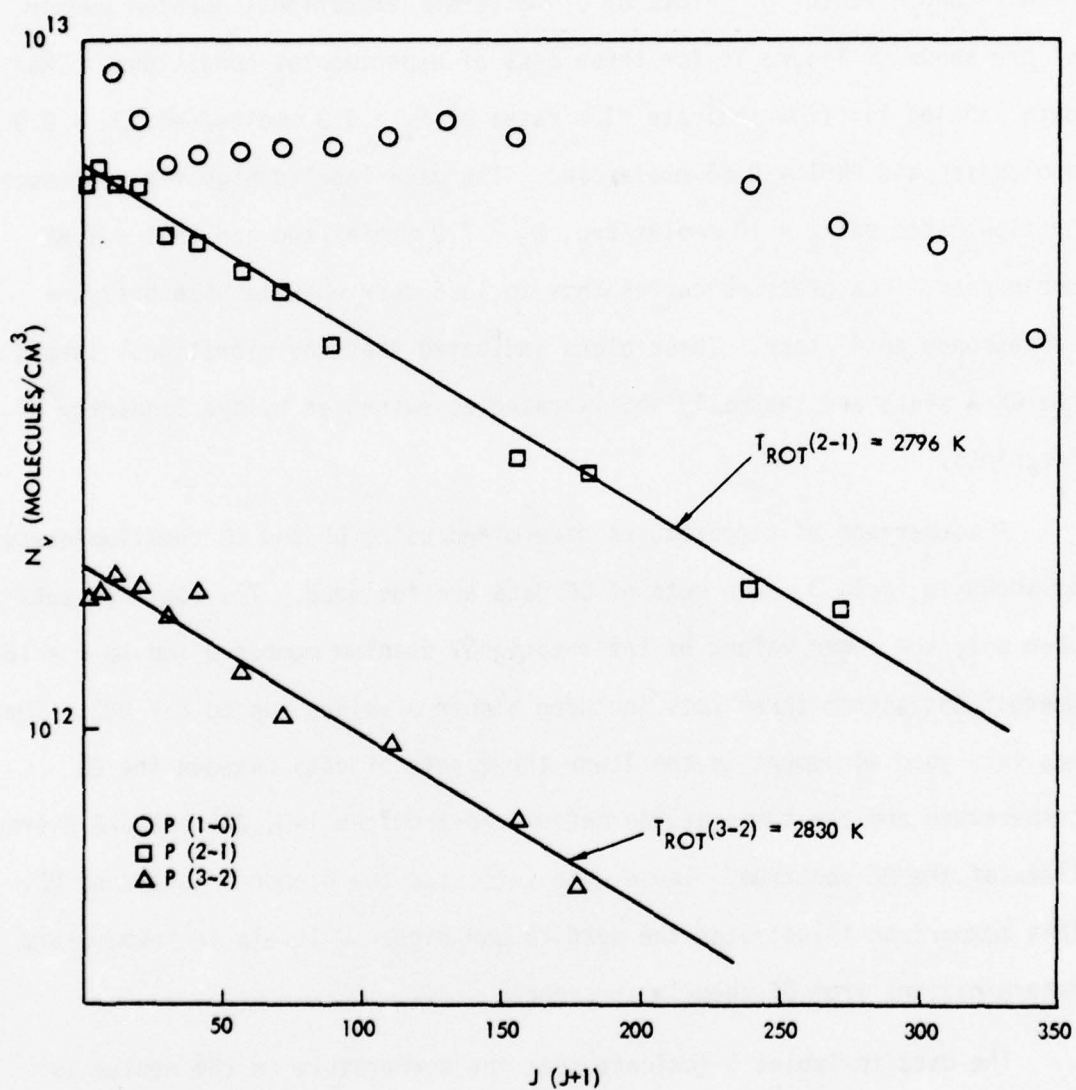


Figure 15. Plots of DF vibrational state number densities versus  $J(J + 1)$ .

The CN vibrational populations are proportional to the intensity of the transition divided by the fourth power of the frequency  $\nu$  and the Franck-Condon factor  $g$ . Plots of  $J/\nu^4 g$  versus vibrational quantum number  $\nu'$  are shown in Figure 16 for three sets of experimental conditions. The data labeled low flow indicate flow rates of  $F_2 = 3.3$  mmol/sec,  $D_2 = 2.9$  mmol/sec and  $CNCl = 0.65$  mmol/sec. The data labeled high flow corresponds to flow rates of  $F_2 = 10$  mmol/sec,  $D_2 = 7.9$  mmol/sec and  $CNCl = 1.69$  mmol/sec. Low pressure corresponds to 19.6 torr whereas high pressure corresponds to 41 torr. These plots indicated that the vibrational levels of the CN A state are thermally equilibrated as evidenced by the linearity of the plots.

A comparison of temperatures determined using DF and CN chemiluminescence is shown in Table 3. Two sets of DF data are included. The top five sets used only the lower values of the rotational quantum number  $J$  (up to  $J = 16$ ) whereas the bottom three sets included higher  $J$  values (up to  $J = 28$ ). There was very good agreement in the lower three sets of data between the CN temperature and the temperatures determined from the 1-0, 2-1 and 3-2 P-branch lines of the DF spectrum. These data sets used the higher  $J$  levels of DF. This comparison illustrates the need to use higher  $J$  levels in temperature determinations from DF chemiluminescence.

The data in Tables 3 indicate that the temperature in the medium is only a function of flow and is not a function of pressure. Thus, for a given set of flow conditions, it is necessary to determine the temperature only once. It also is sufficient to determine temperatures using only CN spectra. This observation significantly reduced the time required to obtain needed temperature data.

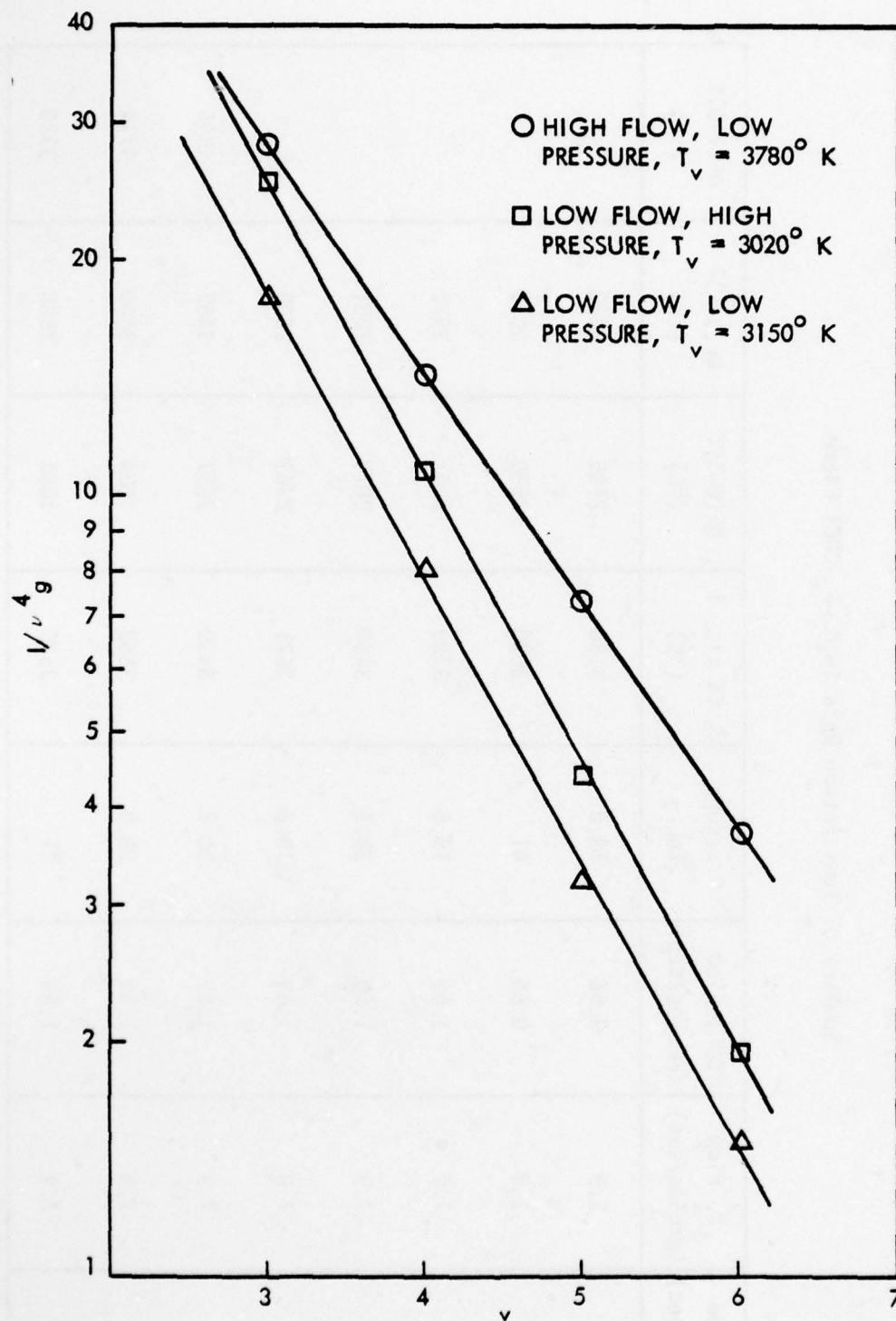


Figure 16. Plots of relative number densities in vibronic levels of CN versus  $V$  to allow determination of CN vibrational temperature.

Table 3.

Summary of Temperature Data in  $D_2$ - $F_2$ -CNC1 Flame

$F_2$ Flow (mmoles/sec)	$D_2$ Flow (mmoles/sec)	CNC1 Flow (mmoles/sec)	Pressure (torr)	CN vib. T (°K)	DF(2-1)T (°K)	DF(3-2)T (°K)	DF(1-0)T (°K)
3.2	2.9	0.65	19.6	3.50	2796	2830	*
3.2	2.9	0.65	41	3020	2630	3010	
10	7.9	1.69	19.6	3780	2851	3972	
10	7.9	1.69	30.5	3480	2879	2881	
10	7.9	1.69	19.6	3671	2761	2809	
*1							
*10	7.9	1.69	30.7	3439	3637	3462	3890
*10	7.9	1.69	20.0	3553	3584	3660	3774
*10	7.9	1.69	41	3530	3600	3688	3920

\*Data includes higher J levels.



#### 2.3.4 Spatial Intensity Distributions in $F_2/D_2/CNCl$ Flames

Some discrepancies were observed between intensity versus pressure data taken on the previous contract<sup>(6)</sup> and that taken in the current studies. Figure 17 is from the previous contract report and illustrates the dependence of emission on pressure in an  $F_2/H_2/CNCl$  flame. In this study, a relatively sharp maximum in intensity was observed at 8 to 10 torr total pressure. In most of the tests run with the present system, the intensity continued to increase as the pressure was increased. To understand this discrepancy, careful observations of the  $F_2/D_2/CNCl$  flame were made. To monitor variations in flame structure, a Polaroid camera with black and white film was focused on the chemiluminescence window in the laser cavity. The window had the dimensions of 5.7 cm long by 5 cm wide. The nozzle was 15 cm long so only a central portion of the flow field was observed. Figure 18 shows examples of photographs taken at flow conditions of  $F_2 = 7.7$  mmol/sec,  $D_2 = 6.1$  mmol/sec and  $CNCl = 1.3$  mmol/sec and pressures of 5, 10 and 15 torr. Similar photographs are shown in Figure 18 for flow conditions of  $F_2 = 3.3$  mmol/sec,  $D_2 = 3.9$  mmol/sec and  $CNCl = 0.65$  mmol/sec for pressures of 5, 10 and 15 torr. The critical information gained from these photographs is that the position of the flame in the cavity moves as the pressure in the cavity is varied, probably due to a change in gas velocity as the pumping speed is changed. This information can be combined with the fact that observations of emission intensity were made at a fixed position to explain observed discrepancies. In the current studies, observations were made close enough to the nozzle that the most intense part of the flame was probed at high pressures. The observations under the previous contract were made further downstream. This would account for the sharp rise in emission

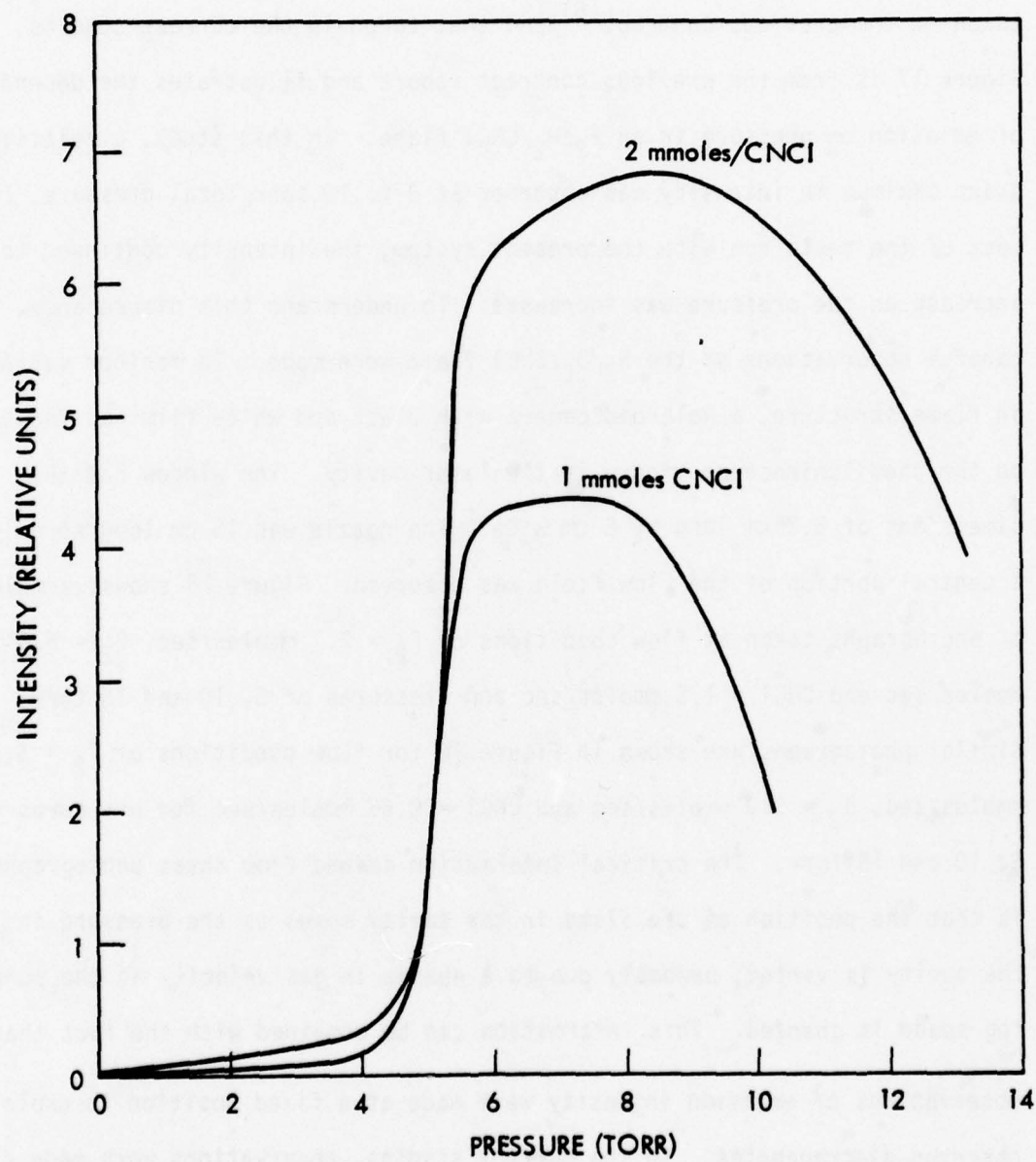
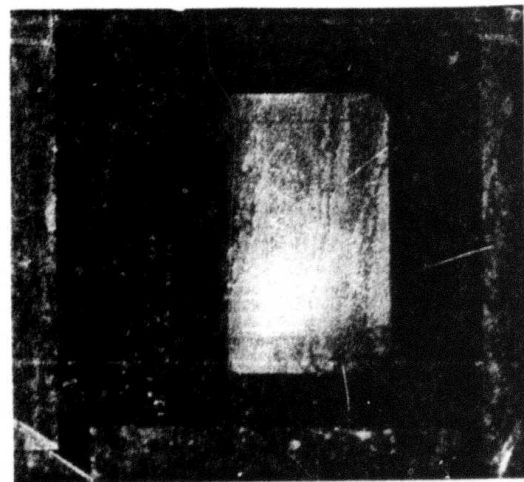
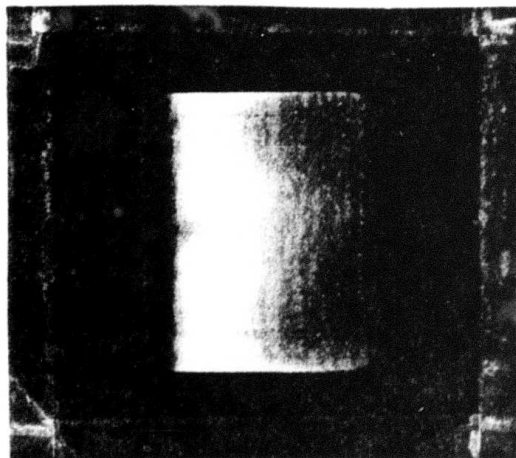


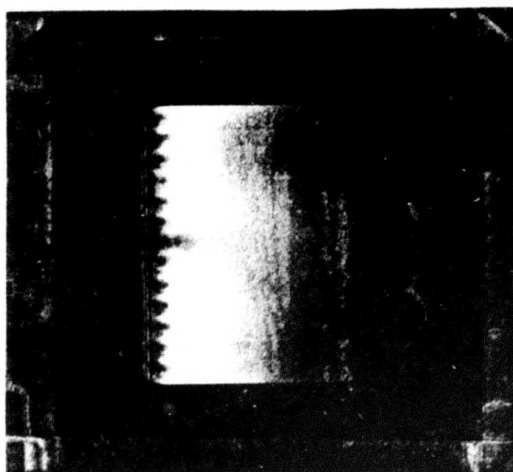
Figure 17. Plot of CN emission intensity versus cavity pressure obtained on prior contract.



P = 5 torr



P = 10 torr



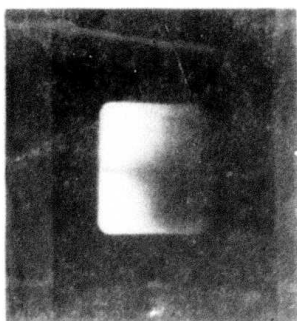
P = 15 torr

Figure 18.  $F_2$ ,  $D_2$ , CNC1 flame at several cavity pressures.  
 $F_2 = 7.7$  mmol/sec,  $D_2 = 3.9$  mmol/sec, CNC1 = 0.65 mmol/sec

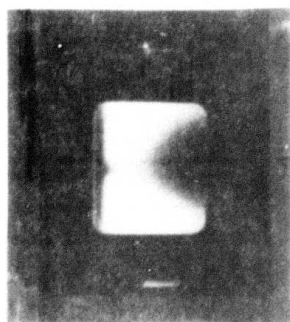
as the flame came within the viewing range of the spectrometer and the gradual drop in intensity as the flame became more compressed near the nozzle at high pressures. Thus, trends in emission intensity are very dependent on observation position. The photographs in Figure 19 show non-uniformities in the flow in both the x and y directions. This type of flow field would certainly not be likely to produce gain.

The spatial variations in intensities in the flame were studied more quantitatively by installing a mechanism which allowed the spectrometer to scan in the x (width) and y (height) directions along the side window as shown in Figure 20. For simplification, the spectrometer was set to observe the peak of the (3,0) band of the CN red system at  $6954\text{\AA}$ . Scans were first made in the horizontal direction. The vertical position was then changed and a new scan was made in the horizontal direction. Results of these scans are illustrated in Figures 21 through 23. Figure 21 corresponds to the flow condition in Figure 18 with a pressure of 10 torr. Scans over three y positions are shown in this figure. These scans illustrate that the intensity is low near the nozzle, increases towards a maximum at  $y = 2\text{ cm}$  and decreases again near the bottom of the cavity. Note there are some variations in intensity along the x-axis although the sharp drop at  $x = 5.6\text{ cm}$  is probably due to the limited field of view of the spectrometer near the edge of the cavity. These variations certainly imply uneven number densities of CN excited states across the cavity. The data in Figures 20 and 21 correspond to flows of  $F_2 = 3.3\text{ mmol}/\text{sec}$ ,  $D_2 = 3.9\text{ mmol}/\text{sec}$  and  $\text{CNCI} = 0.65\text{ mmol}/\text{sec}$  at pressure of 5 and 10 torr respectively. For the 5 torr case in Figure 22, the intensity is seen to gradually increase as y is increased to approximately 0.8 inches. Beyond this point the flame became unstable until y became equal to 1.6 inches where a stable region of intensity was

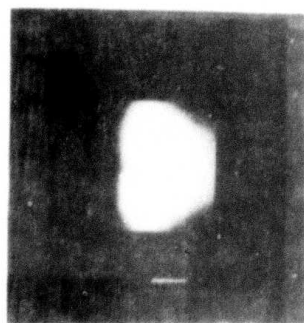




15 torr



10 torr



5 torr

Figure 19.  $F_2$ ,  $D_2$ ,  $CnCl$  flames at several pressures.  
 $F_2 = 3.3$  mmol/sec,  $D_2 = 3.9$  mmol/sec,  $CnCl = 0.65$  mmol/sec

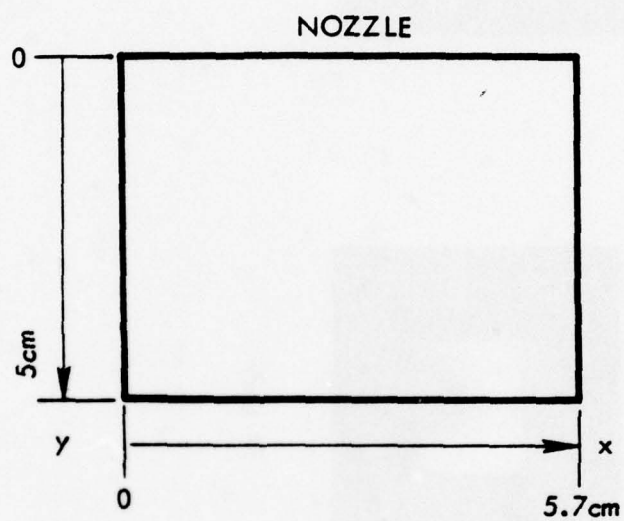


Figure 20. Chemiluminescence side window showing directions of intensity versus distance scans.

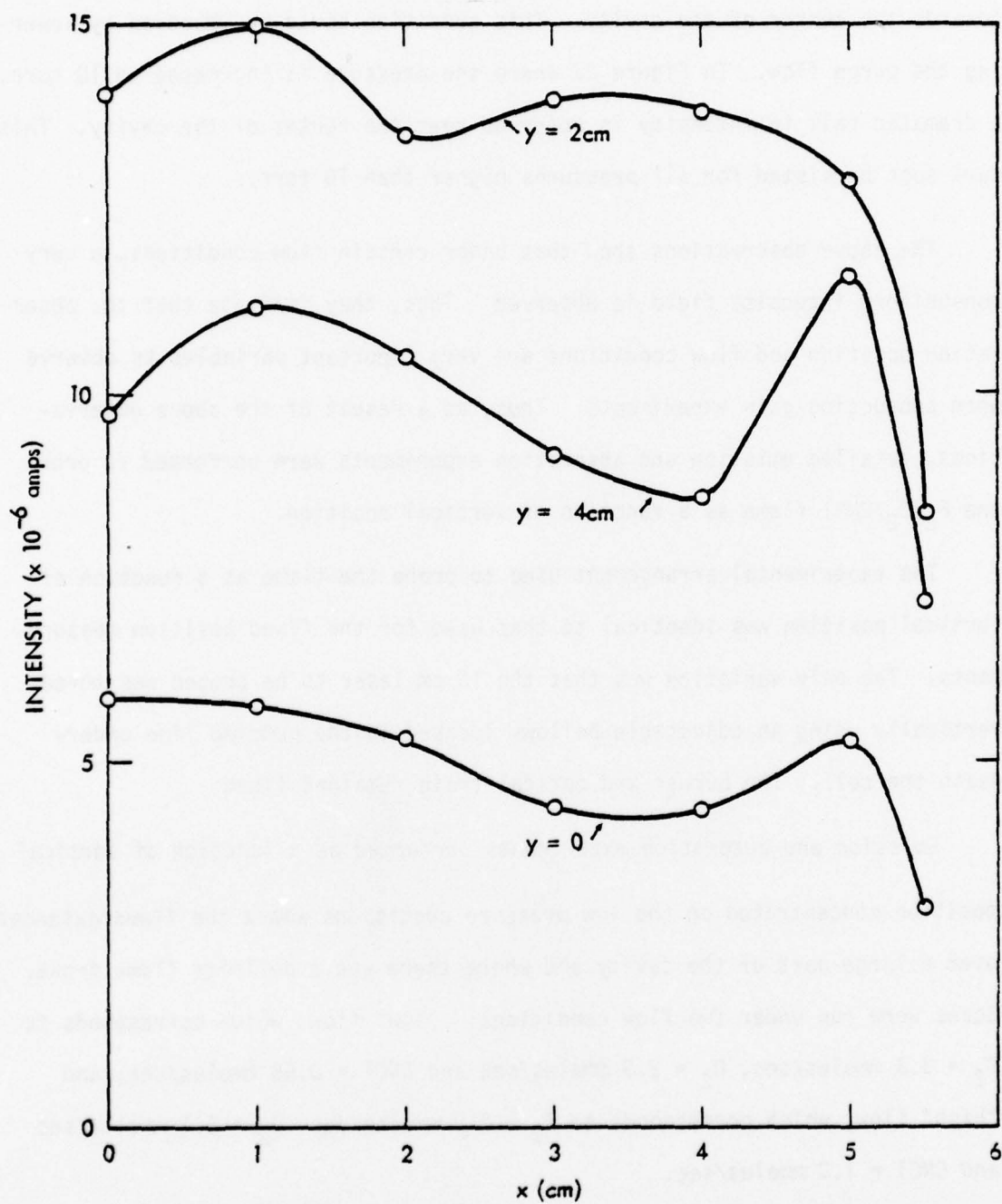


Figure 21. Scan of intensity versus position of the  $D_2$ ,  $F_2$ ,  $CNCl$  flame. High flow with pressure = 10 torr.

again observed. The fall in intensity at the edges is real in this case. Some of it could be attributed to the nitrogen window purge pushing the flame towards the center of the cavity. This condition could be improved by lowering the purge flow. In Figure 23 where the pressure is increased to 10 torr, a dramatic fall in intensity is observed near the center of the cavity. This dark spot persisted for all pressures higher than 10 torr.

The above observations show that under certain flow conditions, a very non-uniform intensity field is observed. Thus, they indicate that the observation position and flow conditions are very important variables to observe when conducting gain experiments. Thus, as a result of the above observations, detailed emission and absorption experiments were performed to probe the  $F_2/D_2/CNCl$  flame as a function of vertical position.

The experimental arrangement used to probe the flame as a function of vertical position was identical to that used for the fixed position measurements. The only variation was that the 15 cm laser to be probed was moved vertically using an adjustable bellows located in the pumping line underneath the cell. The burner and optical train remained fixed.

Emission and absorption experiments performed as a function of vertical position concentrated on the low pressure conditions where the flame extended over a large part of the cavity and where there was a definite flame front. Scans were run under two flow conditions: "low" flow, which corresponds to  $F_2 = 3.3$  mmol/sec,  $D_2 = 2.9$  mmol/sec and  $CNCl = 0.65$  mmol/sec; and "high" flow, which corresponds to  $F_2 = 7.0$  mmol/sec,  $D_2 = 6.1$  mmol/sec and  $CNCl = 1.3$  mmol/sec.

Figure 24 shows plots of emission and absorbance versus vertical dis-



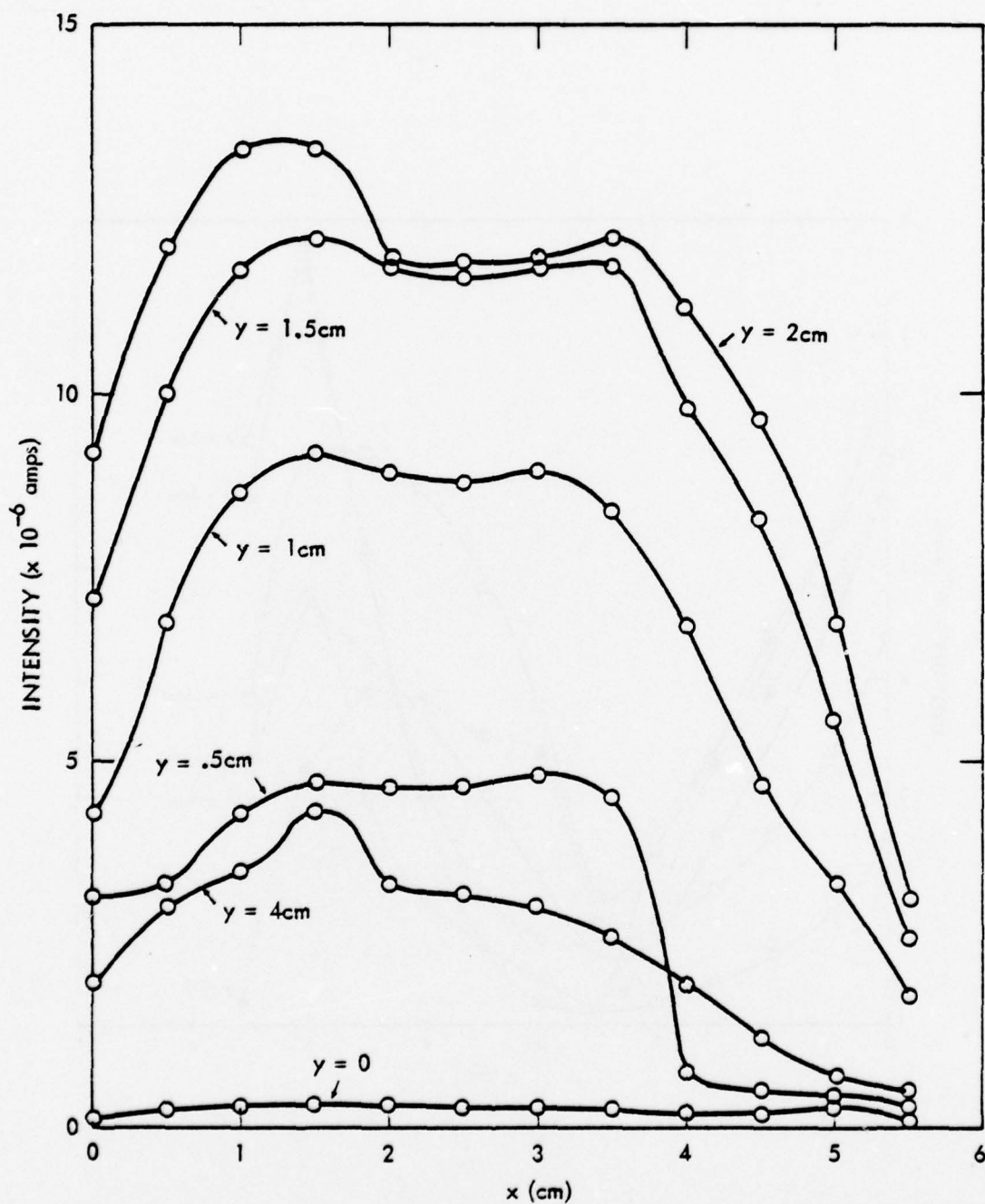


Figure 22. Scan of intensity versus position of the  $D_2$ ,  $F_2$ ,  $CNCl$  flame. Low flow with pressure = 5 torr.

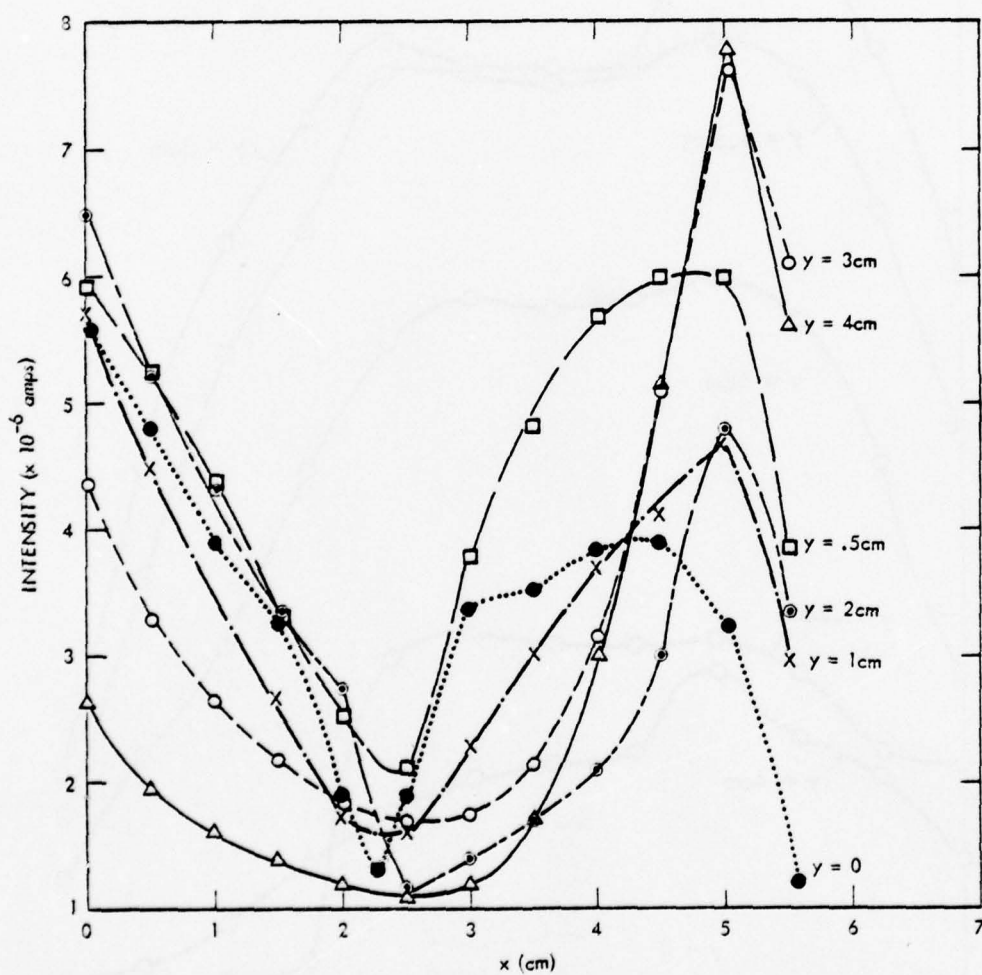


Figure 23. Scan of intensity versus position of the  $D_2, F_2, CNCl$  flame. Low flow with pressure = 10 torr.

tance for the "high" flow condition. Four pressure conditions are included on this plot. Figures 25 and 26 show plots of emission and absorbance versus vertical distance for the "low" flow condition at 5 and 10 torr respectively. For this flow condition, the effect of changing the purge flow on the emission and absorbance was studied. This was motivated by the data in Figures 22 and 23 which shows a drop in intensity near the edges of the window. This indicated that the purge tends to drive the flame inward. The data in Figure 25 illustrate that there is more emission at low purge flows. However, as the pressure is increased as in Figure 26, the purge tends to have less effect. Conversion of this data to number densities will be discussed in Section 2.3.7.

#### 2.3.5 Effects of Total Pressure

The data in Figures 25 and 26 showed the effects of purge flow on emission and absorbance. During the course of obtaining this data it was observed that the total pressure in the cavity was critical in determining emission intensities. For example, if flows and pumping speed were held constant and window purge gas flow increased with no additional pressure adjustment, the intensity increased dramatically. However, if the pressure was then readjusted to its initial value the intensity dropped back near its original level. This effect could be achieved only through addition of purge which did not affect the actual flame. When diluent (He) was added with the fluorine, a dramatic drop in intensity of A state emission was observed as soon as any diluent was added. Temperature determinations showed a corresponding drop in temperature.

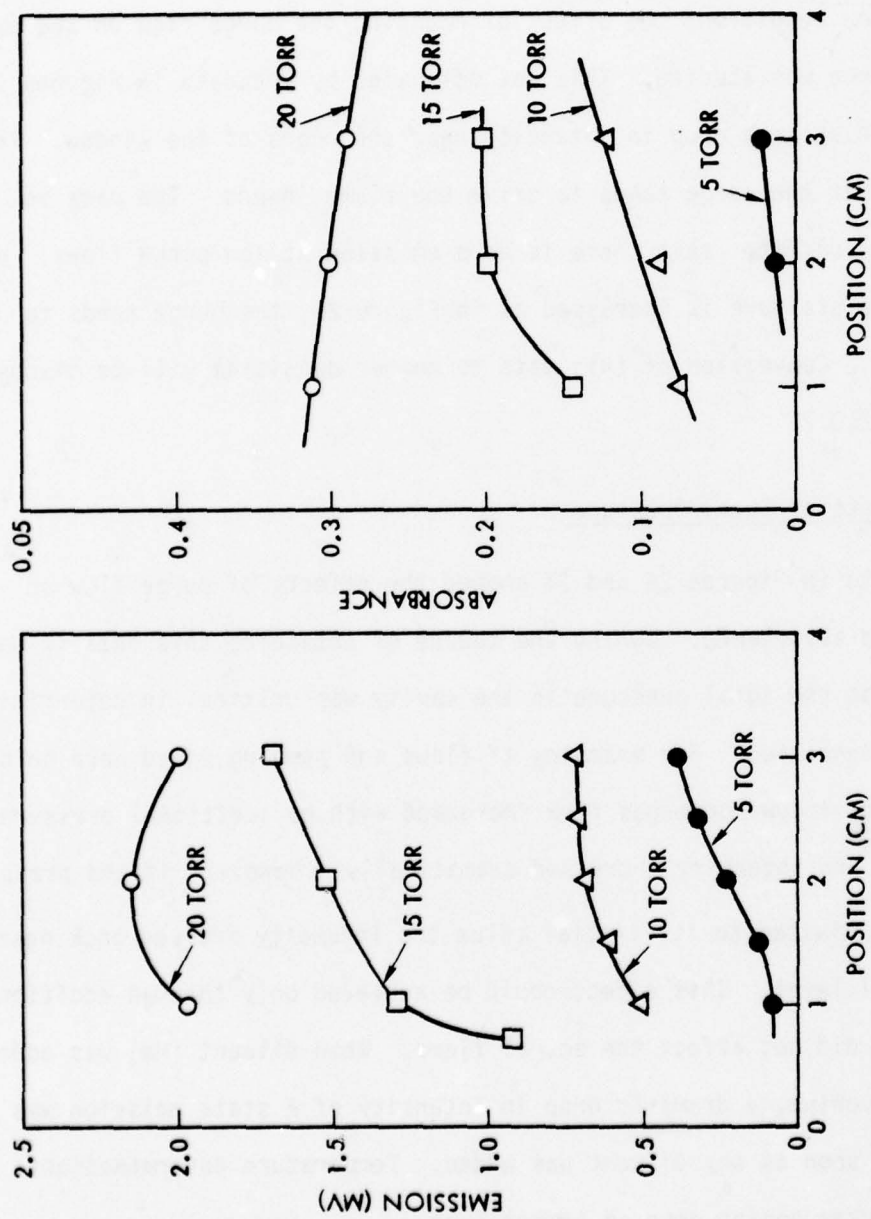


Figure 24. Plots of emission and absorbance versus distance from the nozzle for high flows and several cavity pressures.



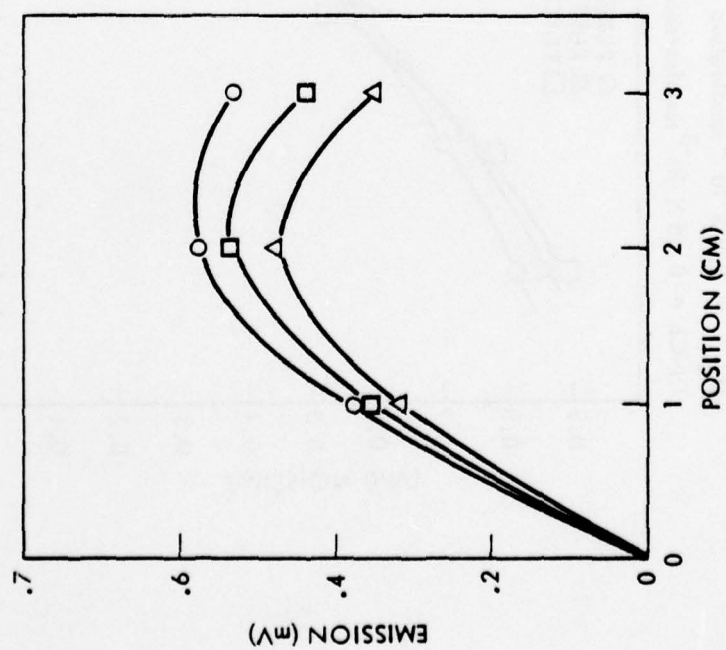
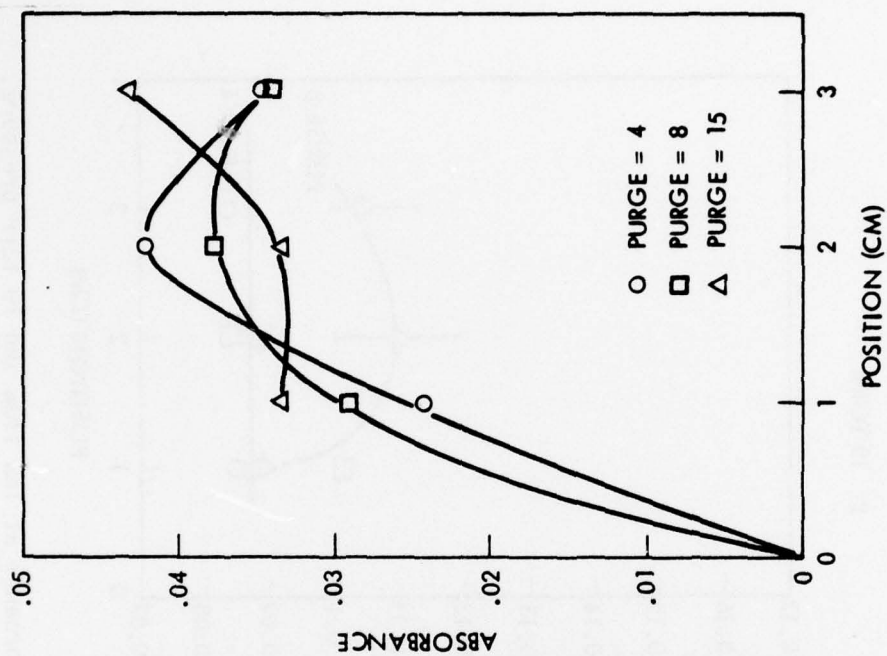


Figure 25. Plots of emission and absorbance versus distance from the nozzle for low flow at 5 torr.

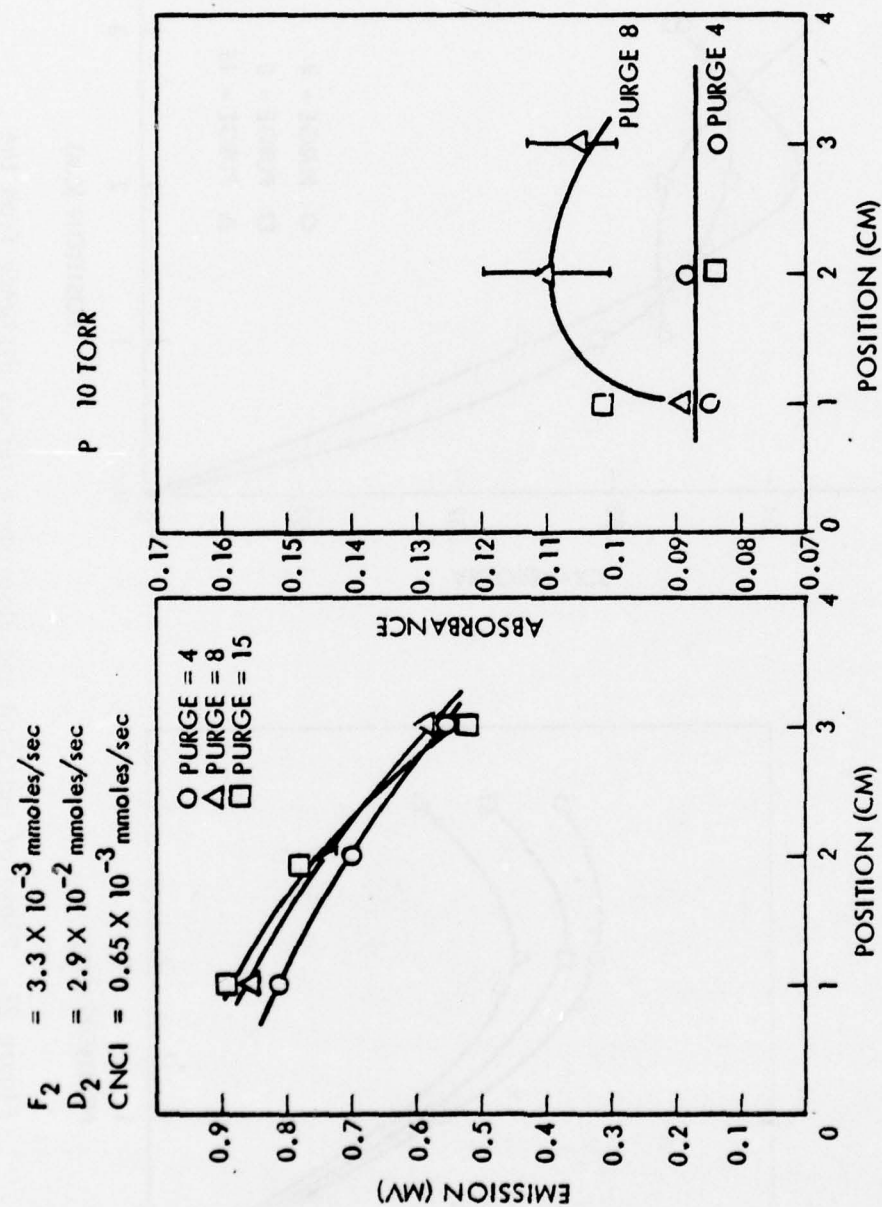


Figure 26. Plot of emission and absorbance at low flow and 10 torr pressure.

### 2.3.6 Visible Spectroscopy

Detailed visible spectra were taken to aid in understanding of the processes involved in the excitation of the CN to its A state. A log plot of the visible spectrum from 300 to 900 nm for two conditions is shown in Figure 27. These spectra were taken for flows of  $F_2 = 3.3$  mmol/sec,  $D_2 = 2.9$  mmol/sec and  $CNCl = 0.65$  mmol/sec and pressures of 20 and 60 torr. The main features are CN ( $B^2_{\Sigma} \rightarrow X^2_{\Sigma}$ ) violet bands,  $C_2$  ( $A^3_{\Pi_g} \rightarrow X^3_{\Pi_u}$ ) Swan bands, and CN ( $A^2_{\Pi} \rightarrow X^2_{\Sigma}$ ) red bands. This spectrum was taken using the 0.3 m spectrometer with a 1200 line/mm grating blazed at 5000Å. An RCA C31034A photomultiplier was used as a detector. In the figure, no correction is made for the spectral response of the detector system. The major difference in the two scans appears to be that a continuum is present under the other features at higher pressures. Also, the intensity of the  $C_2$  Swan bands relative to the other features in the spectrum has increased. This is in agreement with the fact that the flame appeared white at the higher pressure.

Calibrated intensities were used to compare the integrated intensities in the (2,0) band of the CN red system with the (0,0) band of the CN blue system. These intensities were converted to values proportional to total densities in the  $v' = 2$  level of the CN red band and the  $v' = 0$  level of the CN blue band by dividing by appropriate Franck-Condon factors. This comparison gives the ratio  $CN(B^2_{\Sigma}, v' = 0)/CN(A^2_{\Pi}, v' = 2)$  equal to  $4.5 \times 10^{-4}$ . The temperature of the medium for this run was  $3000 \pm 200^\circ K$ . The experimental value of B to A emission corresponds to a temperature of  $2400^\circ K$  if the B and A states were in thermal equilibrium. This does not provide conclusive proof of whether the excitations in the flame are caused by purely thermal processes. Further discussion of this will be given in Section 2.4.

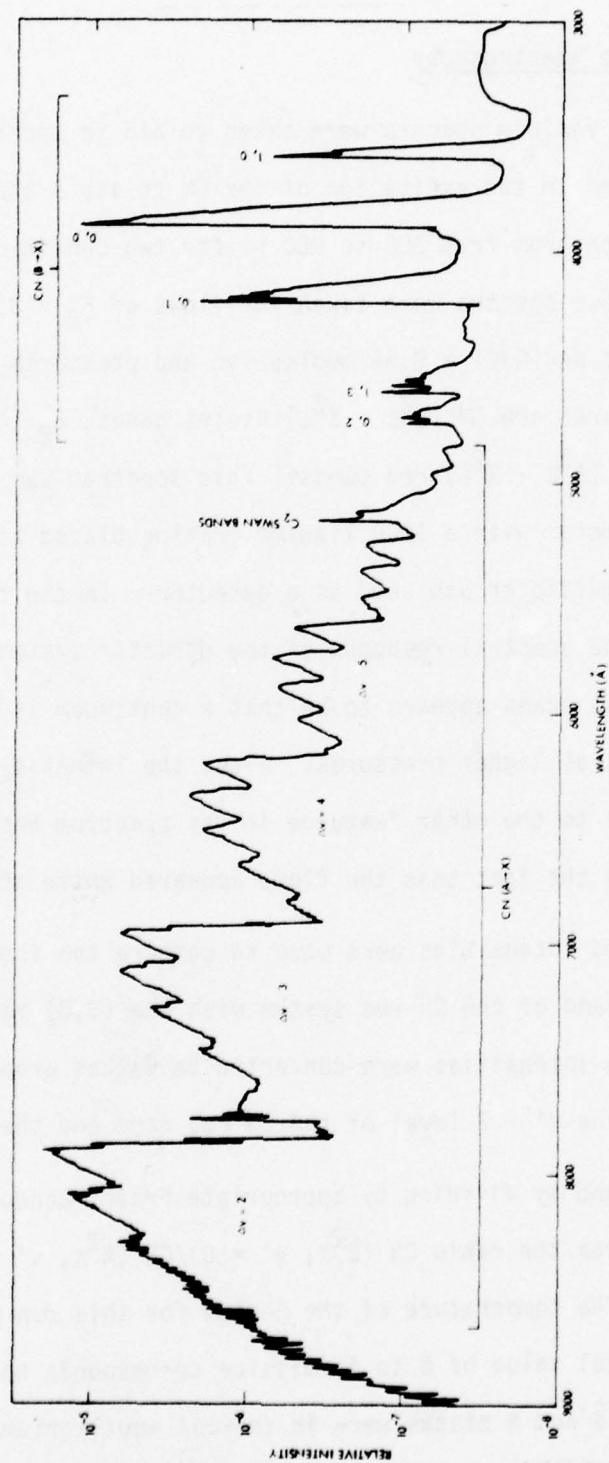


Figure 27. Spectrum of  $F_2/D_2/CNCl$  flame from 300 to 800 nm.



### 2.3.7 Data Reduction

The data presented in the earlier sections gave emissions in terms of volts and absorbances. In order to be meaningful, these numbers must be reduced to number densities. In the analysis that follows, the assumption is made that the source and absorbing medium are both Doppler broadened.

From Mitchell and Zemansky,<sup>(7)</sup> the expression for absorption of an isolated Doppler broadened rotational line by a medium that is also Doppler broadened and contains the same species is

$$A = \frac{k_0 \ell}{(1 + \alpha^2)^{1/2}} \quad (6)$$

where  $\ell$  is the pathlength,  $\alpha$  is the ratio of Doppler widths in the source and absorbing CN and  $k_0$  is the absorption coefficient. Mitchell and Zemansky also define the absorption coefficient as

$$k_0 = \frac{2}{\Delta v_D} \sqrt{\frac{\ln 2}{\pi}} \frac{\pi e^2}{mc} \cdot N_{v''j''} \cdot f \quad (7)$$

where  $\Delta v_D$  is the Doppler width in  $\text{sec}^{-1}$ ,  $N_{v''j''}$  is the number density in the lower vibration-rotation level and  $f$  is the appropriate f-number. From Schadee,<sup>(8)</sup> the f-number for transitions between two rotational levels in the X and A states of CN is

$$f_{j'j''} = \frac{\lambda_{v'v''}}{\lambda_{j'j''}} f_{e1} \frac{q_{v'v''} S_j}{2j'' + 1} \quad (8)$$

where  $\lambda_{v'v''}$  and  $\lambda_{j'j''}$  are wavelengths of the bandhead and absorption line, respectively,  $f_{e1}$  is the electronic f-number which is tabulated for CN,<sup>(8)</sup>  $q_{v'v''}$  is the Franck-Condon factor and  $S_j$  is the rotational line strength. Combining equations (7) and (8) gives

$$k_0 = \frac{2}{\Delta v_D} \sqrt{\frac{\ln 2}{\pi}} \frac{\pi e^2}{mc} N_{v''J''} \frac{\lambda_{v'v''}}{\lambda_{J'J''}} \cdot f_{el} \cdot \frac{q_{v'v''} S_J}{2J'' + 1} \quad (9)$$

Number densities in the lower state can then be calculated by combining equations (6) and (9).

For emission, the number densities in the upper  $v'$ ,  $J'$  level can be calculated from equation (3) using the appropriate Einstein coefficient. Using the expressions of Schadee for the Einstein coefficient,  $A_{J'J''}$ , the number density of the upper level can be expressed as

$$N_{v'J'} = I_{em} \left( \frac{m}{8\pi^2 h e^2} \right) \left( \frac{\lambda_{J'J''}^4}{\lambda_{v'v''}} \right) \frac{2(2J' + 1)}{q_{v'v''} \cdot f_{el} \cdot S_J} \quad (10)$$

where  $I_{em}$  is the emission intensity in units of ergs/sec  $\text{cm}^3$ .

In evaluating the above expressions, care was required in using the correct expression for the Hönl-London (HL) factor  $S_J$ . The expressions given by Schadee assumed that

$$\sum_{J''} \sum_{J'} S_J = (2S + 1)(2J' + 1) = 2(2J' + 1) \quad (11)$$

The expressions for the HL-factors for a  ${}^2_{\Pi} - {}^2_{\Sigma}$  transition are given by Earls<sup>(9)</sup>. However, when his HL-factors are summed over all transitions from or to a given rotational level the sum is  $(2J' + 1)/2$ . Thus, the HL-factors of Earls had to be multiplied by a factor of 4 to be applicable in the above expressions.

Numerical values were applied to the above expressions. For absorption, the number density is slightly dependent on temperature. For a temperature of 2900°K, the expression for the number density in the lower level is

$$N''_{0,24} = 2.72 \times 10^{12} \text{A} \quad (12)$$

while for a temperature of 3600°K

$$N''_{0,24} = 2.84 \times 10^{12} \text{A} \quad (13)$$

For emission, data was taken at two different slit widths: The  $F_2/H_2/CNCl$  data being taken with 60 $\mu$  slits and the  $F_2/D_2/CNCl$  data being taken with 100 $\mu$  slits. Calibrations were compared to insure that the data taken with the two slit widths was compatible. For 60 $\mu$  slits

$$N'_{0,24} = 1.05 \times 10^9 \cdot S(\mu v) \quad (14)$$

while for 100 $\mu$  slits

$$N'_{0,24} = 1.48 \times 10^8 \cdot S(\mu v) \quad (15)$$

where  $S(\mu v)$  is the emission signal in  $\mu v$  and the number densities have units of molecules/cm<sup>3</sup>.

The data reported in earlier sections was reduced using the above formulas. Figure 28 shows the number densities of CN in the  $v' = 0, J' = 24$  and  $v'' = 0, J'' = 24$  levels of the  $A^2\Pi$  state for  $F_2/H_2/CNCl$  data presented in Figures 10 and 11. Figure 29 shows the same number densities for the  $F_2/D_2/CNCl$  data presented in Figures 12 and 13. It should be noted that number densities are very similar, regardless of whether  $H_2$  or  $D_2$  is present in the flame. Figures 30 and 31 show the results of number densities versus vertical position in the flame for the  $F_2/D_2/CNCl$  system. This corresponds to the data presented in Figures 21 through 23. In all these figures the densities in the X state are given by the top set of curves and the densities in the A state are given by the lower set of curves. In all instances, the

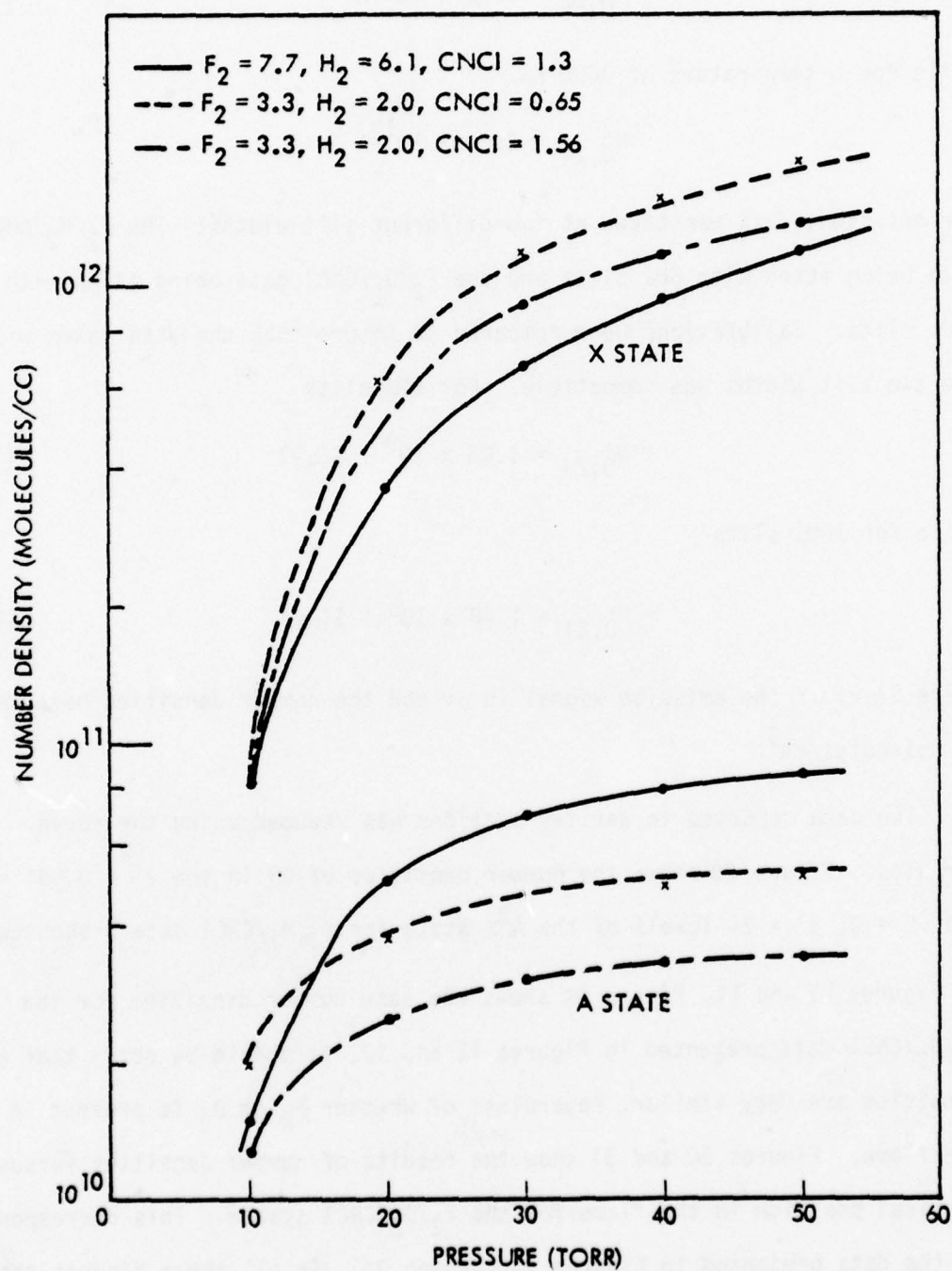


Figure 28. Number densities of CN A and X states in  $F_2/H_2/CNCl$  flames - reduction of data in figures 9 and 10.



lower state density in the  $v'' = 0, J'' = 24$  state exceeds the upper state density in the  $v' = 0, J' = 24$  state by the order of a factor of 10.

#### 2.3.8 CN-Donors Other Than CNCI

The initial program plan included the study of HCN and  $\text{CF}_3\text{CN}$  as CN-donors along with CNCI. With this in mind, HCN was purchased from Fumico and  $\text{CF}_3\text{CN}$  was purchased from PCR, Incorporated.

Difficulties were encountered with HCN because of its relatively low vapor pressure. As HCN was drawn off, the remainder of the HCN liquid in the tank cooled, causing the pressure to drop. Thus, run times were too short to allow quantitative collection of data. Qualitatively, it appeared that emission intensities of the CN band comparable to those obtained with CNCI could be obtained with very low flows of HCN. The flame also appeared very stable and uniform. An attempt was made to warm the HCN bottle but with little success. There were warnings of explosion changes due to rapid polymerization if the HCN cylinder were heated above approximately  $50^\circ\text{C}$ . Thus, only limited testing was conducted with HCN with no conclusive results.

When  $\text{CF}_3\text{CN}$  was added to the  $\text{F}_2, \text{H}_2$  flame, very intense chemiluminescence was obtained. The flame appeared white near the nozzle and became pink toward the end of the viewing region. A spectral scan of this flame showed that the CN blue band intensities were much more intense than in CNCI,  $\text{H}_2$ ,  $\text{F}_2$  flames. In fact, the (0,0) band of CN ( $B^2_\Sigma - X^2_\Sigma$ ) emission was the most intense feature in the spectrum. The intensity of the  $\text{C}_2$  Swan bands was also considerably enhanced compared with the CNCI flames. This indicated that some chemistry was taking place in the system, some of which involved the  $\text{CF}_3$  radical. From the visible portion of the CN spectrum the CN vibrational

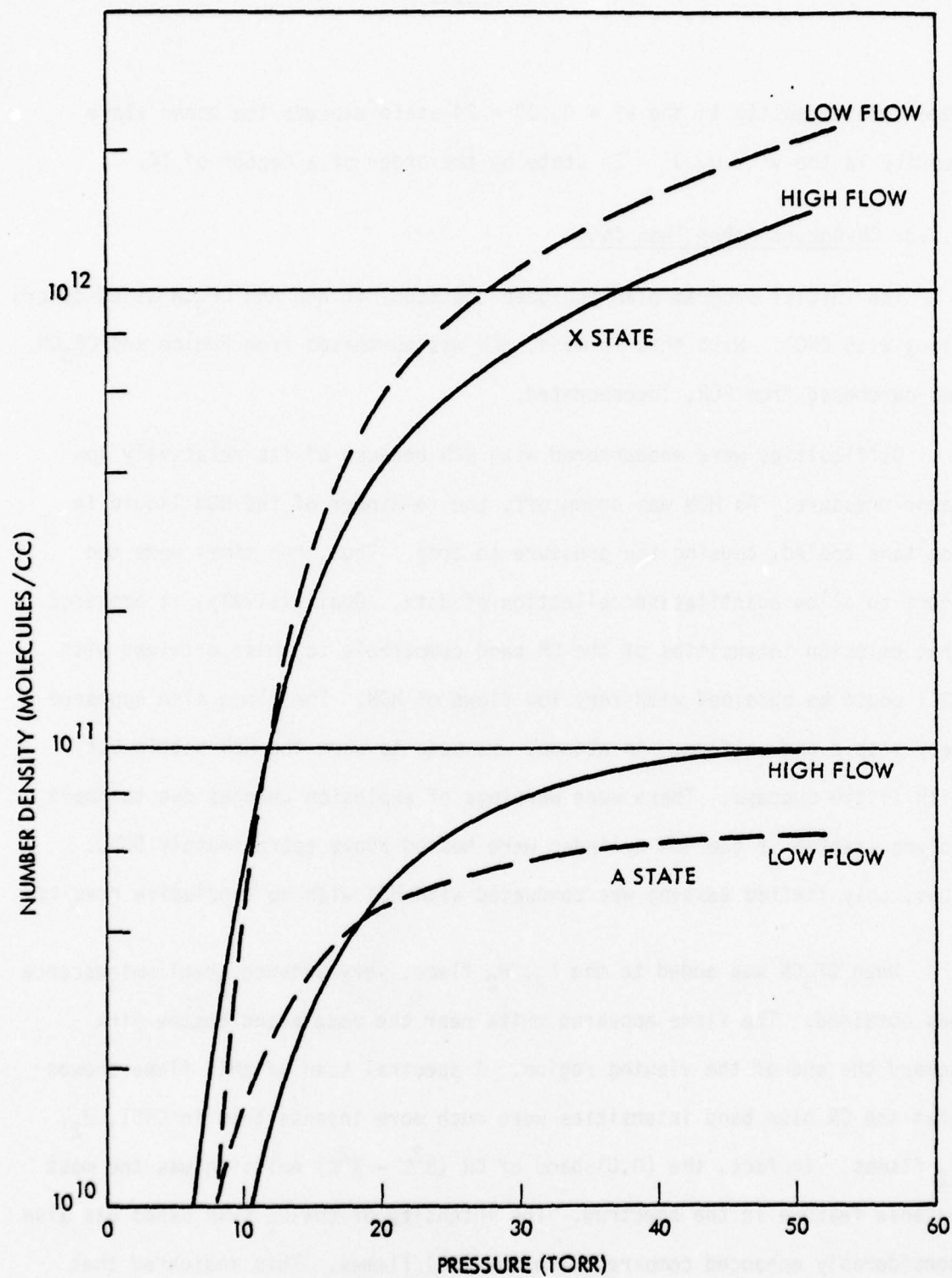


Figure 29. Reduced data for  $F_2/D_2/CNCl$  flows. Raw data is shown in figures 11 and 12.

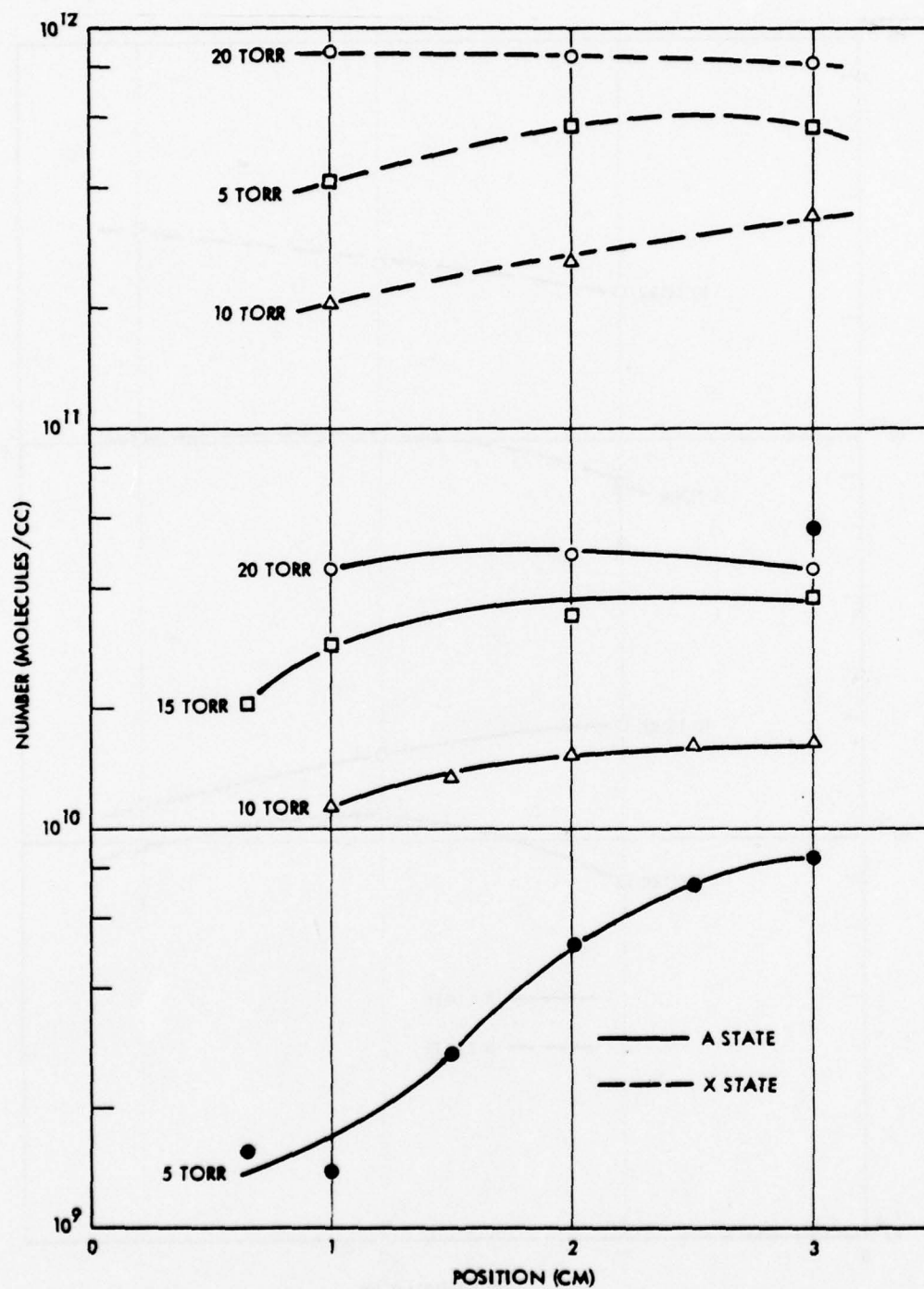


Figure 30. Number densities versus position for  $F_2 = 7.7$ ,  $D_2 = 6.1$  and  $CNCl = 1.3$  mmol/sec. Data is shown in figure 19.

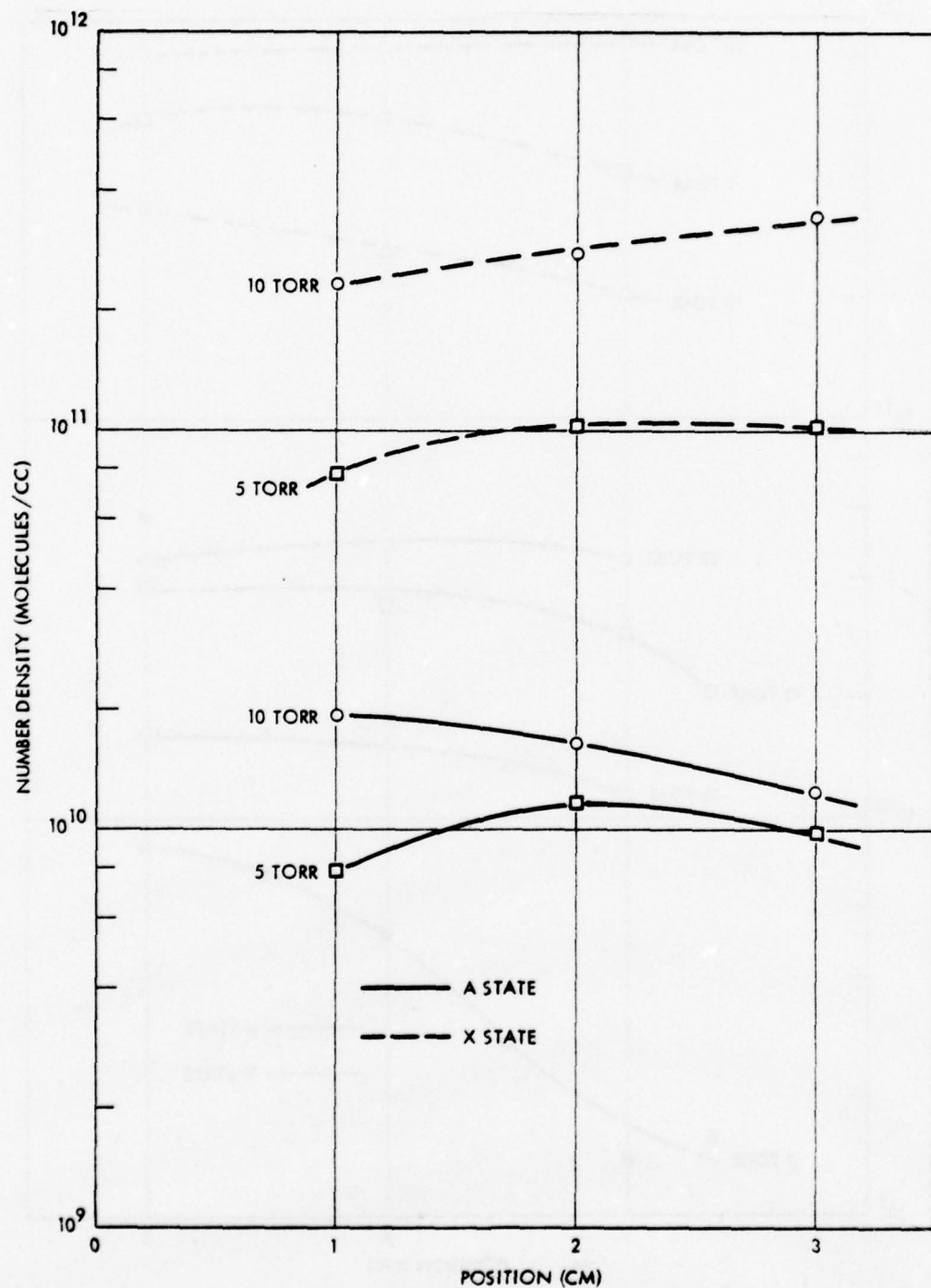


Figure 31. Number densities versus position for  $F_2 = 1.7$ ,  $D_2 = 6.0$  and  $CNC1 = 1.3$  mmol/sec. Data is shown in figures 20 and 21.



levels appeared to be in thermal equilibrium with a vibrational temperature of 2800°K. Since this temperature is comparable to that in flames with CNCl, the white emission could not be attributed to a higher temperature. Flow rates were  $F_2 = 4.6$  mmoles/sec,  $D_2 = 3.3$  mmoles/sec and  $CF_3CN = 0.7$  mmoles/sec.

## 2.4 DISCUSSION

The objective of the current program was to evaluate chemical pumping of the  $A^2\Pi$  state of the CN molecule for potential as a chemical laser system. The present discussion of the data obtained will therefore stress the laser aspects of the CN-system.

The most important parameter to consider in evaluating a laser system is gain. For a diatomic molecule, the gain  $G$  is

$$G = \left( \frac{\ln 2}{\pi} \right)^{1/2} \frac{g'A}{4\pi} \frac{\lambda^2}{\Delta\nu_D} \left( \frac{N'_{v'J'}}{g'} - \frac{N''_{v''J''}}{g''} \right) \quad (16)$$

For the CN  $A^2\Pi$  state,  $g' = 4(2J' + 1)$  while for the CN  $X^2\Pi$  state,  $g'' = 2(2J'' + 1)$ . If a Q-branch transition is considered with  $J' = J''$ , equation (15) can be simplified to

$$G = \left( \frac{\ln 2}{\pi} \right)^{1/2} \frac{A}{4\pi} \frac{\lambda^2}{\Delta\nu_D} \left( N'_{v'J'} - 2N''_{v''J''} \right) \quad (17)$$

where  $A$  is the Einstein coefficient for the desired transition. Number densities for  $N'_{0,24}$  and  $N''_{0,24}$  were shown in Figures 28 - 31 for several conditions. These data, combined with equation (16), show that there is no gain in the (0,0) transition of the  $A^2\Pi - X^2\Pi$  CN transition. It is useful to extrapolate this data to the  $v'' = 1$  and  $v'' = 2$  levels of the  $X^2\Pi$  state.

If thermal equilibrium is assumed

$$N''_{v',24}/N''_{0,24} = \exp \left[ -(E''_{v',24} - E''_{0,24})/kT \right] \quad (18)$$

Two temperatures will be considered. The first is 2800°K which applies for the "low" flow cases and the second is 3600°K which applies for the "high" flow cases. The most probable transition where gain could be achieved is the  $v' = 0, v'' = 2$ . Therefore, population in  $N''_{2,24}$  will be considered. The energy difference between  $v'' = 2, J'' = 24$  and  $v'' = 0, J'' = 24$  is  $8.075 \times 10^{-13}$  erg. Thus, using equation (17),  $N''_{2,24} = 0.1055 \cdot N''_{0,24}$  at 2800°K and  $N''_{2,24} = 0.197 \cdot N''_{0,24}$  at 3600°K. Two cases can be taken for illustration. From Figure 28, for the lowest flow case ( $T = 2800^\circ\text{K}$ ),  $N'_{0,24}$  equals  $3.9 \times 10^{10}$  and  $N''_{0,24}$  equals  $6.2 \times 10^{11}$ . From this,  $N''_{2,24}$  equals  $6.5 \times 10^{10}$ . Therefore, the gain is proportional to

$$G \propto (N'_{v',J'} - 2N''_{v'',J''}) = -9.1 \times 10^{10} \quad (19)$$

With the higher flow case ( $T = 3600^\circ\text{K}$ ), the gain is proportional to  $-9.6 \times 10^{10}$ . This indicates absorption for both cases. Similar results are obtained in choosing other data for analysis. The best result indicated that the lower state density would need to be a factor of at least 3 lower to reach a condition of equal gain. Unfortunately, no change in conditions could achieve this change.

From the above analysis, it appears that if the flow could be cooled such that the A state density remained the same but the vibrational levels in the ground state were in thermal equilibrium, a chance of gain in the (0,2) transition would exist. However, it is possible that density in the

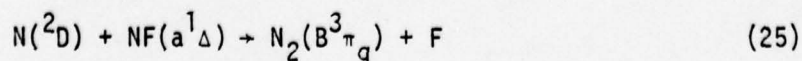
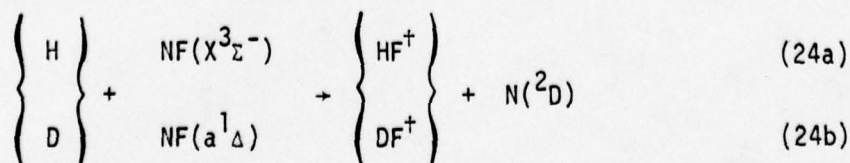
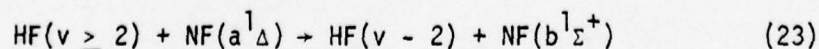
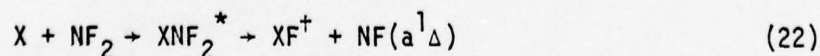
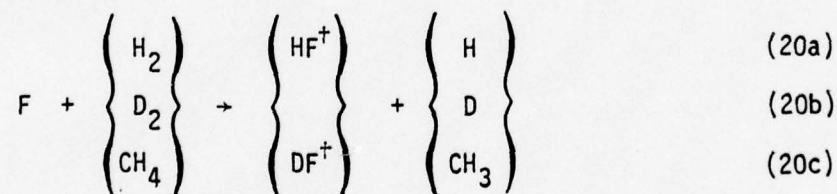
A state would also be lost in such a cooling process. Thus, at the present time, the hope for a CN laser using fluorine hydrogen flames for pumping appears remote.

The other point which deserves discussion is the mechanism whereby the CN is excited. Density measurements and comparison of A and B state intensities indicate that the numbers observed in the A state are greater than would occur by a strictly thermal mechanism. However, it is very difficult to postulate a believable mechanism to account for A state excitation.

The CN system was abandoned after all data appeared to show at least a factor of 10 between the  $v' = 0, J' = 24$  and  $v'' = 0, J'' = 24$  levels. Thus, the remainder of the contract was spent on the chemical pumping of NF which will be reported in the next section.

### 3.0 CHEMICAL PRODUCTION OF NF EXCITED STATES

Emission from the NF ( $b^1\Sigma^+$ ) state was first reported in  $\text{NF}_3 - \text{H}_2$  and  $\text{N}_2\text{F}_4 - \text{H}_2$  flames by Goodfriend and Woods<sup>(10)</sup> in 1965 although they did not assign the state or propose a production mechanism. Clyne and White<sup>(11)</sup> observed that metastable, electronically excited NF ( $b^1\Sigma^+$ ) and NF ( $a^1\Delta$ ) molecules were produced by reaction of hydrogen, oxygen or nitrogen atoms with  $\text{NF}_2$  radicals. They also noted the formation of nitrogen atoms in the  $\text{H}/\text{NF}_2$  reaction. Later, Herbelin and Cohen<sup>(12)</sup> re-examined the hydrogen atom/ $\text{NF}_2$  system and clarified the mechanism by which NF excited states are formed in this system. The mechanism they proposed to account for their experimental observations is:



In the above, X denotes H, D, or  $\text{CH}_3$ .



These early experiments were conducted in a flow tube where  $\text{NF}_2$  radicals were produced by a discharge through  $\text{NF}_3$ . Later, a subsonic laser device in which F atoms were generated in a discharge through  $\text{SF}_6$ , and  $\text{N}_2\text{F}_4$  and hydrogen were added to the heated flow to produce  $\text{NF}_2$  radicals and H atoms, allowed scaling of NF ( $a^1\Delta$ ) production to  $1.4 \times 10^{15}$  molecules/cc.<sup>(13)</sup>

Concurrently, experiments at TRW in which  $\text{NF}_3$  had been used as a fuel in a CW HF chemical laser indicated that NF excited states were produced in a strictly chemical system.<sup>(6)</sup> At this time, experiments were also performed to study energy transfer from NF metastable states to other species which would be potentially better laser candidates. However, results from these tests were minimally encouraging.

Because of the success of Herbelin *et. al.* at Aerospace Corporation in scaling NF production making use of F atoms to generate H atoms needed for HF production, it was desirable to study NF production in a system where all species, including F atoms, were produced chemically. It was also desirable to use heat generated in production of F atoms by combustion of  $\text{F}_2$  and  $\text{H}_2$  to dissociate  $\text{N}_2\text{F}_4$  into  $\text{NF}_2$  radicals. The existing CW laser facility located in the Penthouse laser facility at TRW seemed ideal for this study. Thus, the last part of the contract was spent in pursuing these studies. The following sections present the results of these studies.

### 3.1 EXPERIMENTAL

#### 3.1.1 Experimental Apparatus

The apparatus chosen for these studies is the smallest of TRW's CW HF chemical laser devices. A drawing of the laser assembly is shown in

Figure 32. The laser hardware is constructed in a building block arrangement. Table 4 summarizes the characteristics of the laser. A photograph of the device is shown in Figure 33. For experiments with  $N_2F_4$ , the combustor was modified to include injection ports 1, 2 and 3 inches from the nozzle. The ports were simply holes located on opposite sides of the diameter of the combustor. The holes were located  $90^\circ$  from the cooling water ports shown in Figure 32. For some experiments, longer Brewster angle windows were used to allow study of emission as a function of distance from the mixer. A bellows section located below the heat exchanger allowed adjustment of laser position.

\* It was desirable to perform some experiments in a device with a longer gain length. For these studies, the laser described in Section 2.2 for the CN work was used. A photograph of the nozzle and mixer used for these experiments is shown in Figure 34. This is called a "side-on" injector because fuel is injected through holes along each side of the nozzle. For the NF experiments,  $N_2F_4$  was injected through the holes in one side of the mixer while hydrogen was injected through holes in the other side. This device has a 15 cm gain length and was used to study an alternate mixing concept. The hardware used in these experiments is described in even greater detail elsewhere.<sup>(14)</sup>

### 3.1.2 Diagnostics

The major diagnostic used to monitor the experiments was chemiluminescence spectroscopy. A 0.3 m McPherson spectrometer with a 1200 lines/mm grating blazed at  $7500\text{\AA}$  was used for the spectral measurements. An RCA C31034A gallium arsenide photodetector was used to detect the radiation. The

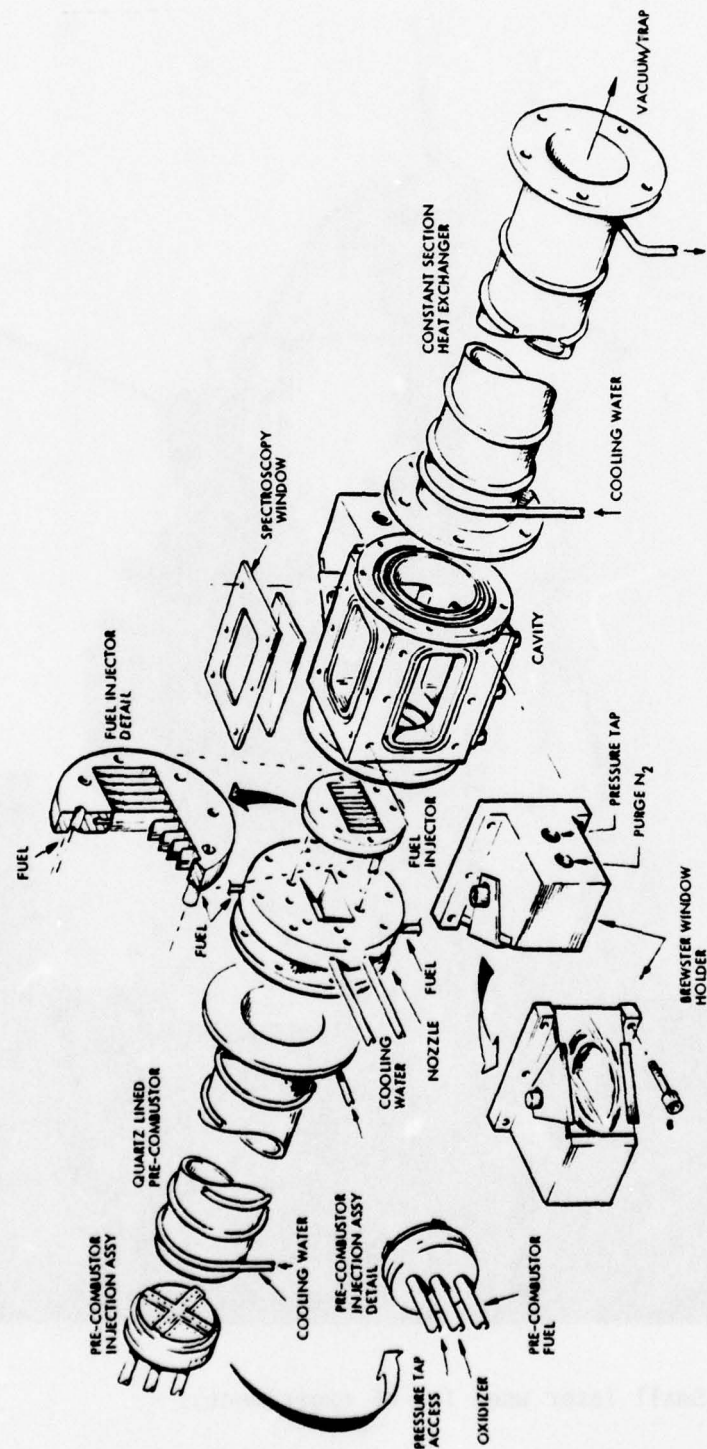


Figure 32. Schematic of small laser used for NF experiments.

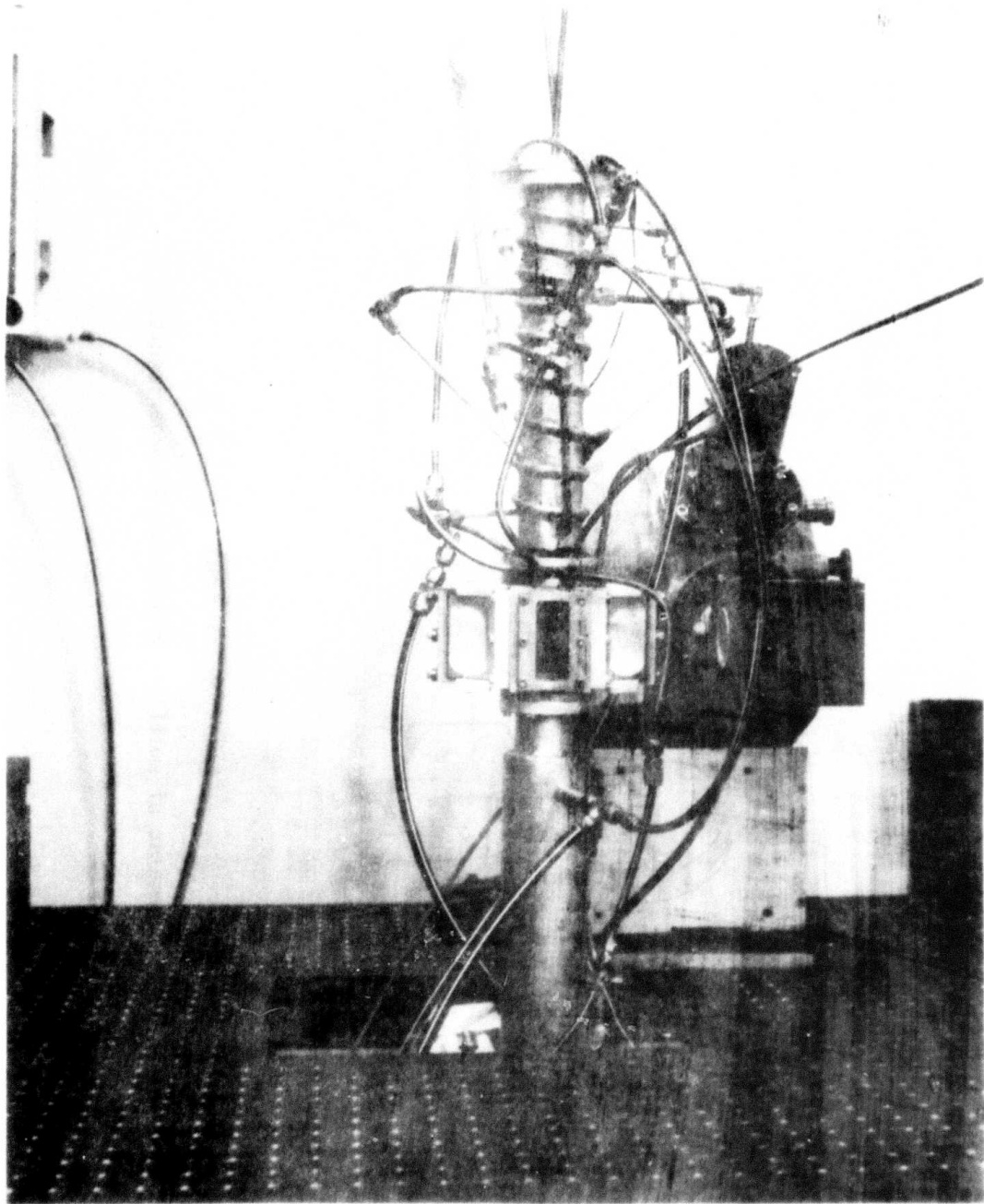


Figure 33. Small laser used for NF experiments.



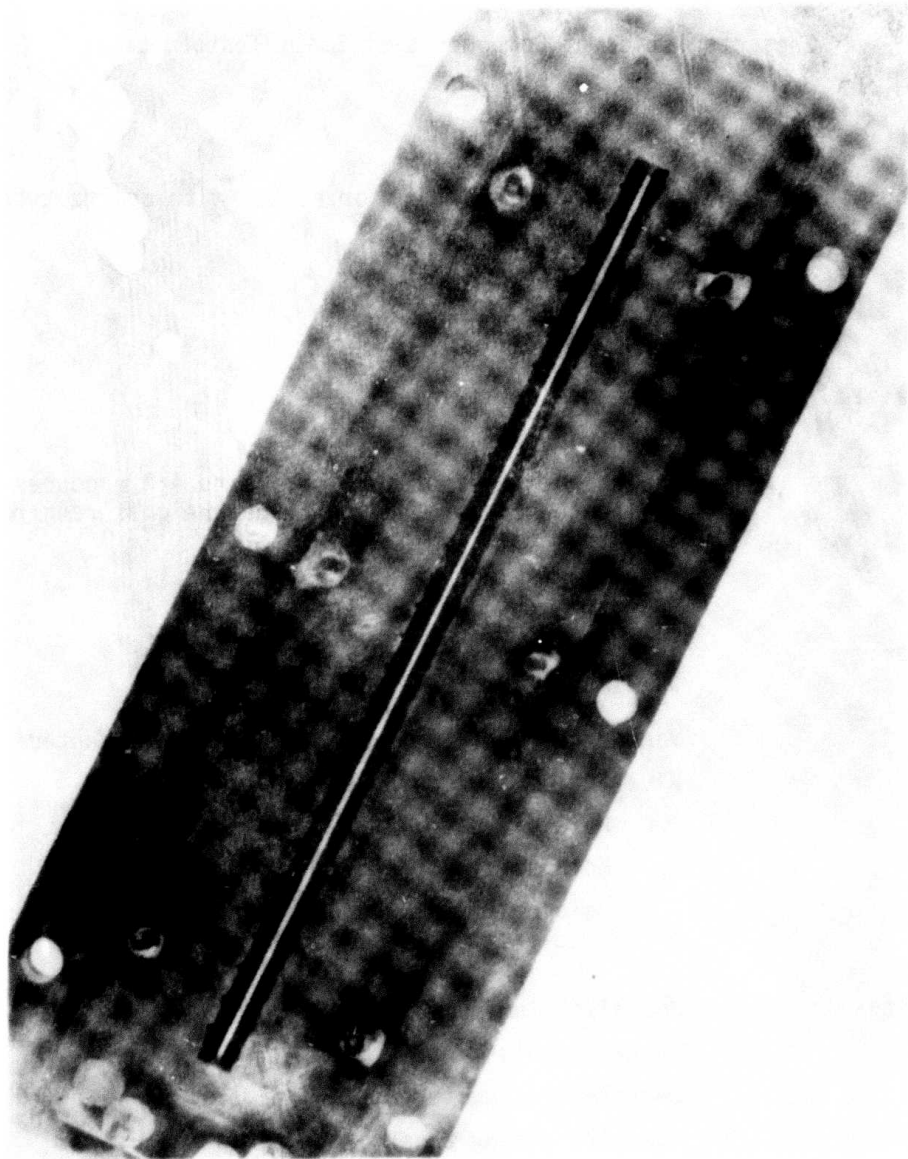


Figure 34. "Side-on" injector nozzle.

Table 4.  
Characteristics of Components of Small Testbed Laser

Combustor:	Water cooled aluminum or nickel with quartz tube insert Length: 30 cm Diameter: 3.8 cm "Raised post burner"
Nozzle:	Water cooled stainless steel Height at exit plane = 1.2 cm Expansion ratios of 13:1, 8:1, and 4:1 produces with duplicate hardware having throat heights ranging from 3 mm to 1 mm. Gain length: 6 cm
Mixer:	Uncooled copper "Busemann biplane" design Vane spacing of 3 mm and 5 mm center to center Five fuel injection holes/vane Hole diameter: 0.5 mm Hole spacing: 2.5 mm Hole position: Staggered on opposite sides of vane centerline
Cavity:	Uncooled aluminum Inner diameter = 8.9 cm Detachable Brewster window holders Sapphire window observation parts
Heat Exchanger:	Water cooled aluminum Constant section: 8.9 cm I.D. Length: 30 cm

spectrometer was used on its side as the slit image was horizontal. A 4-inch focal length toroidal mirror was used to give a 1:1 image of the 300  $\mu\text{m}$  x 1 cm slits. A 4800 $\text{\AA}$  cut on filter was used in all experiments to eliminate any second order radiations from shorter wavelengths. The spectrometer-photomultiplier assembly was calibrated using an Eppley filament lamp to allow determination of absolute light flux. The slit image of the spectrometer was placed on the filament and was smaller than the lamp source.

The total photon flux from an emitting state is proportional to the integrated area under the emission curve. However, experimentally it is more convenient to monitor the peak height. Therefore, to make data accumulation easier, several scans over desired emission curves were run and ratio of peak height to area determined. This ratio was found to be constant over a wide range of intensities. Therefore, for data collection, only the peak height was monitored and the peak height to area ratio used to convert the data to absolute photon fluxes. As will be discussed later, it was virtually impossible to isolate the NF ( $a^1\Delta$ ) state emission from nitrogen first positive and HF overtone emissions. Consequently, most measurements of absolute photon flux were made using NF ( $b^1\Sigma^+$ ) state emission. A radiative lifetime for this state of .016 sec<sup>(15)</sup> was used to reduce photon fluxes to number densities of b state.

The laser device used in these studies has been characterized extensively in the past<sup>(14)</sup> as to F atom concentrations produced in the laser precombustor. These measurements indicated that the fluorine atom flows were from 75% to 90% of the  $\text{F}_2$  flow. These measurements were not repeated for this program. No convenient diagnostic was found for  $\text{NF}_2$  radical concentration. This type

of measurement would have been very useful in characterizing the system as there is a question as to the concentration of  $\text{NF}_2$  radicals entering the mixing region.

Temperatures in the active region were determined using HF chemiluminescent spectroscopy. A toroidal mirror was used to focus a 1:1 image of the laser cavity onto the spectrometer entrance slit. An indium-antimonide detector was used. The entire optical system was flushed with dry nitrogen to eliminate absorption of the HF lines by water vapor in the air. The slits of the "HF" spectrometer were located vertically to the nozzle so good spatial resolution in the flow direction was not available. However, trends in temperatures under different flow conditions were obtainable.

Pressure transducers are located in both the combustor and cavity to allow the pressure to be probed under several run conditions.

### 3.1.3 Gas Handling

All the constituents used under the program were gaseous. Fluorine was handled using standard procedures with remotely operated valves at critical points. Flows were measured by monitoring the pressure on the high pressure side of calibrated orifices. These flows were calibrated using Matheson flow transducers. The tetrafluorohydrazine was obtained from Hercules Incorporated. It was handled in the same manner as fluorine. All lines which came into contact with tetrafluorohydrazine were passivated with fluorine before  $\text{N}_2\text{F}_4$  was admitted.

## 3.2 RESULTS

Experiments were run with four separate configurations. The first



three sets were run using the small HF laser device with 13:1, 8:1 and 4:1 expansion ratio nozzles. The fourth set was run with the 15 cm device and the "side-on" injector nozzle.

### 3.2.1 Preliminary Experiments

Initial experiments were conducted using a quartz-lined nickel combustor which contained only one port for introduction of  $N_2F_4$ . This port was simply a line entering the side of the combustor and was located 5 cm upstream from the expansion nozzle.

Before introduction of  $N_2F_4$ , tests were conducted to verify that the system was functioning properly as a DF laser. For these tests,  $F_2$  and  $H_2$  were burned in the combustor to produce F atoms and  $D_2$  was added through the mixer. The first mixer tested was a "side-on" injector with a 1 x 3 cm exit area and a 13:1 area expansion ratio nozzle. This particular mixer had never been tested on the small device. Only 1 watt DF power was produced with this nozzle. A "Busemann biplane" nozzle was then installed with a 13:1 area ratio nozzle. With this system, 7 watts of CW DF power were obtained with the same flow conditions as with the "side-on" injector. This indicated that the "side-on" injector was not mixing properly in this laser. Therefore, tests in this system were conducted using the nine vane, four hole biplane injector with several different area ratio nozzles.

The first tests using  $N_2F_4$  were run to verify that the system was working properly. Flows were 2 mmoles/sec fluorine, 0.88 mmoles/sec hydrogen, 2 mmoles/sec helium, 2 mmoles/sec deuterium and 2.8 mmoles/sec nitrogen purge. The flow of  $N_2F_4$  was 0.165 mmoles/sec. These flows produced a

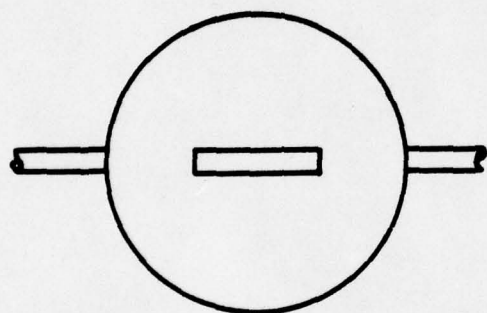
yellow flame that was extinguished when  $D_2$  was turned off. A spectral scan showed the emission was nitrogen first positive which overlapped the region where the NF ( $a^1\Delta$ ) state emits. When hydrogen was substituted for  $D_2$  in the cavity, the green emission band from NF ( $b^1\Sigma$ ) appeared as well as the nitrogen first positive emission. The intensity of b state emission increased linearly with  $N_2F_4$  flow up to a flow of 0.22 mmoles/sec. Again, all emissions ceased when the cavity hydrogen was turned off.

Methane was next added to the cavity in the place of hydrogen. Blue emission resulted which was attributed to  $C_2$  swan bands. The emission of NF ( $a^1\Delta$ ) could barely be discerned in the HF,  $\Delta v = 2$  overtone emission.

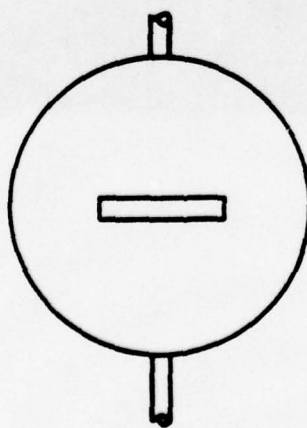
Photographs were taken of the emissions to determine spatial distribution. A photograph of the emission with a single inlet port for  $N_2F_4$  is shown in Figure 35. The emission is not uniform over the cavity. This can be noticed near the mixer where there is a dark region on the right-hand side of the photograph. There are also dark areas on the sides of the cavity. To attempt to correct this, and also to study the effect of the position where  $N_2F_4$  is added a new precombustor was built of aluminum with three pairs of holes for addition of  $N_2F_4$ . The holes could be aligned either parallel or perpendicular to the slot of the expansion nozzle. This is illustrated in Figure 36. These pairs of injectors were located at distances 3.8, 8.9 and 14 cm above the nozzle. When the  $N_2F_4$  was added parallel to the nozzle, a dark region appeared in the center of the cavity as shown in Figure 37. Thus, it appears that the  $N_2F_4$  did not mix well with the other combustor gases before expanding through the nozzle. When the injection ports were turned at right angles to the nozzle, the emission in the cavity became very uniform as illustrated in Figure 38. Thus, it was found necessary to insure that the



Figure 35. Emission with one  $\text{N}_2\text{F}_4$  injector port.



A. ADDITION OF  $N_2F_4$  PARALLEL TO NOZZLE AXIS



B. ADDITION OF  $N_2F_4$  PERPENDICULAR TO NOZZLE AXIS

Figure 36. Schematic of location of  $N_2F_4$  injection ports.



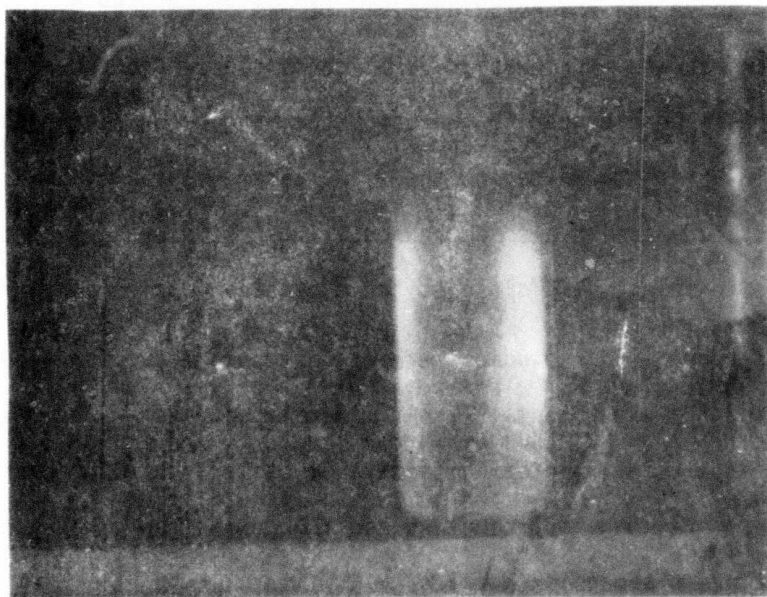


Figure 37. NF emission with  $N_2F_4$  added through two ports parallel to nozzle axis.

$N_2F_4$  was added properly. It would have been even more desirable to have had a more sophisticated mixer for  $N_2F_4$ .

Studies were also made of the effect of position where  $N_2F_4$  is added to the cavity. The three sets of ports were located at distances 5 cm, 10 cm and 15 cm above the expansion nozzle. It was found that NF ( $b^1\Sigma^+$ ) signals were strongest when  $N_2F_4$  was added at ports closest to the nozzle. When the  $N_2F_4$  was added higher in the combustor, the color of the flame changed from yellow-green to white and the flame became unstable. The intensity of NF b state emission also decreased. These studies indicated that it was desirable to inject  $N_2F_4$  close to the expansion nozzle.

These preliminary studies were conducted to establish general procedures for running the experiments. Their major impact was in determining how to add  $N_2F_4$  and in determining which mixing nozzle to use for hydrogen. These conditions were then kept constant and then experiments were conducted using three different expansion nozzles.

### 3.2.2 Experiments with the 13:1 Area Expansion Ratio Nozzle

As mentioned above, three nozzles with different area expansion ratios were available. The nozzle tested first had a 13:1 area expansion ratio. Experiments were run with this nozzle that aimed at optimizing NF ( $b^1\Sigma^+$ ) state emission for a given  $N_2F_4$  flow. The manner in which experiments were conducted was to first turn on the fluorine, helium and both hydrogen flows. These flows were initially set for optimum HF lasing. The  $N_2F_4$  was then added and this flow set to some predetermined value. The NF ( $b^1\Sigma^+$ ) emission line at  $5288\overset{\circ}{\text{\AA}}$  was then monitored while other flows were adjusted. The order

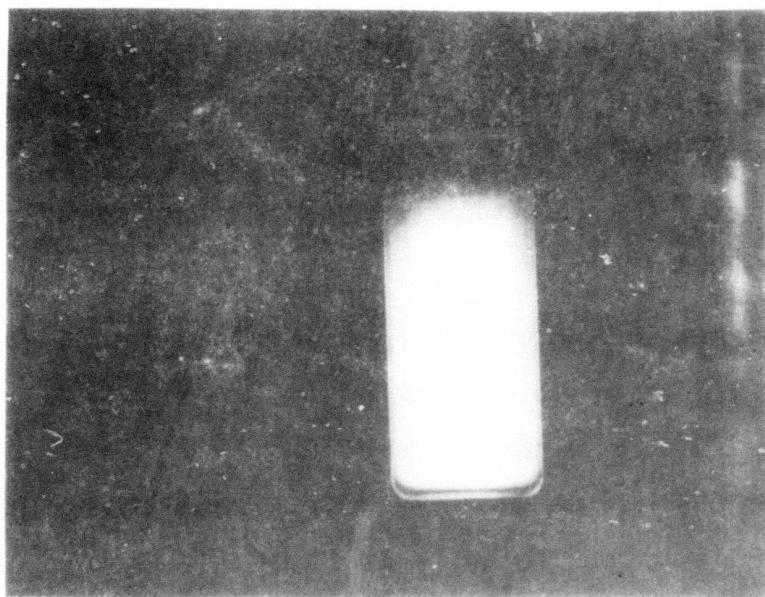


Figure 38. NF emission with  $\text{N}_2\text{F}_4$  added through two ports perpendicular to nozzle axis.

in which flows were optimized was first fluorine, second combustor hydrogen, and finally, cavity hydrogen. It was found that the intensity was extremely dependent on the fluorine and combustor hydrogen flows and relatively insensitive to cavity hydrogen flow once this flow reached a critical value.

A study of the effect of helium diluent flow was also made after the other flows had been optimized. Increasing helium caused the flame to become unstable and the NF signal to drop. The other flows were readjusted but the flame remained unstable. A decrease in helium also caused a decrease in NF signal. Again, a readjustment of other flows did not bring the signal up to previous levels.

A summary of flows of the various gases for optimum NF ( $b^1\Sigma^+$ ) emission at  $5288\text{\AA}$  is given in Table 5 accompanied by the number density of NF ( $b^1\Sigma^+$ ) determined from the spectrometer calibration. This data is plotted in Figure 39 to illustrate the manner in which the NF emission scales with  $N_2F_4$  flow. Note that the plot is not linear and bends over at the higher  $N_2F_4$  flows, even though intensity of NF emission still increases with increasing  $N_2F_4$ .

Scans of the intensity of b state emission versus distance from the mixing nozzle in the flow direction,  $X_c$ , were performed. A typical scan is shown in Figure 40. For all  $N_2F_4$  flows run with this nozzle, the intensity peaked at  $X_c = 1.3$  cm. The intensities reported in Table 5 correspond to those observed at this distance.

Scans of the region near  $8742\text{\AA}$  where the NF ( $a^1\Delta - X^3\Sigma$ ) transition emits were made at several flows of  $N_2F_4$ . A scan at optimum b state emission for an  $N_2F_4$  flow of 0.25 mmoles/sec is shown in Figure 41. In this figure the



Table 5.  
Summary of Flow Conditions and Number Densities of  
NF ( $b^1\Sigma^+$ ) for 13:1 Nozzle

Flows (mmoles/sec)					Pressure (torr)		[NF ( $b^1\Sigma^+$ )]
N <sub>2</sub> F <sub>4</sub>	F <sub>2</sub>	H <sub>2</sub> (comb)	H <sub>2</sub> (cav)	He	Combustor	Cavity	Molecules/cc
0.07	1.78	0.57	1.14	2	16.9	1.44	$7.5 \times 10^{11}$
0.11	1.68	0.64	1.16	2	18.0	1.42	$1.17 \times 10^{12}$
0.14	1.80	0.72	1.34	2	20.3	1.50	$1.40 \times 10^{12}$
0.18	1.86	0.75	1.34	2	21.5	1.56	$1.50 \times 10^{12}$
0.21	2.16	0.85	1.46	2	24.5	1.68	$1.68 \times 10^{12}$
0.25	2.26	0.97	1.46	2	26.6	1.70	$1.79 \times 10^{12}$

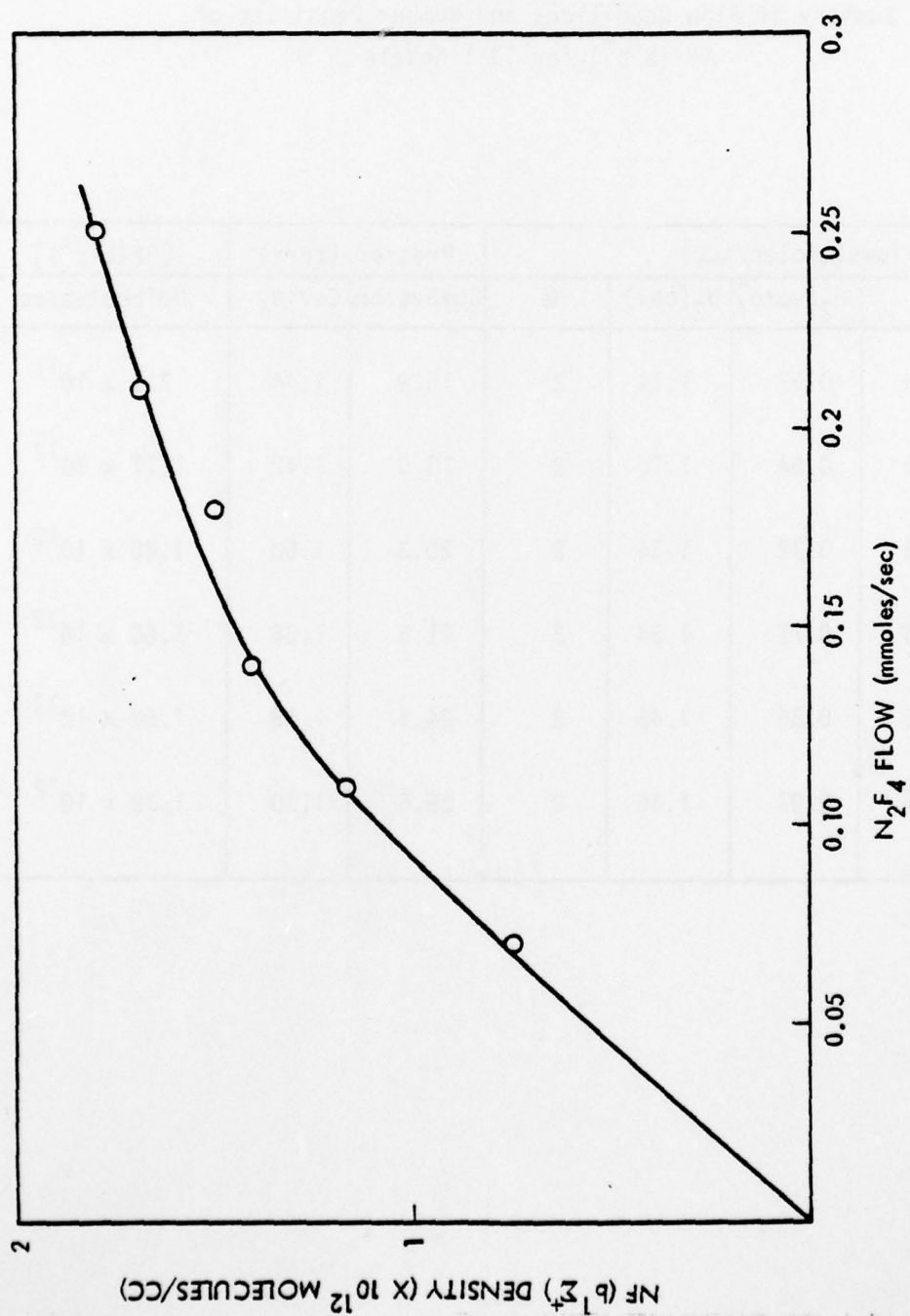


Figure 39. Plot of NF density versus N<sub>2</sub>F<sub>4</sub> flow for 13:1 nozzle.

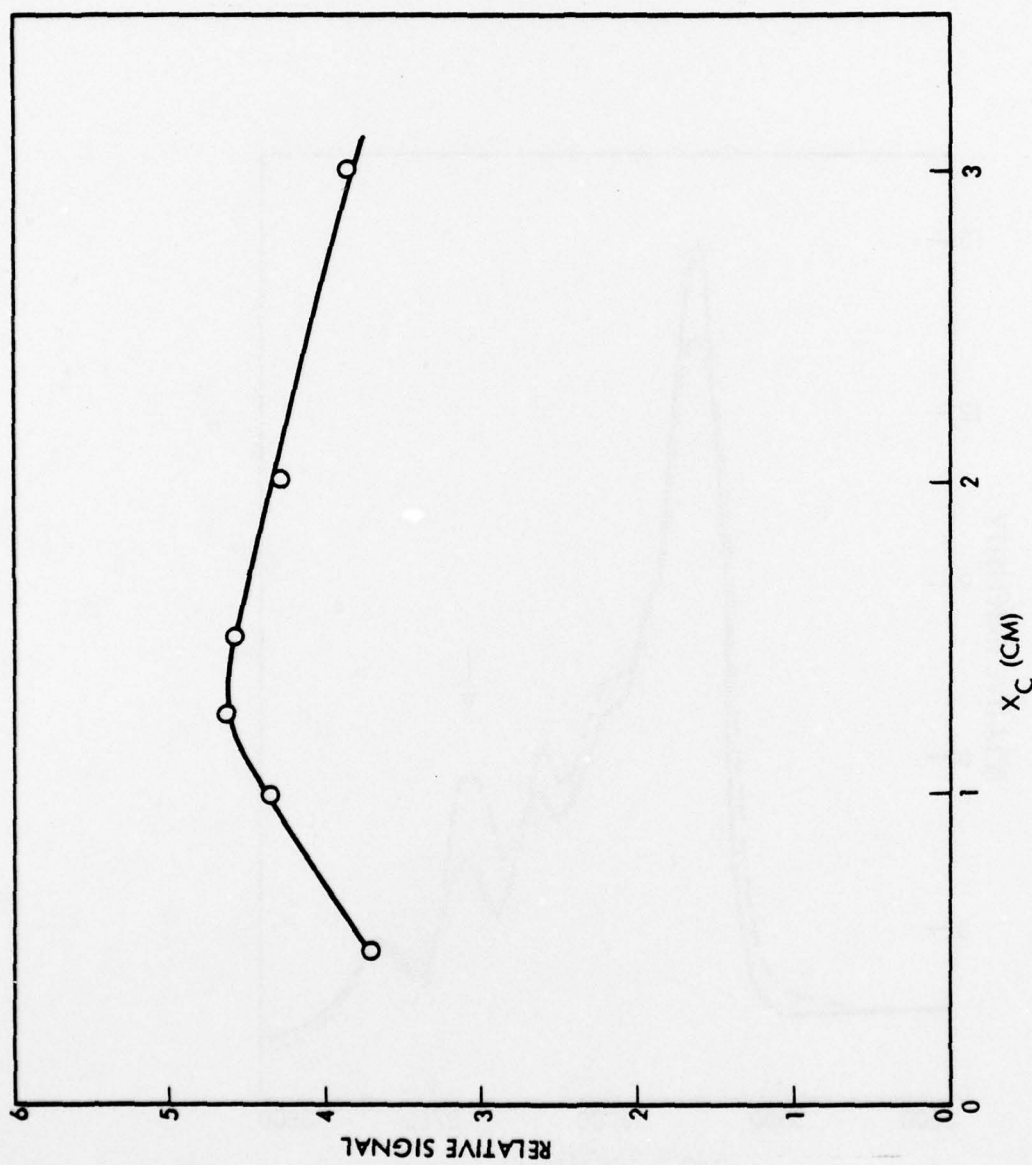


Figure 40. Variation of NF signal with distance from mixer for 13:1 nozzle.

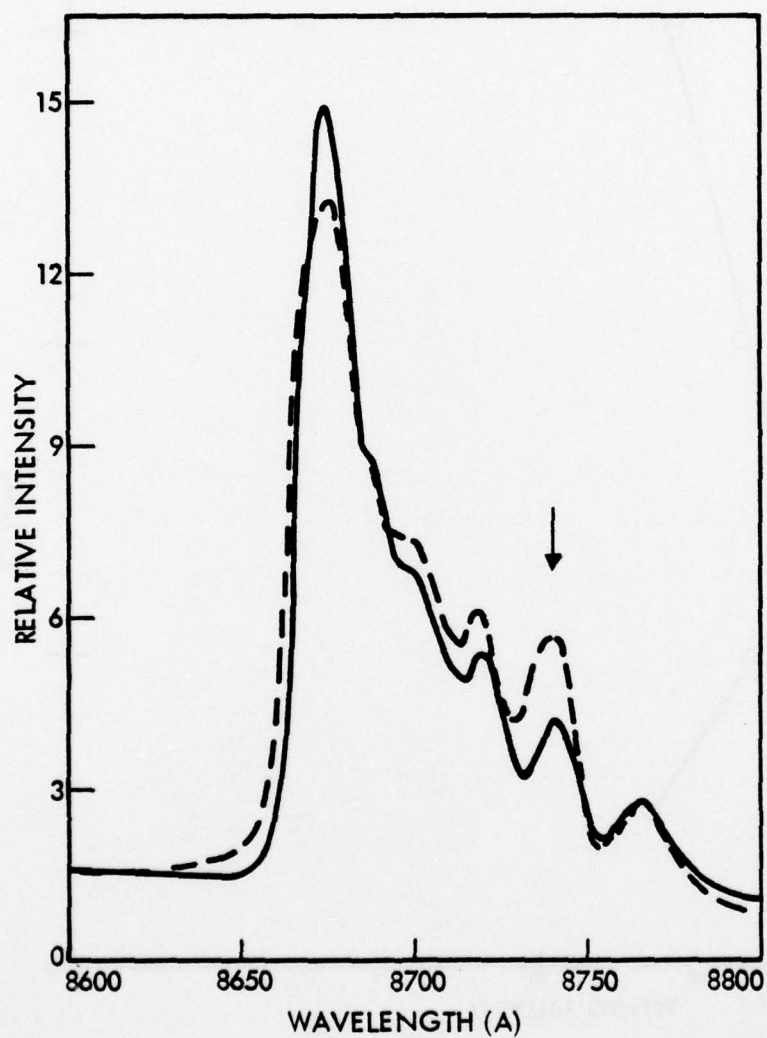


Figure 41. Emission spectrum of flame from small laser. Solid line is with no  $N_2F_4$ , broken line is with  $N_2F_4 = 0.25$  mmol/sec.



solid line is a scan with only the fluorine and combustor and cavity hydrogens. The broken line is a scan with added  $N_2F_4$ . The  $R_2$  line of the 3-0 HF overtone lies at  $8740\overset{\circ}{\text{\AA}}$  and is indicated by the arrow in the figure. The  $R_3$  line of the 3-0 HF overtone lies at  $8719\overset{\circ}{\text{\AA}}$ . Notice that the intensity at both these lines increased with addition of  $N_2F_4$  while the intensity of the main band of the R branch of HF near  $8670\overset{\circ}{\text{\AA}}$  decreased. The increase in intensity of the lines at  $8719\overset{\circ}{\text{\AA}}$  and  $8740\overset{\circ}{\text{\AA}}$  is due to the  $a^1\Delta$  state of NF radiating at  $8742\overset{\circ}{\text{\AA}}$  and the 2,1 band of  $N_2$  first positive radiation at  $8722\overset{\circ}{\text{\AA}}$ . If this interpretation is correct, an estimate of the NF(a) state intensity can be made by comparing the peak heights at  $8742\overset{\circ}{\text{\AA}}$  with and without  $N_2F_4$ . Such a procedure gives an estimate of the a state density of  $8 \times 10^{13}$  molecules/cc for this particular flow condition.

Temperatures in the laser cavity were studied for two sets of flow conditions using HF chemiluminescence data. HF scans were first run with only fluorine and hydrogen flows at distances of 0.5 and 2 cm.  $N_2F_4$  was then added and the same scans repeated. The data is summarized in Table 6. The temperatures were lower near the nozzle, increasing with distance. Addition of  $N_2F_4$  lowered the temperature significantly in all cases, even though it constituted a small fraction of the total flow.

At the conclusion of the tests with this nozzle, the system was changed to include a 4:1 area expansion ratio nozzle. Results of tests with this nozzle are summarized in the next section.

### 3.2.3 Experiments with the 4:1 Area Expansion Ratio Nozzle

Experiments were conducted in the same manner described in the last section, i.e., flows were adjusted to give maximum emission at  $5288\overset{\circ}{\text{\AA}}$  for

Table 6.  
Temperatures in Active Region with the 13:1 Nozzle

Flow Conditions*	N <sub>2</sub> F <sub>4</sub>	X <sub>c</sub> (cm)	T(°K)
Set 1	No	0.5	980
Set 1	Yes	0.5	920
Set 1	No	2.0	1500
Set 1	Yes	2.0	1150
Set 2	No	0.5	800
Set 2	Yes	0.5	640
Set 2	No	2.0	1050
Set 2	Yes	2.0	750

\*Flow conditions (mmoles/sec)

Set	F <sub>2</sub>	H <sub>2</sub> (comb)	H <sub>2</sub> (cav)	N <sub>2</sub> F <sub>4</sub>	H <sub>e</sub>	Purge N <sub>2</sub>
1	2.40	0.88	1.14	0.186	2.8	2.0
2	1.40	0.57	1.00	0.07	2.8	2.0

a given  $N_2F_4$  flow. Results of these experiments are summarized in Table 7 and plotted in Figure 42. The optimum flows with this nozzle differ from those observed with the 13:1 nozzle in that there is less variation in the optimum fluorine and hydrogen flows as  $N_2F_4$  is increased. The major difference between the two systems is the pressure at which the precombustor operates; the 13:1 nozzle producing a pressure three times higher than the 4:1 nozzle. The variation of precombustor pressure with  $N_2F_4$  flow is plotted in Figure 41. This plot is linear illustrating that addition of  $N_2F_4$  probably changes the performance of the combustor. The cavity pressures with the two nozzles were almost the same as they were determined by the pumping speed of the pump. In general, number densities obtained with this nozzle were higher than those obtained with the 13:1 nozzle, especially at higher  $N_2F_4$  flows. A study of the effect of helium in the system was made. For fixed flows, increasing the helium flow caused the NF signal to decrease. However, it was found that when fluorine and hydrogen flows were readjusted, the NF signal increased. Thus, for an  $N_2F_4$  flow of 0.186, the signal was 1.59 units with helium flow 2 mmoles/sec, fluorine flow 1.88 mmoles/sec, combustor hydrogen flow 0.95 mmoles/sec and cavity hydrogen flow 0.86 mmoles/sec. When the flows were adjusted to  $He = 3.2$  mmoles/sec  $F_2 = 2.1$  mmoles/sec, combustor  $H_2 = 0.95$  mmoles/sec and cavity  $H_2 = 1.2$  mmoles/sec, the signal was 1.65 units. This is only a small increase but did indicate that there is a range of flows at which optimum intensity can be obtained.

Scans of intensity versus  $X_c$  were made. These scans illustrated that for all flows, intensities were a maximum for the range of  $X_c$  from 1.0 to 1.5 cm.

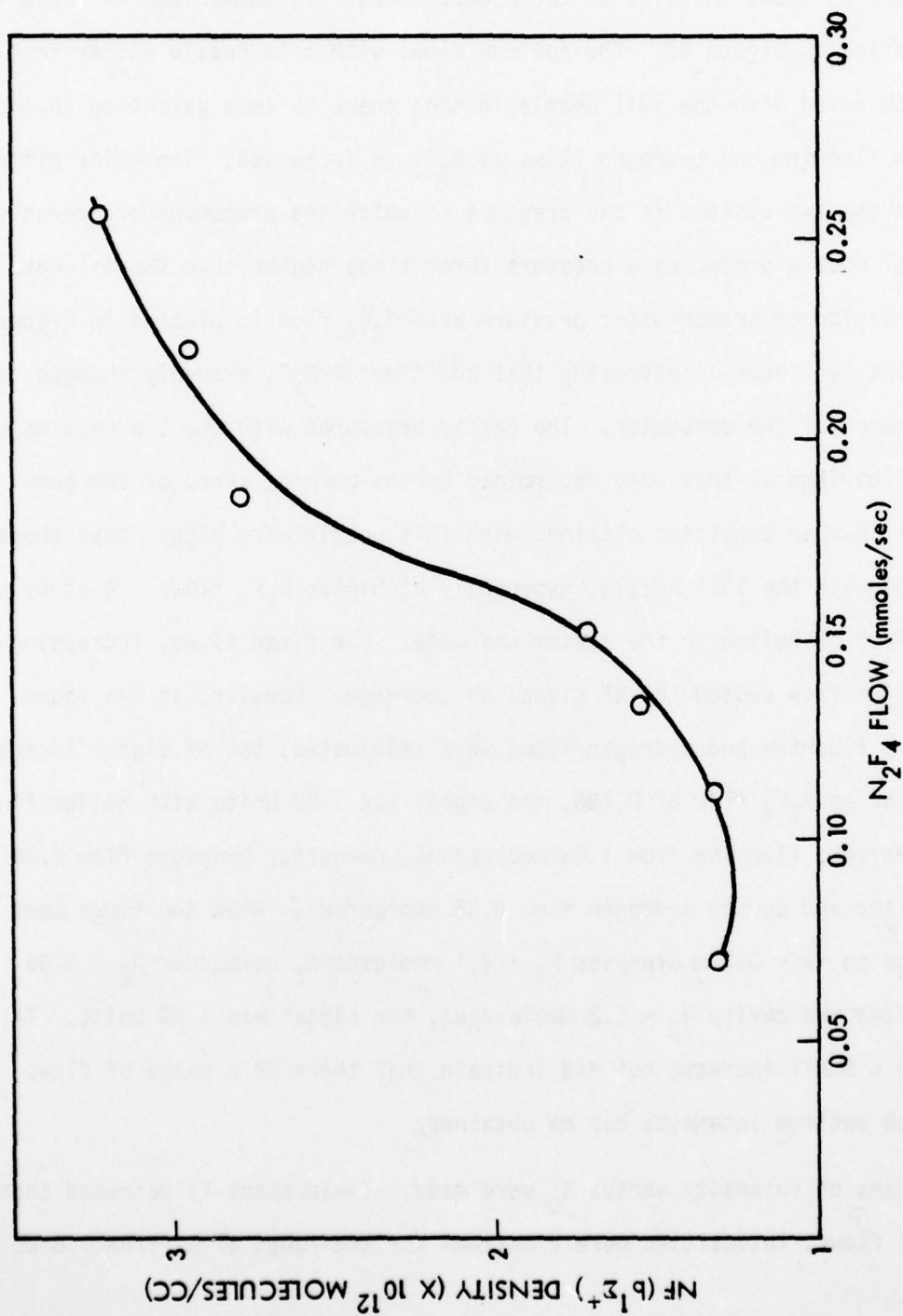


Figure 42. Plot of NF density versus N<sub>2</sub>F<sub>4</sub> flow for 4:1 nozzle.



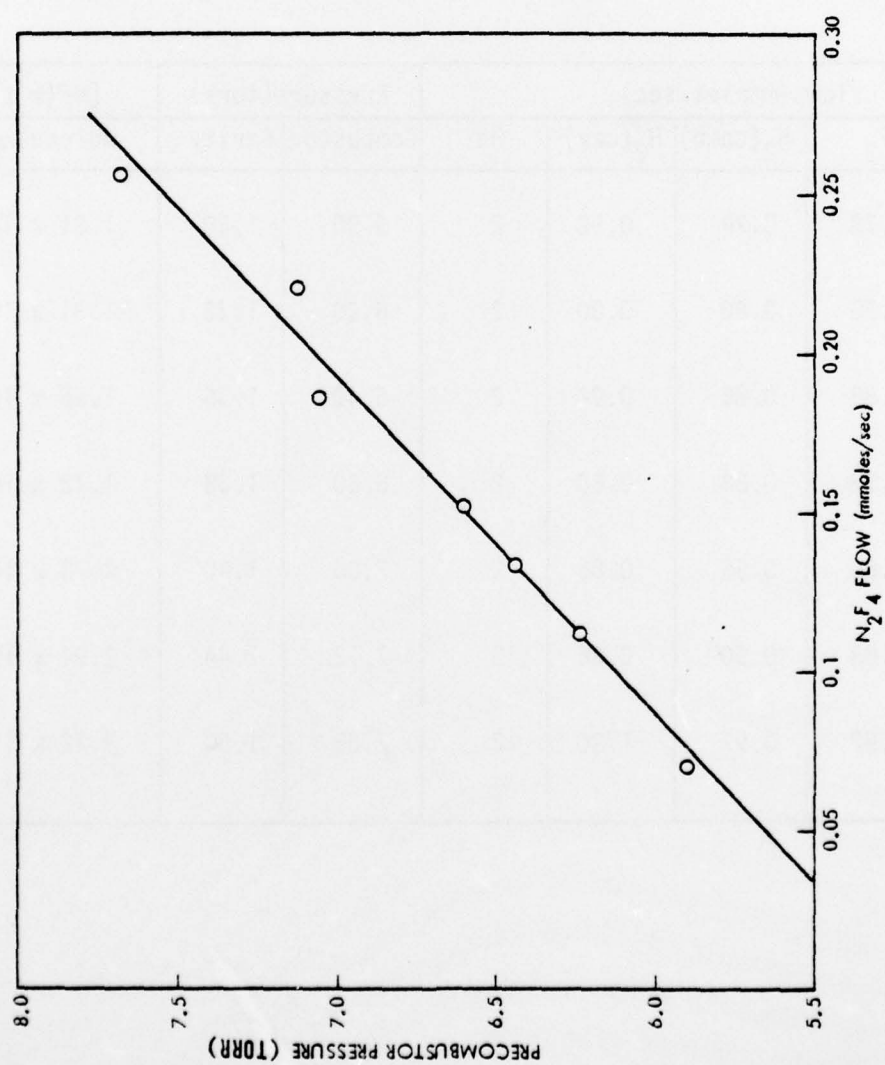


Figure 43. Variation of precombustor pressure with  $N_2F_4$  flow.

Table 7.  
Summary of Flow Conditions and Number Densities of  
NF ( $b^1\Sigma^+$ ) for 4:1 Nozzle

Flows (mmoles/sec)					Pressure (torr)		[NF( $b^1\Sigma^+$ )]
N <sub>2</sub> F <sub>4</sub>	F <sub>2</sub>	H <sub>2</sub> (comb)	H <sub>2</sub> (cav)	He	Combustor	Cavity	Molecules/cc
0.07	1.78	0.79	0.92	2	5.90	1.30	$1.31 \times 10^{12}$
0.112	1.78	0.80	0.80	2	6.20	1.33	$1.31 \times 10^{12}$
0.133	1.88	0.80	0.92	2	6.40	1.36	$1.55 \times 10^{12}$
0.152	1.78	0.88	0.80	2	6.60	1.38	$1.72 \times 10^{12}$
0.186	1.88	0.95	0.86	2	7.06	1.40	$2.78 \times 10^{12}$
0.221	1.88	0.90	0.86	2	7.12	1.44	$2.94 \times 10^{12}$
0.256	1.92	0.97	1.20	2	7.68	1.50	$3.22 \times 10^{12}$

Temperature data using HF chemiluminescence were taken for typical run conditions used with this nozzle. All data were taken at the position where optimum emission was obtained, i.e.,  $X_c = 1.0$  cm. A summary of temperatures obtained for various  $N_2F_4$  flows is given in Table 8. For this nozzle, the temperature tended to remain constant, regardless of the amount of  $N_2F_4$  added.

The increase of intensities of NF emission with a change from a 13:1 to a 4:1 nozzle indicated that the expansion ratio of the nozzle is crucial in determining NF concentrations. Thus, studies were next made with an 8:1 expansion ratio nozzle to round out the studies.

#### 3.2.4 Experiments with the 8:1 Area Expansion Ratio Nozzle

Experiments with this nozzle were conducted in the same manner as described previously; the  $N_2F_4$  flow was set and then other flows were adjusted to give optimum NF  $b^1\Sigma$  state emission at  $5288\text{\AA}$ . Results of these experiments are summarized in Table 9 and plotted in Figure 44. As the  $N_2F_4$  flow was increased, the flows of fluorine and hydrogen in the combustor had to be increased to obtain optimum emission. However, the intensity of NF emission was relatively insensitive to the flow of cavity hydrogen and this flow remained constant, regardless of the  $N_2F_4$  flow.

The main thing to note about the number densities obtained with this nozzle is that they are higher than those obtained with either the 13:1 or 4:1 expansion ratio nozzles. This tends to indicate that the combustor conditions obtained with this nozzle produce more favorable F and  $NF_2$  concentrations than obtained with the other nozzles.

The NF ( $b^1\Sigma^+$ ) concentration was still increasing as  $N_2F_4$  increased.

Table 8.

Summary of Temperatures with 4:1 Nozzle at  $X_c = 1$  cm

Flow $N_2F_4^*$ (mmoles/sec)	Temperature (OK)
0	$1100 \pm 100$
0.07	$1100 \pm 100$
0.133	$1200 \pm 100$
0.186	$1100 \pm 100$
0.256	$1000 \pm 100$

\*Other flow rates:  $F_2 = 1.78$  mmoles/sec

$H_2$  (comb) = 0.8 mmoles/sec

$H_2$  (cab) = 0.92 mmoles/sec



Table 9.  
Summary of Flow Conditions and Number Densities of  
NF ( $b^1\Sigma^+$ ) for 8:1 Nozzle

Flows (mmoles/sec)					Pressure (torr)		[NF ( $b^1\Sigma^+$ )]
N <sub>2</sub> F <sub>4</sub>	F <sub>2</sub>	H <sub>2</sub> (comb)	H <sub>2</sub> (cav)	He	Combustor	Cavity	Molecules/cc
0.07	1.76	0.58	1.26	2	11.5	1.36	$1.80 \times 10^{12}$
0.105	1.89	0.65	1.26	2	12.8	1.40	$2.63 \times 10^{12}$
0.14	1.89	0.65	1.26	2	13.0	1.46	$3.17 \times 10^{12}$
0.175	1.89	0.72	1.26	2	14.0	1.36	$3.52 \times 10^{12}$
0.210	1.89	0.82	1.26	2	15.1	1.34	$3.68 \times 10^{12}$
0.244	2.08	0.90	1.26	2	16.8	1.42	$3.83 \times 10^{12}$
0.268	2.14	0.95	1.26	2	17.7	1.48	$3.94 \times 10^{12}$
0.280	2.14	0.95	1.26	2	17.6	1.44	$3.83 \times 10^{12}$
0.294	2.21	1.02	1.26	2	18.7	1.46	$4.10 \times 10^{12}$
0.338	2.26	1.05	1.26	2	19.5	1.58	$4.32 \times 10^{12}$

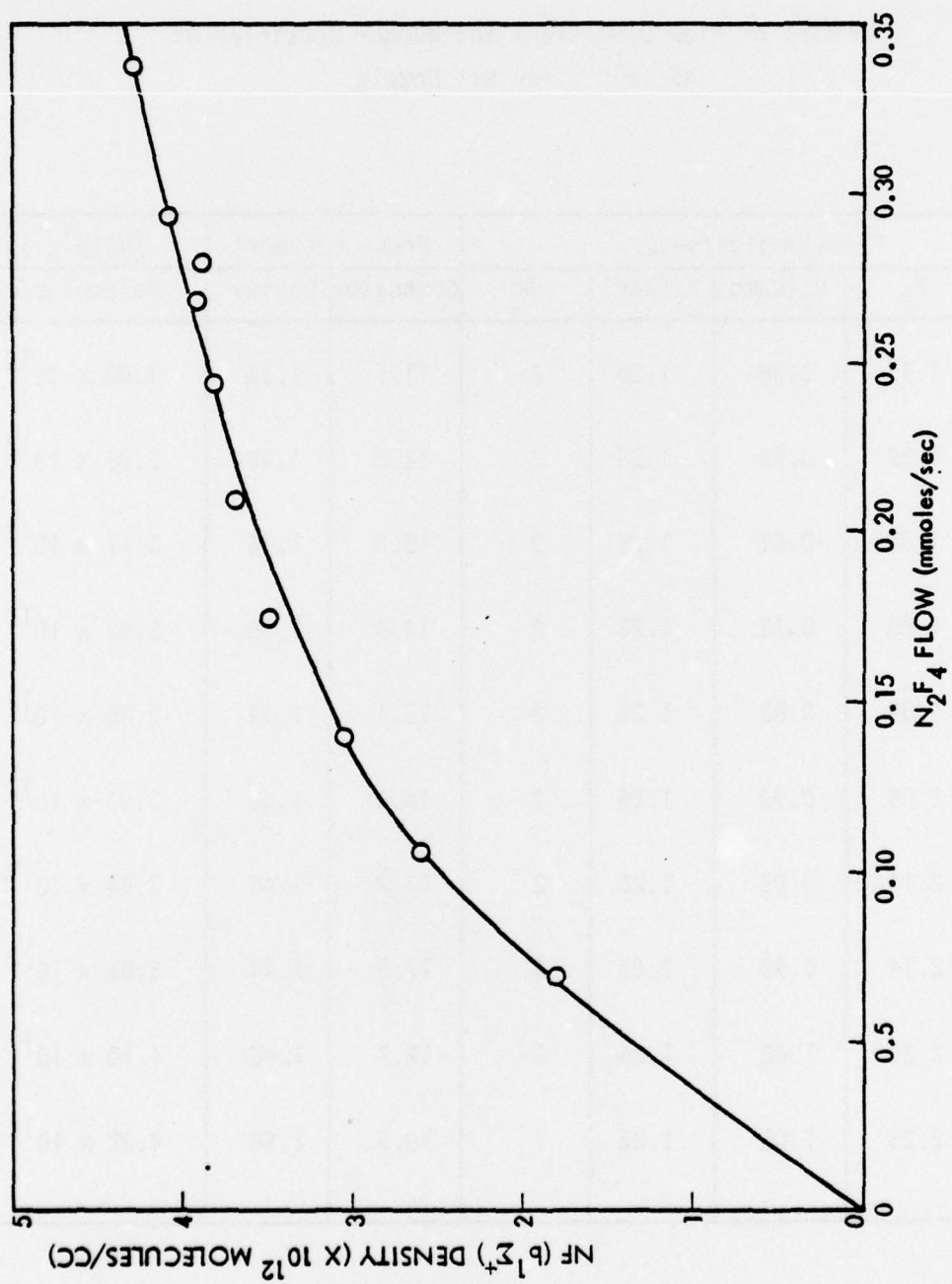


Figure 44. Plot of NF density versus N<sub>2</sub>F<sub>4</sub> flow for an 8:1 nozzle.

However, the slope of the plot of NF emission intensity was smaller at higher  $N_2F_4$  flows than at low  $N_2F_4$  flows.

Experiments were also conducted to determine the effect of cavity pressure on NF emission intensities. For these tests, the pump was throttled to increase the pressure. Flows were then readjusted to give optimum NF emission. When the cavity pressure was increased in this manner, the flame changed color from yellow-green at normal pumping speeds to yellow for medium pressures to white at higher pressures. The flame also moved in the cavity. At low pressures, the cavity was filled almost uniformly whereas at higher pressures the flame concentrated near the nozzle. Although temperatures were not measured under the high pressure conditions, past experience indicates that temperatures may have increased from 1500°K to 2500°K. The white flame was due to continuum radiation. This could be blackbody radiation caused by high temperatures. Table 10 summarizes the number densities obtained for two pressures at two  $N_2F_4$  flowrates. The NF density increased almost linearly with pressure. The  $X_c$  at which maximum intensities occurred was nearer to the nozzle at the higher pressure.

It is interesting to note color changes which occur under normal run conditions. At the lower flows, the flame appeared yellow-green. As flows increased a transition in color occurred until the flame became bright orange. The orange was enhanced nitrogen first positive emission. The enhancement at higher pressures could indicate a three-body mechanism for formation.

### 3.2.5 Experiments with the 15 cm Device

Some experiments were performed with a laser with a 15 cm gain length. For these experiments, only fluorine and hydrogen were burned in the com-

Table 10.  
NF Densities as a Function of Cavity Pressure

$X_c$ (cm)	Flows (mmoles/sec)				Pressure (torr)		[NF( $b^+ \Sigma^+$ )] Molecules/cc
	$N_2F_4$	$F_2$	$H_2$ (comb)	$H_2$ (cav)	Combustor	Cavity	
1.5	0.07	1.62	0.60	1.04	11.0	1.34	$1.9 \times 10^{12}$
0.2	0.07	1.30	0.62	2.00	9.7	3.44	$4.04 \times 10^{12}$
1.5	0.27	2.66	1.35	2.2	22.0	1.54	$3.26 \times 10^{12}$
0.5	0.27	2.52	1.38	2.14	21.4	3.2	$5.60 \times 10^{12}$



bustor to form fluorine atoms. The  $N_2F_4$  and additional hydrogen were added to the cavity on opposite sides of the "side-on" injector nozzle described in Section 3.1.1. Thus, these experiments differed from those performed with the smaller laser in which the  $N_2F_4$  was added.

Experiments were performed to characterize the performance of this laser. A photograph of the flame in this device taken through the Brewster angle window looking at the two sides of the injector is shown in Figure 43. This shows a separation of the flow near the nozzle with the flame becoming uniform near the bottom of the cavity. Because of the asymmetry of the flame, it was difficult to probe the system along the laser axis. Thus, chemiluminescence measurements were made through the side window perpendicular to the laser axis.

Studies were made of the variation of intensity of NF ( $b^1_\Sigma$ ) emission with variations in flow. Figure 46 shows the intensity versus fluorine flow for flows of  $N_2F_4$  equal to 0.25 mmol/sec, combustor hydrogen equal to 1.05 mmol/sec and cavity hydrogen equal to 3 mmol/sec. Figure 47 is a plot of intensity versus combustor hydrogen flow. In both plots, the intensity is peaked at a decisive maximum. Figure 48 is a plot of intensity versus cavity hydrogen flow. The intensity is a strong function of hydrogen flow only at low flows. At higher flows there is little dependence of intensity on hydrogen flow. Table 11 summarizes experiments performed with varying  $N_2F_4$  flow. For these experiments, the  $N_2F_4$  flow was set and the other flows adjusted to give maximum NF emission. The number densities in the table could be in error as much as a factor of two due to difficulties in determining the viewing depth. Scans of density of NF versus distance from the nozzle are also shown in Table 11. Note the NF density reaches a local



Figure 45. NF emission with "side-on" injector. Camera was looking through a Brewster angle window.

Table 11.  
Summary of Experiments With 15 cm Gain Length,  
Side-on Injector Nozzle

$x_c$	Flows (mmoles/sec)				Pressure (torr)		$[NF(b^+)]$
(cm)	$N_2F_4$	$F_2$	$H_2$ (comb)	$H_2$ (Cav)	Combustor	Cavity	Molecules/cc
.6	0.25	4.3	1.05	3.00	18.9	0.36	$1.4 \times 10^{12}$
.6	0.53	4.0	1.15	3.00	19.0	0.40	$1.59 \times 10^{12}$
.6	1.03	3.7	1.00	4.00	17.4	0.50	$1.78 \times 10^{12}$
.6	1.36	3.8	1.20	4.60	18.9	0.56	$1.96 \times 10^{12}$
1.0	1.36	3.8	1.20	4.60	18.9	0.56	$1.52 \times 10^{12}$
1.5	1.36	3.8	1.20	4.60	18.9	0.56	$1.31 \times 10^{12}$
2.0	1.36	3.8	1.20	4.60	18.9	0.56	$2.07 \times 10^{12}$
2.5	1.36	3.8	1.20	4.60	18.9	0.56	$2.94 \times 10^{12}$
3.0	1.36	3.8	1.20	4.60	18.9	0.56	$3.38 \times 10^{12}$
4.0	1.36	3.8	1.20	4.60	18.9	0.56	$3.73 \times 10^{12}$

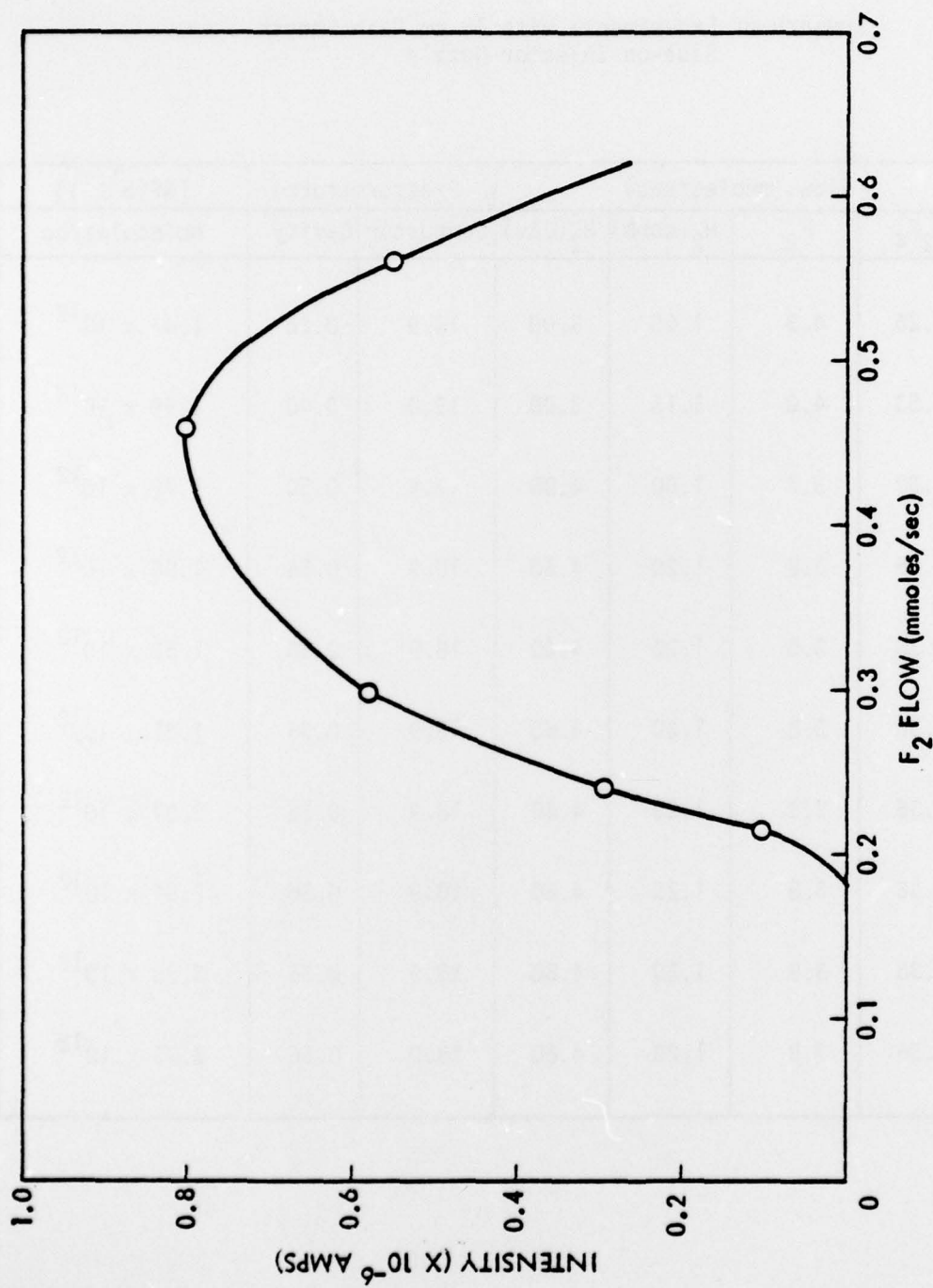


Figure 46. Variation of NF intensity with fluorine flow for 15 cm device.



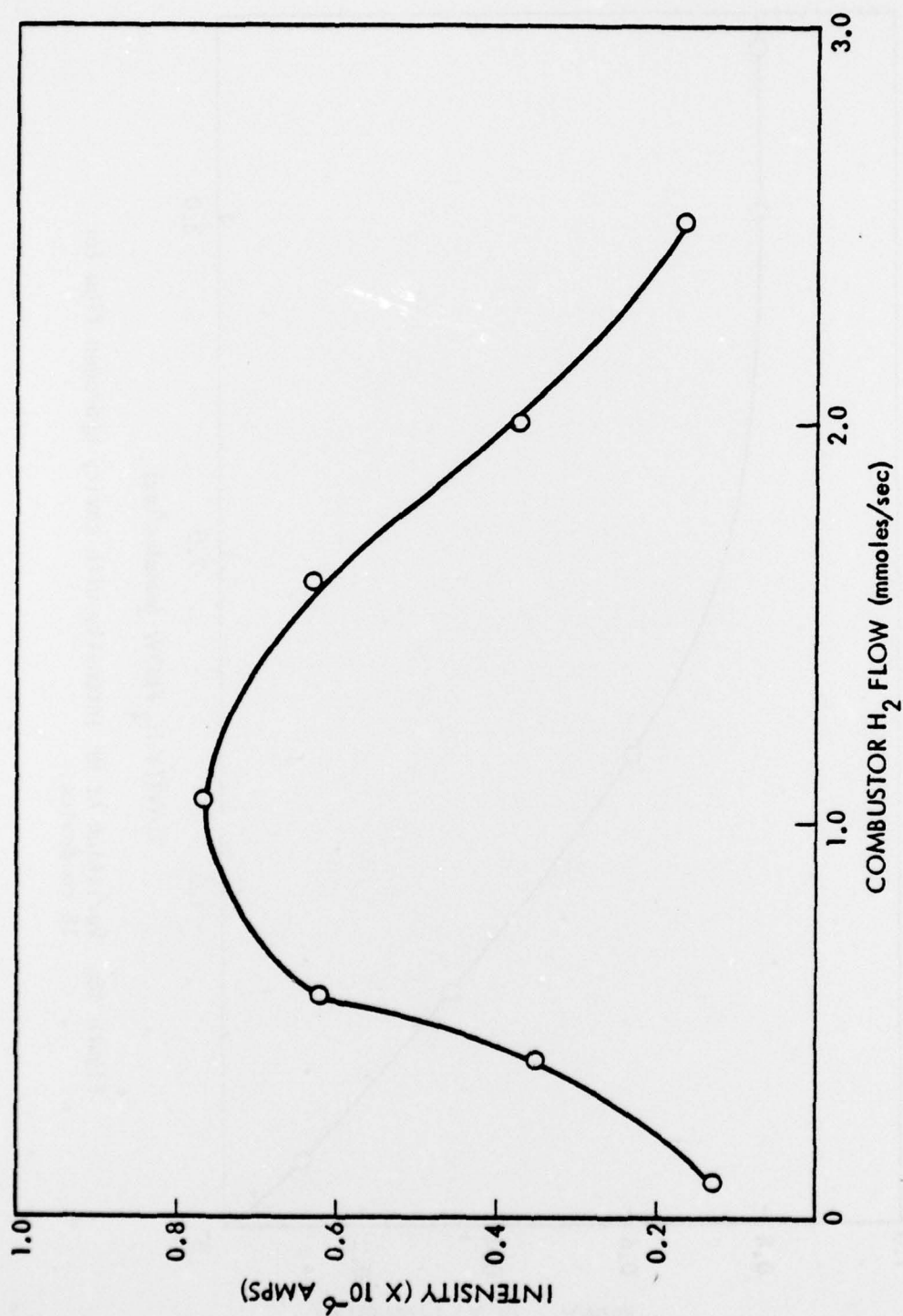


Figure 47. Variation of NF intensity with combustor hydrogen flow for 15 cm device.

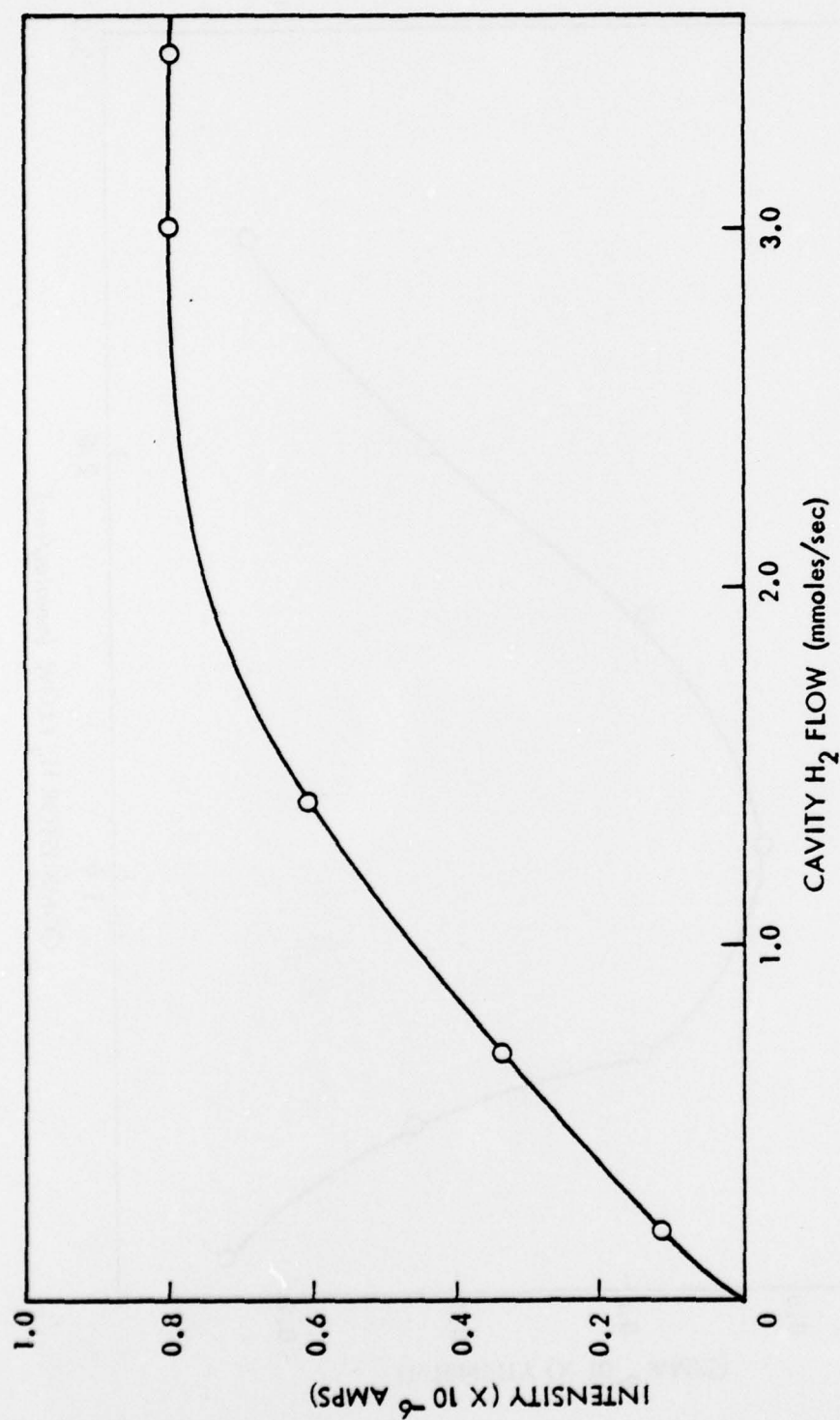


Figure 48. Variation of NF intensity with cavity hydrogen flow for 15 cm device.

maximum at  $X_c = 0.6$  cm, decreases to a minimum at 1.5 cm and then continues to increase for the viewing length that could be scanned. It was found that maximum intensities were obtained with no diluent flow. Intensities dropped sharply when any helium was added to the flow.

The temperature in the flame was determined using HF chemiluminescence. The temperature was found to be determined by the fluorine and hydrogen flows. With no diluent, temperatures ranged from 900°K near the nozzle to 1600°K at the bottom of the cavity. Thus, the temperature was certainly sufficient to convert the  $N_2F_4$  to  $NF_2$  radicals. The no-diluent operation suggested that high temperatures are desirable for NF b state production.

Experiments with this system were limited by inadequate mixing. It was also difficult to increase flows sufficiently to attain higher cavity pressures than 0.6 torr. These limitations will be discussed in the next section.

### 3.3 DISCUSSION

The major purpose of these experiments was to determine what number densities of NF excited states could be achieved in a combustion system using existing hardware. For all experiments, densities of NF ( $b^1\Sigma^+$ ) were reported. These ranged from  $7 \times 10^{11}$  to  $5 \times 10^{12}$  molecules/cc. However, densities of the NF ( $a^1\Delta$ ) state are expected to be larger as this state is formed by a more direct mechanism than is the NF ( $b^1\Sigma^+$ ) state. Unfortunately, the emission from the "a" state was always overlapped by emission from HF or nitrogen first positive, making direct determination of density in this state impractical. Kinetic rate calculations were performed to aid in estimating "a" state densities from "b" state densities. For these

Table 12.

Kinetic Rates Used for NF RESALE Calculations

Reaction	Log A	$\eta$	E(kcal/mol)
1. $\text{H} + \text{NF}_2 \rightarrow \text{HF}(0) + \text{NF}(a^1\Delta)$	$13 \pm .3$	.5	$1.2 \pm 1$
2. $\text{H} + \text{NF}(b^1\Sigma^+) \rightarrow \text{HF}(0) + \text{N}$	$13 \pm .3$	.5	$2.3 \pm 3$
3. $\text{H} + \text{NF}(a^1\Delta) \rightarrow \text{HF}(0) + \text{N}$	$13 \pm .3$	.5	$3.0 \pm 2$
4. $\text{H} + \text{NF}(X^3\Sigma^-) \rightarrow \text{HF}(0) + \text{N}$	$13 \pm 1$	.5	$1.2 \pm 2$
5. $\text{N} + \text{NF}_2 \rightarrow \text{N}_2 + 2\text{F}$	$12.4 \pm .7$	.5	
6. $\text{N} + \text{NF}(X^3\Sigma^-) \rightarrow \text{N}_2 + \text{F}$	$12.6 \pm .7$	.5	
7. $\text{N} + \text{NF}(a^1\Delta) \rightarrow \text{N}_2 + \text{F}$	$12.6 \pm .7$	.5	
8. $\text{N} + \text{NF}(b^1\Sigma^+) \rightarrow \text{N}_2 + \text{F}$	$12.6 \pm .7$	.5	
9. $2\text{NF}(X^3\Sigma^-) \rightarrow \text{N}_2 + 2\text{F}$	$12 \pm 1$	.5	
10. $2\text{NF}(a^1\Delta) \rightarrow \text{N}_2 + 2\text{F}$	$12 \pm 1$	.5	46.
11. $2\text{NF}(b^1\Sigma^+) \rightarrow \text{N}_2 + 2\text{F}$	$12 \pm 1$	.5	3.
12. $\text{NF}(b^1\Sigma^+) \rightarrow \text{NF}(X^3\Sigma^-)$	$1.8 \pm .1$	(sec <sup>-1</sup> )	
13. $\text{NF}(a^1\Delta) \rightarrow \text{NF}(X^3\Sigma^-)$	$0 \pm .15$	(sec <sup>-1</sup> )	
14. $\text{NF}(a^1\Delta) + \text{NF}(b^1\Sigma^-) \rightarrow \text{N}_2 + 2\text{F}$	$12 \pm 1$	.5	24.
15. $\text{NF}(X^3\Sigma^-) + \text{NF}(b^1\Sigma^+) \rightarrow \text{N}_2 + 2\text{F}$	$12 \pm 1$	.5	
16. $\text{NF}(X^3\Sigma^-) + \text{NF}(a^1\Delta) \rightarrow \text{N}_2 + 2\text{F}$	$12 \pm 1$	.5	17.
17. $\text{NF}(b^1\Sigma^+) + \text{NF}_2 \rightarrow \text{N}_2\text{F}_2 + \text{F}$	$12 \pm .7$	.5	$1.6 \pm 2$
18. $\text{NF}(a^1\Delta) + \text{NF}_2 \rightarrow \text{N}_2\text{F}_2 + \text{F}$	$12 \pm .7$	.5	$4 \pm 3$
19. $\text{NF}(X^3\Sigma^-) + \text{NF}_2 \rightarrow \text{N}_2\text{F}_2 + \text{F}$	$12 \pm .7$	.5	$1.6 \pm 3$
20. $\text{N}_2\text{F}_2 + \text{NF}_2 \rightarrow \text{NF}_3 + \text{N}_2 + \text{F}$	$12 \pm 1.5$		30.
21. $\text{HF}(2) + \text{NF}(a^1\Delta) \rightleftharpoons \text{HF}(0) + \text{NF}(b^1\Sigma^+)$	$11.5 \pm .3$ $11.5 \pm .3$	.5 .5	$.83 \pm .1$
22. $\text{HF}(3) + \text{NF}(a^1\Delta) \rightleftharpoons \text{HF}(1) + \text{NF}(b^1\Sigma^+)$	$12.4 \pm .7$ $12.4 \pm .7$	.5 .5	$.14 \pm .1$



Table 12. (Continued)

Kinetic Rates Used for NF RESALE Calculations

Reaction	Log A	$\eta$	E(kcal/mol)
23. $\text{NF}_3 + \text{He} \rightarrow \text{NF}_2 + \text{F} + \text{He}$	$16.6 \pm .7$		$48 \pm 5$
24. $\text{F} + \text{H}_2 \rightarrow \text{HF}(1) + \text{H}$	13.4	0	1.6
25. $\text{F} + \text{H}_2 \rightarrow \text{HF}(2) + \text{H}$	13.9	0	1.6
26. $\text{F} + \text{H}_2 \rightarrow \text{HF}(3) + \text{H}$	13.6	0	1.6

calculations, the rates in Table 12 were used. This set of rates was obtained from John Herbelin at Aerospace Corporation. The  $F + H_2$  rates were added to the set of NF rates. One limitation of this set of rates is the HF rates. None of the quenching rates for  $HF(v)$  were included to keep computer times short. This could lead to an overestimation of NF ( $b^1\Sigma^+$ ) state densities since the principal pumping mechanisms for this state are reactions 21 and 22 which involve vibrationally excited HF.

The rates in Table 12 were put into the RESALE-1 computer program with initial conditions approximating those present in the combustion experiments. The principal uncertainties in the initial conditions were in the amounts of  $F^{\bullet}$  and  $NF_2$  radicals present. Most runs were made assuming that the F-atom concentration was equivalent to that obtained if all the  $H_2$  in the combustor was converted to HF and F. It was also assumed that the  $N_2F_4$  was totally dissociated to  $NF_2$  radicals. The version of RESALE used did not include a mixing model although it did allow gas expansion from a nozzle.

The RESALE calculations predicted number densities that were consistently a factor of 10 higher than those observed experimentally. However, on a relative basis, the calculations fit the plots of NF "b" state intensity versus distance very well. They also predicted the behavior of NF density with increasing  $N_2F_4$  flow quite well in a relative sense. Plots of relative intensity from NF "b" state versus  $N_2F_4$  flow are shown in Figure 49. One run was made in which it was assumed that half the  $NF_2$  radicals had recombined with fluorine atoms to produce  $NF_3$ . The densities predicted for this run were only slightly lower than in the equivalent run where there was twice as much  $NF_2$ . The RESALE calculations predicted that the NF "a" state

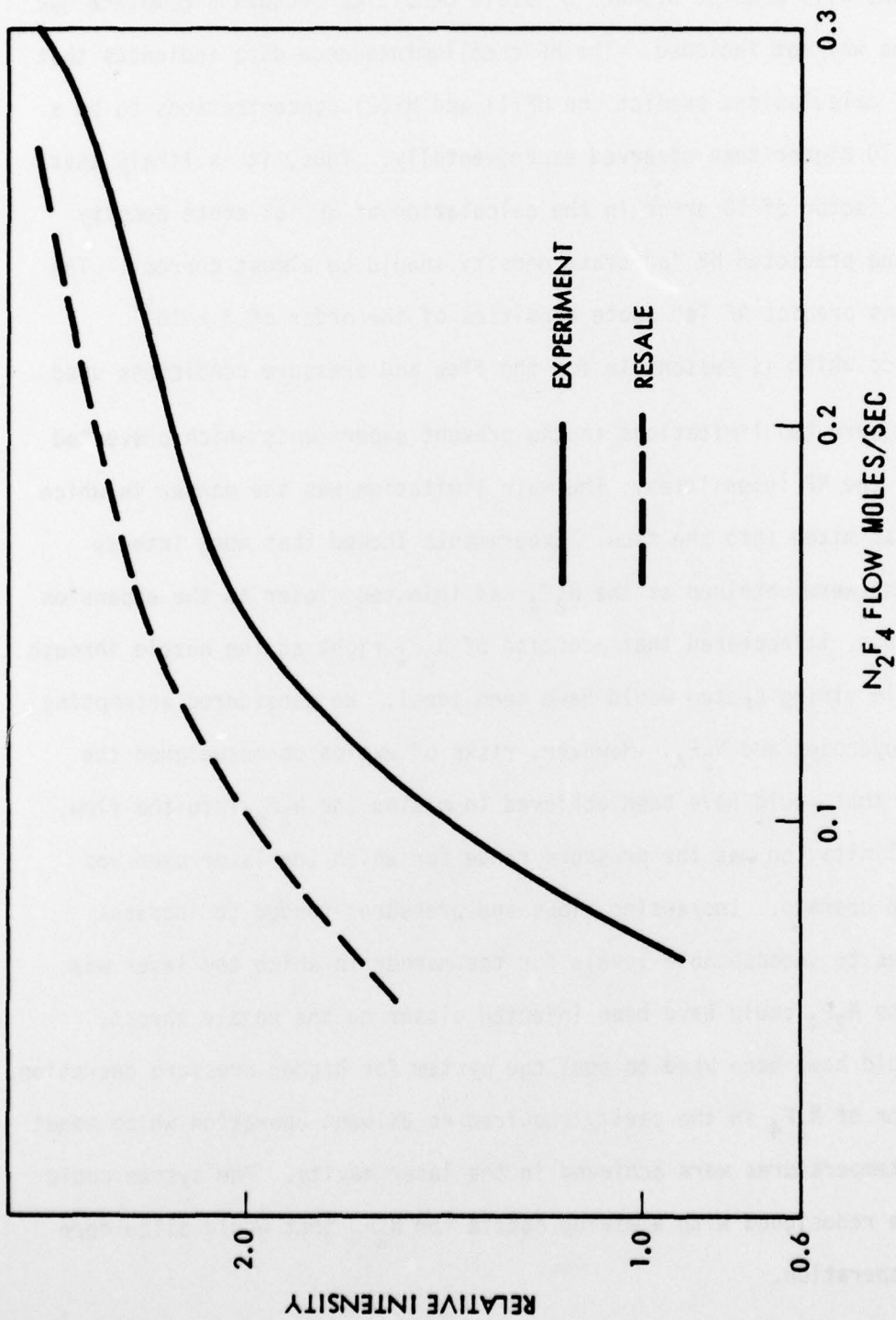


Figure 49. Relative intensity of  $NF(b^1\Sigma^+)$  versus  $N_2F_4$ . Comparison of theory and experiment.

density was a factor of 5 higher than that of the "b" state. However, these calculations will predict higher "b" state densities because a complete set of HF rates was not included. The HF chemiluminescence data indicates that the RESALE calculations predict the HF(1) and HF(2) concentrations to be a factor of 10 higher than observed experimentally. Thus, it is likely that there is a factor of 10 error in the calculation of NF "b" state density but that the predicted NF "a" state density should be almost correct. The calculations predict NF "a" state densities of the order of  $3 \times 10^{14}$  molecules/cc which is reasonable for the flow and pressure conditions used.

There were two limitations in the present experiments which prevented scaling of the NF intensities. The main limitation was the manner in which the  $N_2F_4$  was mixed into the flow. Experiments showed that more intense NF emissions were obtained as the  $N_2F_4$  was injected closer to the expansion nozzle. Thus, it appeared that addition of  $N_2F_4$  right at the nozzle through a reasonable mixing system would have been ideal. We considered attempting to premix hydrogen and  $N_2F_4$ . However, risks of explosion outweighed the advantages that would have been achieved in mixing the  $N_2F_4$  into the flow. The other limitation was the pressure range for which the laser used was designed to operate. Increasing flows and pressures tended to increase temperatures to unacceptable levels for the manner in which the laser was run. If the  $N_2F_4$  could have been injected closer to the nozzle throat, diluent could have been used to cool the system for higher pressure operation. The addition of  $N_2F_4$  in the cavity required no diluent operation which meant very high temperatures were achieved in the laser cavity. The system could probably be redesigned with a mixing nozzle for  $N_2F_4$  that would allow more efficient operation.



The present experiments did not come close to achieving the NF ( $a^1\Delta$ ) state number densities that would be required for lasing. Because of the long lifetime of this state, densities of the order of  $10^{17}$  molecules/cc of the NF ( $a^1\Delta$ ) state would be required to obtain any type of reasonable gain. This is almost a factor of  $10^3$  above the densities achieved in the present system. Increasing pressures from 1.5 torr to 150 torr could give a factor of  $10^2$  but even this would be marginal. It appears that for this reason, the NF ( $a$ ) state may be better used as an energy transfer donor to some other state. However, detailed calculations would be required to fully evaluate whether a system capable of lasing in a CW mode is feasible.

## REFERENCES

1. M. Jeunehomme, "Oscillator Strength for the CN Red Band System", J. Chem. Phys. 42, 4086 (1965).
2. G. Palletto and M. Rigutte, "The  $A^2\Pi$  and  $X^2\Sigma$  States of the CN Molecule from the Berkeley Analysis of the CN Red System", Nuovo Cimento 39, 519 (1965).
3. G. A. West and M. J. Berry, "CN Photodissociation and Predissociation Chemical Lasers: Molecular Electronic and Vibrational Laser Emissions", J. Chem. Phys. 61, 4700 (1974).
4. C. R. Quick, Jr. and Curt Wittig, "Electronic Transition CN Laser Pumped by a Pulsed Electric Discharge", Electron Transition Lasers, J. I. Steinfeld, ed., (The MIT Press, Cambridge, Massachusetts, 1976).
5. S. P. Davis and J. G. Phillips, Red System ( $A^2\Pi - X^2\Sigma$ ) of the CN Molecule, (University of California Press, Berkeley and Los Angeles, California, 1963).
6. J. A. Betts and J. F. Friichtenicht, "Advanced Laser Concepts", Final Report for Contract F29601-73-A-0036-001, 1976.
7. A. C. G. Mitchell and M. W. Zemansky, Resonance Radiation and Excited Atoms, (Cambridge University Press, 1961).
8. A. Schadee, "The Relation Between the Electronic Oscillator Strength and the Wavelength for Diatomic Molecules", J. Quant. Spectrosc. Radiat. Transfer 7, 169 (1967).
9. L. T. Earls, "Intensities in  $^2\Pi - ^2\Sigma$  Transitions in Diatomic Molecules", Phys. Rev. 48, 423 (1935).
10. P. L. Goodfriend and H. P. Woods, "Emission Spectra of Flames of NF-Containing Oxidizers", Combustion and Flame 9, 421 (1965).
11. M. A. A. Clyne and I. F. White, "Electronic Energy Transfer Processes in Fluorine-Containing Radicals: Singlet NF", Chem. Phys. Lett. 6, 465 (1970).
12. J. M. Herbelin and N. Cohen, "The Chemical Production of Electronically Excited States in the H/NF<sub>2</sub> System", Chem. Phys. Lett. 20, 605 (1973).
13. J. M. Herbelin, D. J. Spencer, and M. A. Kwok, "Scale-up of NF ( $a^1\Delta$ ) Produced by the H + NF<sub>2</sub> System in a Subsonic CW Laser Device", J. Applied Phys., (to be published).

14. W. L. Shackelford and H. M. Bobitch, "2 - 5 Micron Chemical Laser", Technical Report AFAL-TR-75-63, May 1975.
15. M. A. Kwok, J. M. Herbelin, and N. Cohen, "Collisional Quenching and Radiative Decay Studies of NF ( $a^1\Delta$ ) and NF ( $b^1\Sigma^+$ )", Aerospace Report No. TR-0074(464)-2, 1976.